Investigating Regulatory Mechanisms Influencing
Oral Cancer-Intrinsic Type I Interferon Production and Signaling

by

Blake Robert Heath

A dissertation submitted in partial fulfillment
of the requirements for the degree of
Doctor of Philosophy
(Immunology)
in the University of Michigan
2021

Doctoral Committee:

Assistant Professor Yu Leo Lei, Chair
Professor Cheong-Hee Chang
Associate Professor Grace Chen
Professor Nisha D'Silva
Professor Mary O'Riordan

Blake Robert Heath

heathbr@umich.edu

ORCID iD: 0000-0001-8656-0532

DEDICATION

To my parents and grandparents, for the wealth of emotional support, and, above all,

unconditional love that brought me to this moment

ACKNOWLEDGMENTS

The work outlined within this dissertation is credited under my name but is the result of patient counsel and wise leadership received from so many. First, I want to thank my mentor, Dr. Leo Lei, for welcoming me into the lab as person number four (or number two if you count my rotation) and trusting me to help build his new research operation. I am forever thankful for his mentorship and brilliant knowledge that has pushed me to think deeper and harder about scientific questions than I may have thought possible. I am additionally thankful for my dissertation committee: Drs. Cheong-Hee Chang, Grace Chen, Nisha D'Silva, and Mary O'Riordan, who provided crucial and encouraging feedback for my projects over the years.

My quality of life in the Lei lab was enhanced by the friendships that I have made. I am thankful to my lab mates for technical assistance, experimental design suggestions, and collegial bonhomie. I also want to acknowledge the numerous collaborators and core facilities I have had the fortune of working with during my time at U of M. In particular, thank you to the University of Michigan Advanced Genomics Core and Dr. Yuying Xie at Michigan State University for continued assistance with bioinformatics and biostatistical analyses.

I feel lucky to have landed in the Graduate Program in Immunology. Thank you to our former program director, Dr. Beth Moore, and current directors, including Dr. Gary Huffnagle, for keeping the needs of students first. I want to additionally thank Drs. Malini Raghavan and Durga Singer for advocating and setting policies to enact the Diversity, Equity, and Inclusion standards

set forth by the university. Lastly, I am thankful for the consistent and kind guidance of Zarinah Aquil, whose capacity for managing program activities is astounding.

I am grateful for my former mentors who helped guide me to this moment: Drs. Thomas Wilkie and Nancy Street at UT Southwestern, and Drs. Silke Paust, Laurie Connor, John Rodgers, and Gayle Slaughter at Baylor College of Medicine. I would not be here without the training and encouragement I received before starting graduate school.

My time at Michigan would not be the same without the friendships I have made; thank you to everyone I have met who made the time special. I am especially appreciative of Giovanny Martinez-Colón and Cara Porsche for assistance with dissertation composition. I would also like to thank my friends in Texas for being excellent sounding boards and sources of enjoyment when I am home.

Lastly, thank you to my family for the support, prayer, and encouragement throughout my time at the University of Michigan. My grandparents, Charles and Sylvia Zeigler, have never wavered in their belief in me and have always extended care in more ways than are imaginable. To my parents, Tony and Pamela Petty, thank you for never putting limits on what I could achieve and providing the stable, loving home that made it all possible.

TABLE OF CONTENTS

LIST OF FIGURES

LIST OF TABLES

ABSTRACT

Head and neck squamous cell carcinoma (HNSCC) is the sixth-leading cause of cancer fatalities worldwide. Furthermore, a societal rise in obesity has coincided with an increased prevalence of head and neck cancers, portending potentially deleterious co-morbidities. The work outlined in this dissertation identifies novel avenues towards our understanding of how tumors mediate immune escape in both lean and obese experimental models, as well as potential limitations and considerations in developing effective immunotherapeutics. Proteins of key importance towards these efforts are type I interferons (IFN-I), characterized as potent activators of anti-tumor immunity. Indeed, this dissertation expands our mechanistic understanding of how stimulator of interferon-inducible genes (STING)-mediated IFN-I production and signaling proves to be a central mechanism in facilitating anti-tumor T-cell and myeloid cell expansions. We find that tumors from obese mouse models display increased tumor burden alongside an immunosuppressed tumor microenvironment. Palmitate, a saturated fatty acid and essential component of adipose tissue, dysregulates IFN-I production in both cancer and immune cells, leading to increased anti-tumor immune responses. Alongside this, the regulatory nucleotide-binding domain and leucine-rich repeat (NLR) protein NLRC3, which has been previously characterized as a negative regulator of IFN-I production in myeloid cells, is identified here as a negative regulator of IFN-I production within human and mouse oral cancer cells. *NLRC3* expression is additionally induced in tumors derived from obesity models, indicating potential linkages between saturated fatty acids and innate immune sensors. Through assessment of the

IFN-I-related metagene *MX1*, we uncovered that downstream paracrine and autocrine IFN-I signaling within oral cancer tumors is subsequently harmful to patient survival and tumor burden, by initiating events leading to the expansion of cancer stem cells. Thus, through this work, we reveal pleotropic nature of IFN-Is in modulating the tumor microenvironment. Cancer-intrinsic IFN-I production promotes pro-inflammatory anti-tumor immune activation, largely dependent on myeloid and cancer cell IFN-I production and myeloid IFN-I downstream signaling, while downstream cancer-intrinsic IFN-I signaling enacts a remodeling of the tumor microenvironment through the expansion of cancer stem cells, supporting cancer immune escape.

CHAPTER 1 – Introduction

The work conducted within this dissertation describes mechanisms that regulate both tumor development and the tumor microenvironment in head and neck squamous cell carcinoma (HNSCC). The underlying theme of the outlined experiments pertains to the role of type I interferon (IFN-I) proteins in mediating both pro-inflammatory immune cell infiltration into tumor sites as well as immune evasion. The following introduction provides context on current research strategies and modalities currently being investigated towards enhancing anti-tumor immunity. The success of immune checkpoint receptor blockade has brought exciting promises for the treatment of HNSCC. While patients who respond to checkpoint inhibitors tend to develop a durable response, fewer than 15% of HNSCC patients respond to immune checkpoint inhibitors, underscoring the critical need to alleviate cancer resistance to immunotherapy. Central genomic events in HNSCC have been found to possess previously unknown roles in suppressing immune sensing. Such inhibitory functions impact both the innate and adaptive arms of tumor-specific immunity. While checkpoint blockade effectively reinvigorates adaptive T-cell responses, additional targeting of the oncogenic inhibitors of innate immune sensing likely informs a novel and potent strategy for immune priming. Thus, the second chapter outlines such a novel mechanism, by which the innate immune sensor NLRC3 negatively regulates the double-stranded DNA-dependent IFN-I pathway, and markedly suppresses Tc1 and T_H1 immune cell responses in mouse tumor models. Additionally, chapter two delineates a mechanism by which obesity mediates increased host tumor burden, through the suppression of IFN-I production and

1

signaling by palmitate. Chapter three examines how downstream cancer-intrinsic IFN-I signaling is detrimental for patient survival and tumor burden, indicating the pleiotropic nature of IFN-Is in cancer immunology. Lastly, chapter four will abridge the importance of the findings outlined in chapters two and three and discuss avenues for future investigation.

Introduction to Head and Neck Squamous Cell Carcinoma

Head and neck cancer is the sixth leading cause of cancer-related death globally, with over 500,000 new cases diagnosed each year (1). Head and neck squamous cell carcinoma (HNSCC), the major subtype of this disease, is responsible for over 90% of new cases (2). Current standard-of-care treatments are often associated with significant morbidity that limits the patient quality of life (3, 4).

Immunotherapy has emerged as a paradigm shift in cancer therapy, with unprecedented durability in patient response and substantially improved patient quality of life. Cancer immunotherapy approaches rely on the pivotal role of the immune system in recognizing and eliminating transformed malignant cells.

Fitting with the well-established observation that the incidence of squamous cell carcinomas is higher in immunocompromised patients (5, 6), the alleviation of cancer-potentiated immune suppression has shown potential in reducing HNSCC tumor burden and improving patient quality of life (7-9). The success of monoclonal antibodies blocking the immune checkpoint receptors (ICRs) signaling has transformed the landscape of emerging cancer therapeutic pipelines. This line of treatment aims to enhance the function of $CD8^+$ cytotoxic T-lymphocytes (CTL), which play a crucial role in recognizing and eliminating tumor cells. Two signals are needed to activate $CD8^+$ T-cells: T-cell receptor interaction with the

MHC-peptide complex (signal 1) and CD28-mediated co-stimulation (signal 2). To prevent excessive immune activation that is often linked to autoimmunity, ICRs are employed to fine tune the magnitude of immune activation. The characterization of two pivotal members of the ICR family, Programmed cell Death protein 1 (PD-1) and Cytotoxic T-Lymphocyte-Associated protein 4 (CTLA-4), informed the clinical advance in ICR blockade therapy. PD-1 pathway dampens signal 1 and CTLA-4 tunes down signal 2 (10). Thus, blocking ICRs can reinvigorate the effector function of CTLs.

Although less than 15% of the patients responded to ICR blockade, the responders developed a durable response (7-9). This important observation is similar to results from phase III immunotherapy trials for other cancer types (11, 12). In this review, we will discuss recently identified pathways that can be further exploited to enhance immune priming for ICR blockade.

Genetic basis for oncogenic suppression of immune sensing of HNSCC

It is well-established that the efficacy of ICR blockade is dictated, at least in part, by a sufficient number of infiltrating CTLs. Somatic mutations give rise to a pool of neoantigens that could be potentially perceived by CTLs. Higher mutation load is found to be associated with better response to immunotherapy (13). Compared to many cancer subtypes, HNSCCs have a high mutational load (14). However, their response rates to ICR blockade remain modest, which raises the possibility that other mechanisms also contribute to HNSCC immunogenicity. The expansion of tumor-specific CTLs depends on proper tumor recognition and antigen processing by the innate immune system, which employs an array of sensors, aka pattern recognition receptors, to become the first responders to abnormal cells. The collective effort in the Cancer Genome Atlas Consortium (TCGA) revealed cancer-specific molecular circuitry with

3

unprecedented details. Emerging evidence suggests certain genetic and genomic alterations specifically interfere with innate and adaptive immune sensing of tumors (Figure 1-1).
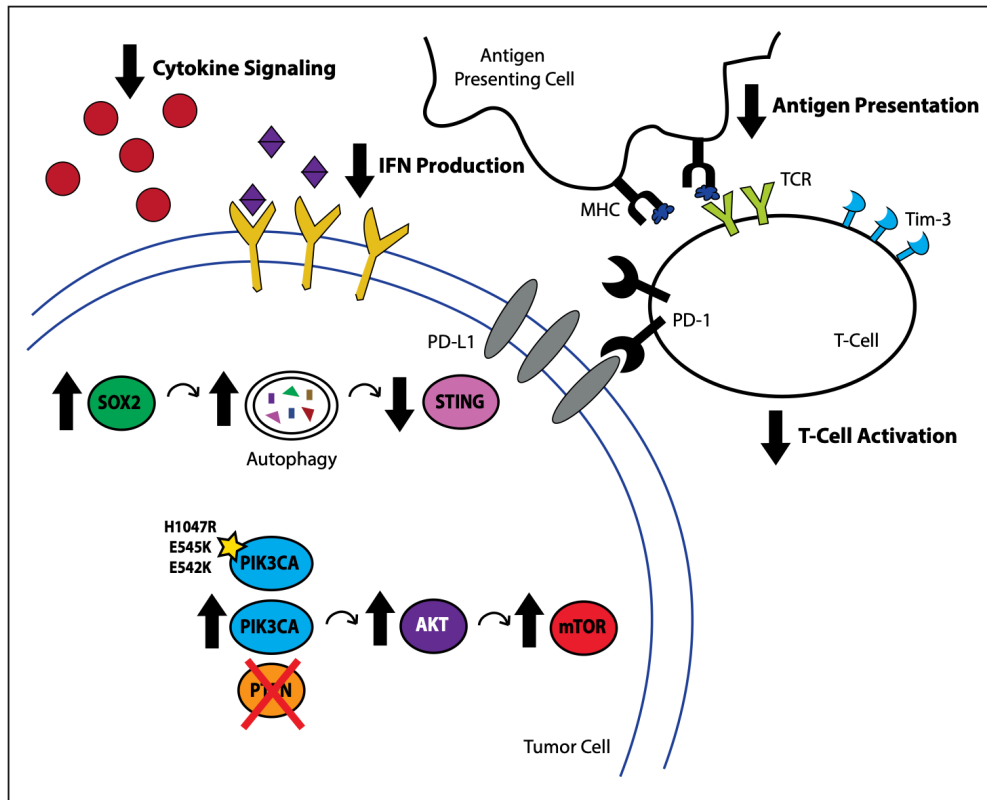
Figure 1-1 – **Genetic abnormalities in HNSCC contributes to poor tumor immunogenicity**

Aberrant signaling resulting from genes controlling processes ranging from self-renewal to metabolism can lead to deficits in cancer immunogenicity. The transcription factor SOX2 has been recently implicated in negatively regulating IFN-I-mediated anti-tumor immune responses, by promoting the autophagosome-mediated degradation of the ER-resident protein STING, leading to decreased immune infiltration. *PIK3CA* is commonly co-amplified with *SOX2* in HNSCC, leading to the activation of the mTOR pathway, which reduces CTL infiltration into the tumor microenvironment.

SOX2 dampens type-I interferon-mediated immune sensing of HNSCC

One such recurrent genetic event, 3q amplification, which occurs in 16% of HNSCC patients from the TCGA and contains transcription factor SRY-box 2 (SOX2), has emerged as a pivotal oncogenic driving event that promotes the initiation, proliferation, and malignant transformation of squamous cell carcinomas (SCCs), in addition to its well-known role in

4

maintaining stemness. *SOX2* is amplified in a wide range of SCCs, and its expression in HNSCC is correlated with decreased patient survival (15), higher incidences of nodal metastasis, and a higher cancer stage at the time of initial diagnosis (16). Among HNSCCs, SOX2 has been demonstrated to promote disease pathogenesis by driving tumor initiation and self-renewal of cancer stem cell populations (17-20).

In addition to these critical functions, recent work has uncovered a surprising role for SOX2 in the potentiation of cancer immune escape in HNSCCs. In particular, *SOX2* emerged from an RNA-Seq-based screen selecting for cancer cell-intrinsic genes associated with the development of resistance to immune killing. Interestingly, in an immunocompetent mouse model of HNSCC, Sox2-overexpressing tumors displayed diminished CD8^{+} CTL infiltration and enhanced tumor growth, suggesting that SOX2 dampens antitumor immunity *in vivo*. Further investigation revealed that these effects are mediated by SOX2-mediated suppression of the stimulator of interferon genes (STING)-dependent type-I interferon (IFN-I) signaling pathway. STING senses cytoplasmic DNA, which is frequently present in cancer cells that are sustaining DNA damage due to unstable genome and treatments, and triggers the production of IFN-I to promote antigen-presenting cell maturation. The centricity of the STING-IFN-I signaling axis has been corroborated in pre-clinical models of several cancer types including HNSCC (16, 21-23). Effective delivery of STING agonists expands tumor-specific CTLs and synergizes with ICR blockade (16, 23). Not surprisingly, suppression of this pathway has emerged as a common strategy used by cancer cells to potentiate immune escape, which is evidenced by frequent loss of STING expression in the tumor cells (24, 25). As a previously unknown mechanism, SOX2 promotes autophagy-dependent turnover of STING, suppressing IFN-I activation. In agreement,

SOX2-high HNSCCs exhibit increased regulatory T-cells and decreased M1-like macrophages infiltration, a phenotype that is commonly seen with a deficiency in STING signaling (16).

Activation of the PI3K pathway promotes adaptive resistance to ICR blockade

Frequent *SOX2* amplification is a defining feature of a major subset of HNSCC. Notably, *SOX2* and *PIK3CA* genes are both located at the 3q26.3 locus and frequently co-amplified in HNSCCs. Aberrant phosphatidylinositol 3-kinase (PI3K) pathway activation, particularly via mutation or amplification of the gene *PIK3CA* is central for the transformation of HNSCC. Data from TCGA HNSCC cohort indicate that the majority of patients with this tumor type display genetic alterations in one or more PI3K pathway members and that over half of these PI3K-altered patients harbor mutations or copy number alterations in *PIK3CA* (26, 27). HNSCC with multiple concurrent PI3K mutations are all advanced, suggesting its critical role in tumor development (28). PIK3CA activates mTOR signaling and promotes HNSCC growth and resistance to EGFR-targeted therapy (29). In addition to its well-characterized role in promoting cancer cell proliferation, emerging evidence suggests that targeting PI3K represents a promising strategy to improve immunotherapy. Such improvement is likely achieved by the pleiotropic effects of PI3K inhibition on both cancer cells and CTLs.

Innate immune priming expands CTLs, and ICR blockade helps to alleviate CTL exhaustion. However, sustained CTL activation entails rapid genome replication, active migration to come in proximity to target tumor cells, production of large amounts of cytokines de novo, and establishment of immunologic synapses. All of these processes are metabolically demanding and require bioenergetics support. Indeed, extracellular glucose is a key nutrient source to maintain CTL effector function, and deprivation of extracellular glucose leads to rapid

CTL exhaustion (30-34). However, a hallmark of cancer is its prioritization of the aerobic glycolysis pathway over oxidative phosphorylation, a phenomenon coined as the Warburg effect (35). PI3K promotes glucose uptake and enhances glycolysis via the mTOR-AKT pathway (36). Tumor cells with activating mutations or amplifications of the *PIK3CA* gene may directly compete with CTLs in the microenvironment for the limited glucose supply. Thus, inhibiting the PI3K pathway is a promising approach to reprogram cancer metabolism in the tumor microenvironment to favor sustained immune effector activation.

In addition to promoting the Warburg effect in tumor cells, PI3K pathway also directly enhances CTL exhaustion in HNSCCs. A potential adaptive resistance mechanism to ICR blockade is the compensatory upregulation of other ICR members. Utilizing clinical HNSCC specimens, a recent study demonstrated that the ICRs PD-1 and T-cell Ig and mucin domain-3 protein (TIM-3) are co-expressed by the most exhausted and dysfunctional CTLs. Interestingly, PD-1 blockade-treated HNSCC patients exhibit upregulated TIM-3 expression by CTLs, and such upregulation is dependent on the activation of the PI3K/AKT pathway (37). Thus, targeting the PI3K pathway can also directly prevent compensatory induction of additional ICR signaling to maintain CTL activation.

Other oncogenic pathways that modulate host immune responses to HNSCC

The amplification of the 3q26.3 locus is not the only event that engages the host-tumor interface. For example, active β-catenin signaling was initially characterized to be associated with a T-cell-poor tumor microenvironment among 266 patients with metastatic cutaneous melanomas. Interestingly, SOX2 was also discovered in this patient cohort as a significant factor driving T-cell exclusion (38), in agreement with another unbiased whole transcriptome screen

that utilizes HNSCC cells (16). Activated WNT/β-catenin drives melanoma resistance to checkpoint blockade (38). In a more recent pan-cancer type bioinformatics analysis of the TCGA database, mutations of β-catenin signaling components were also more frequently found in non-T-cell-inflamed specimens (39).

The human papillomavirus (HPV) is another oncogenic factor that emerges as a regulator of the immune microenvironment. The distinction of HPV$^+$ HNSCC was initially made prominent through a retrospective analysis of the prognostic potential of HPV status. The HPV$^+$ HNSCC subset shows a significantly lower hazard ratio for death (40). However, the impact of HPV on the tumor immune environment and response to immunotherapy is more complex with interesting findings from randomized phase III trials. Two of such trials are CheckMate 141 and KEYNOTE-040. Based on the initial report of CheckMate 141 and a two-year follow-up of the same cohort, the response rates between HPV$^-$ and HPV$^+$ groups were similar with almost identical hazard ratios (7, 8, 41). Similarly, the results from KEYNOTE-040 suggests that the hazard ratio for pembrolizumab vs. standard-of-care was 0.77 with a 95% CI of 0.61-0.97. Interestingly, the hazard ratio for pembrolizumab vs. standard-of-care was 0.97 with a 95% CI of 0.63-1.49 in the HPV$^+$ (p16$^+$) group (9), suggesting that pembrolizumab did not significantly reduce hazard risk of death in this group. In-depth examinations of the T-cell receptor repertoire within HNSCC reveal either similar or worse T-cell clonal expansion in the HPV$^+$ subset (42, 43). Thus, despite the more favorable clinical response to standard-of-care, HPV$^+$ tumors may present not yet fully understood challenges that smolder treatment-induced immune activation.

Strategies to improve innate immune priming to sensitize cold HNSCC

One of the key goals of immune priming is to polarize the immunologically "cold" tumor, which lacks sufficient T-cell infiltration and is resistant to checkpoint protein blockade, towards an immunological milieu which is deemed "hot" or highly T-cell inflamed (44) (Figure 1-2). The innate immune system constitutes the first line of defense against cancer. The innate immune sensors capture conserved molecular patterns that are associated with tissue damage to alert the adaptive arm of immunity. As discussed above, cytoplasmic DNA is a recently identified damage-associated molecular pattern that is commonly present in cancer cells. However, DNA-induced STING-mediated IFN-I activation is often suppressed in a subset of HNSCC by oncogenes. Thus, strategies to bypass oncogenic inhibition of innate immune sensors inform a major class of immune-priming therapies.
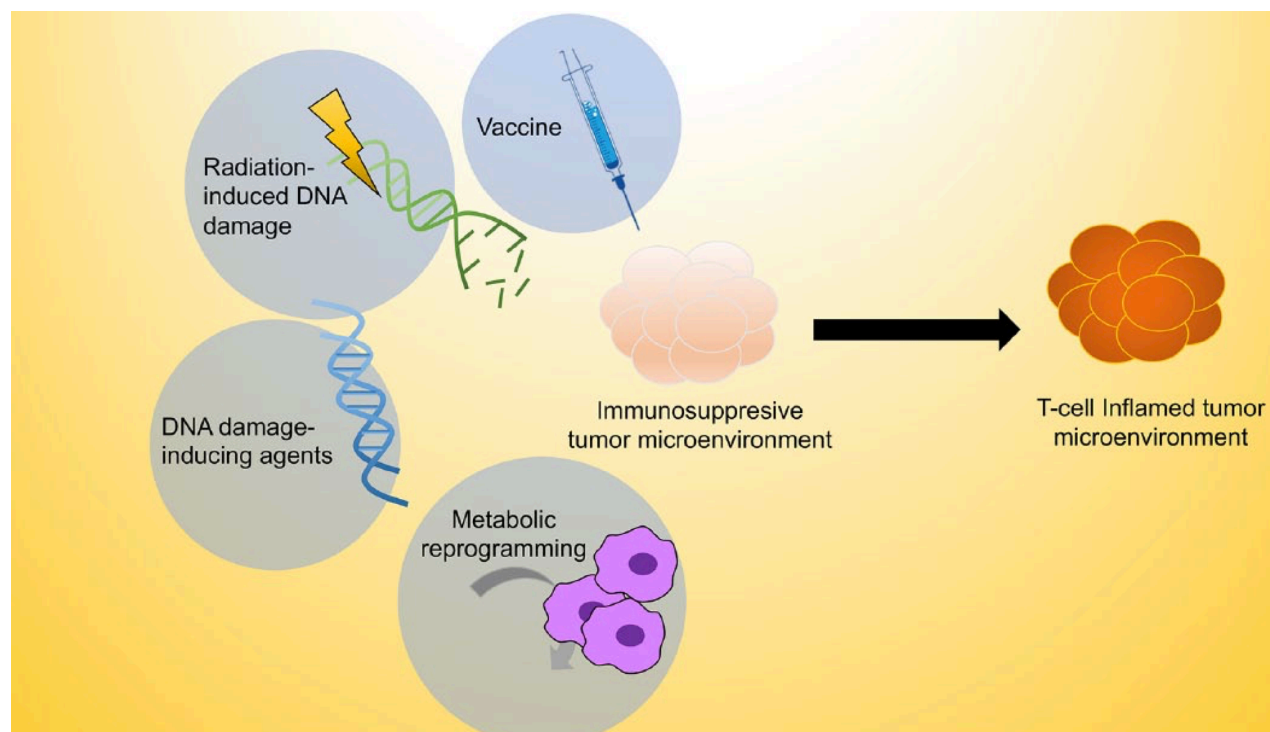
Figure 1-2 – **Strategies to improve innate immune priming to sensitize cold tumors**

A multipronged approach is needed to most effectively prime the tumor microenvironment for ICR blockade. The goal of immune priming is to release frequent oncogenic inhibitors of the innate and adaptive immune signaling, to expand the pool of tumor-specific CTLs, and to metabolically support the activation of antigen-presenting cells and effectors. Some immune-priming approaches have shown promises in HNSCC immunotherapy, including but are not limited to cancer vaccines, radiotherapy, DNA-damage-inducing chemotherapy, and metabolic reprograming agents.

Utilize IFN-I agonists as vaccine adjuvant

From an unbiased transcriptome-wide screen, the IFN-I signaling-centered defense response emerges as the most critical pathway regulating HNSCC cells sensitivity to immune effector-mediated cytotoxicity (16). In addition, IFN-I agonists potently create a T_H1-skewed cytokine milieu to activate macrophages and dendritic cells (45, 46). Indeed, IFN-I-inducing agents show remarkable efficacy in various tumor models. A prototypic experimental vaccine adjuvant is CpG, which induces IFN-I in a Tlr9-dependent fashion. CpG-based vaccines can

significantly expand tumor-specific CD8$^+$ CTLs and improve the tumor response to ICR

blockade (47). However, the TLR9 expression profile in humans is drastically different from that

in mice. Tlr9 is broadly expressed by the myeloid compartment in mice, which underpins the

success of CpG-based formulations in polarizing the antigen-presenting cells towards a

productive anti-tumor immune response. However, TLR9 expression is largely absent in the

human myeloid compartment except for plasmacytoid dendritic cells (48, 49). Thus, novel IFN-

I-inducing adjuvants that are evolutionarily conserved in tissue distribution are explored to

improve cancer immunotherapy.

One of these adjuvants is STING agonist cGAMP. As cGAMP is a highly polar

molecule, several independent groups have reported different delivery system to improve its

pharmacokinetic properties. One such model uses a peptide hydrogel-based system, known as

"STINGel," for delivering STING agonist intratumorally (23). This platform achieves extended

release of drug, due to the semi-solidified state the drug conforms when injected into the tumor.

This technology increases the survival rate of the mice bearing an ICR blockade-resistant

HNSCC model (23).

Emerging nanoparticle-based approaches for immunotherapy have shown remarkable

efficacy in pre-clinical HNSCC models. Nanoparticle classes are comprised of versatile carriers

for an array of treatments, and as a whole, can deliver high-density antigens to the tumor

microenvironment (50). Nanoparticles can be also designed to accumulate in the lymph nodes,

increasing APC uptake of antigen and improving cross-priming (51). One of such examples is a

system coined as the nanosatellite. The nanosatellite vaccine significantly enhances the efficacy

of cGAMP, accumulates in the draining lymph nodes, improves APC maturation, expands

tumor-specific CTL and improves HNSCC response to ICR blockade. Interestingly, the

nanoparticle-based STING agonist delivery system shows better efficacy than using Montanide, one of the strongest clinical-grade adjuvants(16). Overall, new technologies and targeted therapies to bypass oncogenic suppression of innate immune sensors likely substantially improve HNSCC response to ICR inhibitors.

Radiation can prime HNSCC for ICR blockade

Radiation therapy (RT) is a critical component of the standard-of-care for patients with HNSCC. Due to the more favorable response to RT among patients with HPV[+] HNSCC, randomized phase III trials have assessed potential options for treatment de-escalation. Recently, two of such studies confirmed that RT plus cisplatin remains the standard-of-care (52, 53). Conventionally, these responses to RT are found to be dependent on the production of reactive oxygen species, resulting in DNA damage and ER stress, and on the induction of apoptosis. Interestingly, recent evidence suggests that the efficacy of RT depends on an intact immune response as RT loses its efficacy in immunocompromised hosts (21). As a mechanism, following RT-induced DNA damage, the resulting DNA fragments in the cytoplasm likely engage the STING pathway to prime the tumors for ICR blockade therapy (21, 54). MHC class-I genes are downstream targets of IFN-I signaling. It is known that HNSCC exhibits reduced expression of MHC class-I molecules, as a mechanism of immune escape. RT can directly increase MHC class-I expression (55-57), possibly through the STING-IFN-I axis. Improved responses to RT combined with PD-L1 blockade have been reported using an orthotopic mouse model of HNSCC (55). The authors of these studies showed that effects were dependent on infiltration of CD8^{+} T-cells (55, 58). Targeting additional ICRs such as Tim-3 can further enhance responses (59-61).

Despite these promising preclinical data, the most effective combination of RT with immunotherapy remains incompletely understood. Clinically, several factors require further investigation and may necessitate patient- or subgroup-specific treatment protocols. These factors include the patient population of interest (early stage/curative versus recurrent/metastatic), the timing of RT treatment (before or after surgery as well as neoadjuvant, concurrent, or adjuvant with immunotherapy), and the specific dosing and fractionation of radiation treatment. HPV positivity may be also an important biomarker for patient stratification. These considerations are being evaluated in a variety of ongoing clinical trials, which were recently reviewed elsewhere (56).

DNA damage-inducing agents reduces tumor-potentiated immunosuppression

Cytotoxic chemotherapies, in particular DNA damaging agents such as cisplatin and 5-fluorouracil (5-FU), are commonly used in the treatment of HNSCC. Platinum-based chemotherapies bind to DNA and result in the formation of inter- and intra-strand cross-links, while 5-FU is a pyrimidine analogue that inhibits thymidylate synthase. Although through different mechanisms, both inhibit DNA replication. These agents are administered widely, given alone or with radiation, surgery or other cytotoxic agents or targeted therapies.

Although DNA damage agents have conventionally been considered immunosuppressive, recent evidence suggests that they may also have immunostimulatory effects (56, 62). HMGB1 and calreticulin are released following the administration of platinum therapies and activate TLR4-mediated tumor immune responses, although these effects may be specific to oxaliplatin (63, 64). Cisplatin has shown both immunosuppressive and immunostimulatory roles, depending

13

on dosing. A recent study found that sublethal cisplatin helps to increase the expression levels of

antigen-presenting machinery and immunogenic killing. Higher doses of cisplatin dampen the

production of IFN-γ by T-cells (65). Due to the different pharmacokinetics of cisplatin between

murine models and human, additional studies would be informative to determine the optimal

dosing of cisplatin when designing a combination trial. Several DNA damage agents have been

shown to decrease the number and/or function of myeloid-derived suppressor cells (MDSCs)

(66-69); effects on MDSCs, however, may not be specific to this drug class (70-72) and can in

other cases occur in the opposite direction (73). Platinum-based therapies can also activate

cytotoxic T-cells via STAT6-dependent reductions in PD-L2 expression (74) and/or increased

permeability to granzyme B (75). Further supporting the potential role of DNA damaging agents

in improving responses to immunotherapy, inhibition of ATR, a critical component of the DNA

damage response, can promote T-cell killing by preventing the PD-1/PD-L1 interaction (76). An

inhibitor of ATR can prevent RT-induced PD-L1-upregulation and decrease Tregs in the

implantable tumors (77). Finally, *in vivo* data recently published by Tran *et al.* demonstrated the

benefit of combining low-dose cisplatin with PD-L1 inhibitors in an immunogenic model of

HNSCC (65). Ongoing clinical trials, such as NCT02358031, will further inform rational design

of combinatorial strategies to expand the pool of responders to ICR blockade.

Metabolic reprogramming enhances immune effector function

Aberrant metabolic rewiring is a hallmark of cancer. Emerging evidence suggests that

cancer-associated metabolites have a potent impact on intra-tumoral immune cell function. For

example, high levels of lactate, generated as a byproduct of increased glycolysis in cancer cells,

increases the acidity of the TME. This increased acidity subsequently polarizes macrophages

towards an immunosuppressive M2-like phenotype and impairs the activity of CTLs to emit

cytokines such as IFN-γ (78, 79). In addition, the depletion of amino acids from the TME leads

to nutrient restriction, aiding the dysregulated activity of CTLs (80). Recently, findings in

melanoma indicate that pH neutralization of the TME both increases immune cell infiltration and

improves the efficacy of ICR inhibitors anti-PD1 and anti-CTLA-4 (81).

Increased glycolysis is driven by a number of genetic alterations in HNSCC, including

the PI3K-mTOR pathway. The activation of mTOR activity has been shown to promote the

expression of glucose transporter proteins such as GLUT1 and GLUT2, thus boosting glycolytic

flux (82). Interestingly, in addition to the well-characterized function in inhibiting tumor

proliferation, mTOR inhibitors have been found to exhibit previously unknown effect on

immune activation. Inhibition of mTOR pathway may reduce MDSCs and increase the ratio of

M1-/M2-like macrophages in HNSCC models (83). A combination of mTOR inhibitor with ICR

blockade results in improved survival in an immunogenic HNSCC model (84).

Challenges and Future Directions

We have discussed a number of promising immune-priming approaches to sensitize cold

tumors to ICR blockade. Due to the profound efficacy of inhibition of innate immune sensors on

the anti-tumor immune response, there are likely multiple oncogenic inhibitors of the IFN-I

pathway in addition to the published literature. Additional identification of these critical

checkpoints for host innate immune response not only helps identify cold cancers, but also sheds

light to the design of novel adjuvants to maximally prime tumors for immune response.

While therapeutic vaccines are a highly promising approach to synergize with ICR

blockade, many previous cancer vaccine trials have failed to yield promising results. There are

several important considerations when designing the next-generation cancer vaccines. (i) The choice of vaccine antigens is critical. Tumor-associated antigens are also expressed by normal tissue, albeit at lower levels. These antigens may be less immunogenic than tumor-specific antigens, such as HPV oncoproteins and somatic mutation-elicited neoantigens, due to the naturally developed central tolerance. (ii) Novel and robust vaccine adjuvants are crucial to improve efficacy. The extended characterization of the oncogenic inhibitors of innate immune sensors may reveal previously unknown classes of adjuvants to prime the immune system. (iii) The development of next-generation delivery may overcome many common challenges with an emulsion-based vaccine, such as rapid components degradation and inefficient uptake by the antigen-presenting cells. Thus, developing additional nanoparticle and controlled release systems will likely bring transformative changes to immune-priming strategies.

Novel rational combinations need to be tested in a spectrum of immunocompetent animal models. HNSCC is a molecularly heterogenous disease, and thus, no single model can capture the full spectrum of key genetic alterations. New murine HNSCC cell lines that capture distinct genomic features of human disease would be highly desirable to develop the most robust immunotherapeutic. Fully appreciating the critical importance of implantable models, these cell lines are already transformed and able to surpass host-intrinsic immunosurveillance. Thus, they cannot recapitulate the transformation process as pre-malignant cells adopt key genomic events to suppress innate and adaptive immune response and establish an immune privileged niche. New genetically defined transgenic models can further complement the implantable models to rigorously test novel combinatorial immunotherapies.

Overall, exciting breakthroughs have been made by elucidating the mutation landscape in HNSCC and characterizing the efficacy of ICR blockade among this group of patients (27). Built

upon the advances in HNSCC ICR blockade immunotherapy, novel priming strategies are central

to further improving patient outcomes and quality of life.

CHAPTER 2 – The Innate Immune Sensor NLRC3 Influences Obesity-Mediated IFN-I Suppression and Cancer Immune Escape

Abstract

Worldwide, the incidence rates of head and neck squamous cell carcinoma (HNSCC) continue to rise each year. Alongside this, a societal epidemic of obesity has presented unique challenges to our understanding of how adiposity affects tumor progression. In this study, we analyzed the effects of obesity on modulating HNSCC tumors and anti-tumor immune cell infiltrates. We found that administration of murine HNSCC tumors into obese mice led to increased tumor burden and a non-immunogenic cellular profile when compared to normal weight mice. Tumors from obese mice treated with the STING-activating cyclic dinucleotide (CDN) cGAMP exhibited reduced tumor burden, but with a less efficacious rate than normal weight mice. Subsequent analyses revealed that palmitate, a saturated fatty acid and major component of adipose tissue, suppresses cancer-intrinsic type I interferon (IFN-I) responses, while oleate, an unsaturated fatty acid, does not. To then understand what was driving palmitate-mediated suppression of IFN-I production and signaling, we assessed a panel of innate immune sensors and identified the gene *NLRC3*, which is upregulated in tumors from obese mice and HNSCC cells treated with palmitate. To understand the effects of NLRC3 on cancer-intrinsic immunogenic responses, we used NLRC3-deficient human and mouse cell lines to uncover its role as a negative regulator of the cancer-intrinsic IFN-I response. In vivo, NLRC3-deficient tumors grew much smaller than control and exhibited greater effector-cell genetic correlates and anti-tumor immune cell infiltrates. The efficacy of NLRC3-deficiency in mediating an improved

anti-tumor response is directly dependent on both host adaptive immunity and host IFN-I signaling. Overall, this work highlights a novel regulatory mechanism by which adiposity induces an innate immune sensor to drive cancer-intrinsic immunosuppression.

Introduction

Current investigations towards improving treatments for head and neck squamous cell carcinoma (HNSCC) aim to enhance the efficacy of cytolytic and associated anti-tumor immune subsets in combating tumorigenesis (85, 86). It is presently understood that activation of the double-stranded DNA type I interferon (IFN-I) signaling pathway, via engagement of STING, is critical for mediating immunogenic responses to cancer (87, 88). Specifically, this pathway is known to amplify dendritic cell (DC) maturation and cross-presentation (89), support the production of pro-inflammatory cytokines (90) and enhance effector CD8^{+} T-cell compartments (21, 91). As such, first-line treatments for patients with advanced HNSCC, such as radiation therapy, activate multiple priming pathways that sensitize the immunosuppressed tumor microenvironment to become activated (56). However, these treatment regimens are associated with significant co-morbidities, such as dysphagia and osteoradionecrosis (92, 93). Additionally, in a phase I clinical trial examining the efficacy of a cyclic dinucleotide STING agonist towards the treatment of solid tumors, the disease control rate yield was 20% (94), indicating potential discrepancies in our understanding of other immunoinhibitory mechanisms promoting tumor expansion. Alongside this, the dysregulation of inflammatory pathway activation, a hallmark of obesity, is hypothesized to adversely affect cancer patient outcomes (95). In particular, a prospective study assessing the association between body mass and head and neck cancer (HNC) incidence determined that the risk of developing HNCs directly correlates with increased

abdominal weight (96), suggesting potential interplay between fatty acids and cell-intrinsic machinery which promotes cancer immune escape.

In this chapter, we aim to address mechanisms by which obesity promotes tumor growth and suppresses anti-tumor immune responses. We found that saturated fatty acids, major components of adipose tissue, downregulate IFN-I signaling through the promotion of NLRC3, an innate immune sensing protein responsible for inhibiting cancer-intrinsic IFN-I production. We additionally uncover how NLRC3-mediated tumor inhibitory mechanisms are dependent on both adaptive immunity and host IFN-I signaling.

Materials and Methods

Animals

Eight-week-old C57BL/6 (strain 000664), *Ifnar1*$^{-/-}$ (strain 32045-JAX), and *Rag1*$^{-/-}$ (strain 002216) mice were purchased from The Jackson Laboratory and housed under specific pathogen–free conditions in a temperature- and light-controlled environment. To establish obese mouse model, C57BL/6 mice were fed either a normal diet (5L0D, LabDiet, 24.6% protein, 11.4% fat, 57.3% carbohydrate, 4.09 kcal/g) or a 60% kcal% fat diet (D12492, Research Diets, 20% protein, 60% fat, 20% carbohydrate, 5.21 kcal/g) for twelve weeks before tumor implantation. As sex is not a known prognosticator for HNSCC, both sexes were used. Syngeneic HNSCC models were established by inoculation of 1 million empty vector control, shNLRC3, or wild-type MOC2-E6/E7 cells subcutaneously in the right flank. To test drug efficacy, 3 weekly doses of mock (PBS, 100 μL) or 2'3'-cGAM(PS)$_2$ (Rp/Sp) [50 μg/100 μL; catalog no. tlrl-nacga2srs, InvivoGen] were administered intratumorally. Beginning on day 7 after tumor implantation, tumors were measured using a digital Vernier caliper every 2–3 days,

and tumor volume was calculated according to the formula 1/2 (length $\times$ width^2). All mice were euthanized at the indicated time points. After euthanasia, tumors, TILs, and spleens of the mice were resected for subsequent analysis.

Cell culture

The HNSCC cell line PCI-13 was acquired from the University of Pittsburgh. FaDu was purchased from ATCC (HTB-43). Human cell lines were authenticated and maintained in DMEM (10-013-CV, Corning) supplemented with 10% FBS (Gibco, Life Technologies), 100 U/mL penicillin (Gibco), and 100 mg/mL streptomycin (Gibco). The MOC2-E6/E7 cell line was cultured in 60% IMDM (SH30228.01, HyClone) with 30% F12 nutrient mix (11764-054, Gibco), 5% FBS, 4 µg/mL puromycin, 5 µg/mL insulin, 40 ng/mL hydrocortisone, 5 ng/mL EGF, 100 U/mL penicillin, and 100 mg/mL streptomycin. NLRC3–knockout cells were established by transduction of HNSCC cells (PCI-13, FaDu) with an *NLRC3*-targeting CRISPR/Cas9 lentivirus. Control cells were transduced with empty vector virus. EV-MOC2-E6/E7 and shNlrc3-MOC2-E6/E7 cell lines were transduced with empty vector control (EV) or shNlrc3-expressing lentiviruses (MilliporeSigma) followed by puromycin selection (concentration 120 µg/mL). Puromycin was purchased from InvivoGen (ant-pr-1). qPCR on murine *Nlrc3* was performed to validate the knockdown efficiency.

Bone marrow-derived macrophage isolation and differentiation

Bone marrow-derived macrophages (BMDMs) were isolated from adult female mice to assess type I interferon responses in immune compartments. In brief, mice were anesthetized, after which the two posterior femurs, tibias, and fibulas were resected from mice, sterilized with 70% ethanol, and placed within the biosafety cabinet. Bone ends were subsequently cut, and bone marrow was flushed out using a 27 G ½ in needle (305109, BD) and BMDM differentiation media (RPMI media with L-glutamine containing 20% heat-inactivated FBS, 30% L-929 cell supernatant, and 1% penicillin / streptomycin). Bone marrow in differentiation media was then filtered using 70μm cell strainer and split evenly into 6 tissue treated dishes containing 10ml per plate. On day three post-plating, an additional 10ml differentiation media was added to aid cellular growth. On day six post-plating, media was removed, and dishes were washed once with 1X PBS. Cells were then gently removed from the plate in 5ml 1X PBS using a 25cm cell scraper, spun down, and counted. Cells were plated for experimental use in 6-well tissue culture plates, 0.5 x 10^6 cells / well in 2ml BMDM culture media (RPMI media with L-glutamine containing 20% heat-inactivated FBS and 1% penicillin / streptomycin).

Preparation of fatty acid conjugates

Preparation of saturated and unsaturated fatty acids in vitro was performed as previously described (97, 98). In brief, to prepare the BSA solution, 10% (w/v) fatty acid-free bovine albumin (A9418-5G, MilliporeSigma) was gradually added to ultrapure water at 52°C with gentle agitation until the BSA was fully dissolved. To prepare palmitate, 2.6% (w/v) of palmitic

acid (P0500, Sigma-Aldrich) was added to 0.1M NaOH and heated to 70°C until fully dissolved, yielding a concentration of 100 mM. Likewise, sodium oleate was added to ultrapure water at 55°C to yield a concentration of 100 mM. To conjugate fatty acids to BSA, the 100 mM stocks of palmitate and sodium oleate were added to 10% BSA at a ratio of 1:9 and heated at 55°C for 10 minutes. After conjugation, both the 10% (w/v) BSA solution and fatty acid-BSA solutions were filter sterilized using a 0.45µm PES filter (SLHVR33RS, Fisher Scientific), aliquoted and stored at −20◦C. Before use, solutions were warmed to 37◦C. For final use, 200µM of both fatty acid-BSA conjugates were used.

Plasmids, antibodies, inhibitors, and antibiotics

The pcDNA3.1–human STING–HA and pcDNA3.1–murine STING–HA expression plasmids were provided by Glen N. Barber at the University of Miami (Miami, Florida, USA). The lentiCRISPRv2 plasmids were acquired from Addgene (catalog 98290). The single-guide RNA (sgRNA) targeting NLRC3 sequence was 5′-CCGGGTCTCCATCACTATCG-3′. The pcDNA3.1 empty vector (EV) was previously described (99). Poly(dA:dT) (tlrl-patn-1) and cGAMP (tlrl-nacga23-1) were purchased from InvivoGen. Murine pLKO.1-shIFNAR1-puro, pLKO.1-shNLRC3-puro and pLKO.1–empty vector–puro lentiviral constructs were obtained from MilliporeSigma (Clone ID# TRCN0000067279, Clone ID# TRCN0000249396 and catalog number SHC001V, respectively). Lentiviral packaging vectors were provided by Jenny P.Y. Ting at the University of North Carolina at Chapel Hill (Chapel Hill, North Carolina, USA). All cells were maintained in a humidified incubator at 37°C with 5% CO2. Primary antibodies used for immunoblotting were as follows: β-actin (ab49900, Abcam), phospho-TBK1 (Ser172) (5483S, Cell Signaling Technology), TBK1 (3504S, Cell Signaling Technology), phospho-STING (Ser365) (D84FW, Cell Signaling), STING (13647S, Cell Signaling Technology)

phospho-IRF-3 (Ser396) (4D4G, Cell Signaling), and IRF-3 (D83B9, Cell Signaling). The secondary antibodies used for immunoblotting were goat anti-rabbit IgG–HRP (ab97051, Abcam) and goat anti-mouse IgG–HRP (ab97023, Abcam).

Gene expression qPCR and ELISA

Total RNA was extracted using QIAshredder and the RNeasy Plus Mini Kit (catalog 79654 and 74134, respectively; Qiagen). RNA concentration was measured using a Nanodrop Spectrophotometer (Thermo Fisher Scientific). RNA was reverse-transcribed into cDNA using High-Capacity cDNA Reverse Transcription Kit and RNAse inhibitor (4368814 and N8080119, Applied Biosystems). The primers were synthesized by Integrated DNA Technologies. Gene primers utilized were as follows: *ISG15* F 5′-CTGAGAGGCAGCGAACTCAT, R 5′-AGCATCTTCACCGTCAGGTC; *ISG54* F 5′- ACGGTATGCTTGGAACGATTG, R 5′-AACCCAGAGTGTGGCTGATG; *MX1* F 5′-CAATCAGCCTGCTGACATTG-3′, R 5′-TGTCTCCTGCCTCTGGATG-3′; *NLRC3* F 5′-GTGCCGACCGACTCATCTG', R 5′-GTCCTGCACTCATCCAAGC; *HPRT1* F 5′- ATGCTGAGGATTTGGAAAGG, R 5′-CAGAGGGCTACAATGTGATGG; *Ifnb1* F 5′-CCAGCTCCAAGAAAGGACGA, R 5′-CGCCCTGTAGGTGAGGTTGAT; *pan-Ifna* F 5′-CCTGAGAGAGAAACACAGCC, R 5′-TCTGCTCTGACCACYTCCCAG; *Cxcl9* F 5′-GAGCAGTGTGGAGTTCGAGG, R 5′-TCCGGATCTAGGCAGGTTTG; *Cxcl10* F 5′-AATGAGGGCCATAGGGAAGC, R AGCCATCCACTGGGTAAAGG; *Mx1* F 5′-TCTGAGGAGAGCCAGACGAT', R 5′-ACTCTGGTCCCCAATGACAG; *Tnf* F 5′-ATGAGAAGTTCCCAAATGGC-3′, R 5′-CTCCACTTGGTGGTTTGCTA-3′; *Ifng* F 5′-CGGCACAGTCATTGAAAGCCTA, R 5′-GTTGCTGATGGCCTGATTGTC; *Glut1* F 5'-AGCCCTGCTACAGTGTAT, R 5'-

AGGTCTCGGGTCACATC; *Hk1* F 5'-AGGGCGCATTACTCCAGAG, R 5'-
CCCTGTGGGTGTCTTGTGTG; *Pdk1* F 5'-GGACTTCGGGTCAGTGAATGC, R 5'-
TCCTGAGAAGATTGTCGGGGA; *Hif1a* F 5'-ACCTTCATCGGAAACTCCAAAG, R 5'-
ACTGTTAGGCTCAGGTGAACT; *Nlrp3* F 5'-CACGAGTCCTGGTGACTTTGT, R 5'-
GGGGCTTAGGTCCACACAGAAA; *Nlrp12* F 5'-CCTCTTTGAGCCAGACGAAG, R 5'-
GCCCAGTCCAACATCACTTT; *Nlrp3* F 5'-TGCTCTTCACTGCTATCAAGCCCT, R 5'-
ACAAGCCTTTGCTCCAGACCCTAT; *Nod2* F 5'-CACACATGGCCTTTGGTTTCCAGT, R
5'-AAAGAGCTGCAGTTGAGGGAGGAA; *Nlrx1* F 5'-CCTGGATGAGGTGAACTTGG, R
5'-CTGCTGTCAGTGGGTTGTTG; *Nlrc3* F 5'-CACCGTGGGTCACTTGTATCGCACC, R 5'-
AAACGGTGCGATACAAGTGACCCA-3'; *Hprt1* F 5′-GATTAGCGATGATGAACCAGGTT,
R 5′-CCTCCCATCTCCTTCATCACA. Murine IFN-β in the supernatant was quantified using a
LumiKine™ Xpress mIFN-β 2.0 kit (luex-mifnbv2, Invivogen).

Immunoblotting assays

Whole-cell lysates in each well were harvested on ice in RIPA buffer (50 mM Tris-HCl pH 8.0,
1% Triton X-100, 0.05% SDS, 0.25% deoxycholate, 150 mM NaCl, and 50 mM NaF)
supplemented with a protease inhibitor cocktail (11836170001, Roche) and Halt Phosphatase
Inhibitor Cocktail (78420, Thermo Fisher Scientific). The dilutions for the primary antibodies
were as follows: β-actin, 1:100,000; and 1:1000 for other antibodies. All antibodies were diluted
in 5% skim milk. After lysates were harvested on ice in RIPA buffer, the samples were rotated at
4°C for 30 minutes and centrifuged at 13,000 *g* for 10 minutes at 4°C.

AlamarBlue assay

Empty vector control or shNlrc3 MOC2-E6/E7 cells were seeded at a density of 500 cells per well in 96-well microplates with a flat black bottom (3904, Corning). Every 24 hours from day 1 to day 4, corresponding wells were supplemented with 10% alamarBlue (DAL1025, Invitrogen), and the plate was subsequently incubated at 37°C for 4 hours. The fluorescence intensity (excitation 560, emission 590 nm) of these wells was measured using a Biotek plate reader and Gen5 program (version 2.09), and 5 replicates per group were examined simultaneously.

Flow cytometry.

Immune cells from tumors and spleens were purified. Tumors were excised from mice, weighed, and minced into pieces, followed by tissue dissociation and passage through a 70-μm cell strainer to obtain a single-cell suspension. Spleens were processed by mechanical dissociation, followed by lysis of red blood cells (A10492-01, Gibco). Ficoll-Paque PLUS (17-1440-03, GE Healthcare Life Sciences) was added to the bottom of each tube containing single-cell suspensions in RPMI1640, followed by density-gradient centrifugation to purify immune cells. In general, approximately 1×10^6 tumor-infiltrating lymphocytes were extracted from tumors post-Ficoll purification. Cells were subsequently stained for multi-fluorophore flow cytometric analysis with the following antibodies: anti-CD45 (clone 30-F11, BioLegend), anti-CD3 (clone 17A2, Biolegend), anti-TCR beta (clone H57-597, Biolegend), anti-TCR gamma/delta (clone GL3, Biolegend), anti-CD4 (clone RM4-5, BioLegend), anti-CD8 (clone 53-6.7, BioLegend), anti-IFN gamma (clone XMG1.2, Biolegend), and anti-PD-1 (clone 29F.1A12, Biolegend). Cells were also stained for viability using Zombie Aqua (423101, BioLegend) diluted 1:1000 in PBS at 4°C for 30 minutes. Acquisition and compensation were conducted on a Beckman Coulter CytoFLEX

flow cytometer. Approximately 0.5 x 10^5 tumor-infiltrating lymphocytes were acquired per experiment. FlowJo version 10 software was used for data analysis.

Single-cell immune profiling

Whole tumor lysate was treated with ACK Lysing Buffer (A1049201, ThermoFisher), then processed through an EasySep Dead Cell Removal (Annexin V) Kit (17899, STEMCELL Technologies). The cell suspension was submitted in 1× PBS + 0.04% BSA for 10× Genomics 3'-single-cell processing and RNA-Seq at a depth of at least 30,000 reads per cell. We utilized the following criteria to select high-quality transcriptomes: (i) the qualified cells must have unique feature counts between 200 and 7,500; (ii) the mitochondrial reads must be fewer than 10%; (iii) the transcriptomes must have unique molecular identifiers counts over 500. We integrated 5,154 high-quality transcriptomes for downstream analyses. We utilized the sctransform tool to remove the library size effect and the mutual nearest neighbors algorithm to remove the batch effect for final integration. We selected the top 2,025 genes with the highest cell-to-cell variation as well as features to stabilize the immune population structure.

Statistics

Statistical analysis between 2 independent groups was made using unpaired, 2-tailed Student's *t*-tests. Comparisons between more than 2 groups were made using 2-way ANOVA with Šidák's multiple-comparisons post hoc analysis. Tumor burden between groups was compared using both the generalized estimating equation model, unless otherwise specified. Statistical significance is indicated in all figures according to the following scale: *$p < 0.05$; **$p < 0.01$; ***$p < 0.001$; and ****$p < 0.0001$. All graphs are presented as the mean ± SEM.

All animal procedures were performed in accordance with the protocol approved by the Institutional Animal Care and Use Committee at the University of Michigan (PRO00008517). The clinical protocol to obtain HNSCC specimens was approved by the University of Michigan Institutional Review Board (HUM00042189 and HUM00113038), with informed consent obtained from all patients.

Results

Obesity mediates an increased tumor burden and non-immunogenic cellular microenvironment

To understand the effects of obesity on both tumor burden and the associated microenvironment, we first established an obese mouse model by feeding four- to six-week-old C57BL/6 mice either a normal chow diet (consisting of 11.4% kcal fat content) or a 60% kcal high-fat diet for twelve weeks (100), and monitored mouse weights weekly (Figure 2-1 A). After twelve weeks, we utilized the MOC2-E6/E7 syngeneic HNSCC tumor model, which is classified as a non-immunogenic cell line that responds poorly to checkpoint therapies (16, 101). One million MOC2-E6/E7 cells were implanted subcutaneously into the right flank of mice fed either normal chow or a high fat diet and monitored for tumor burden starting one week following implantation (Figure 2-1 B). We found that mice fed a high fat diet (classified as "obese") displayed a higher tumor burden in relation to mice fed normal chow (Figure 2-1 B). It has been previously reported that increased fatty acid synthesis can portend disrupted glucose metabolic responses (102). To understand the potential metabolic differences in tumor burden between groups, we resected tumors at day 21, homogenized, and performed qPCR analysis on intermediates of the glycolysis pathway. We found the tumors from obese mice displayed higher

levels of *Glut1*, *Hk1*, *Pdk1*, and *Hif1a*, indicating metabolic reprogramming of the cancer cell

(Figure 2-1 C-F).
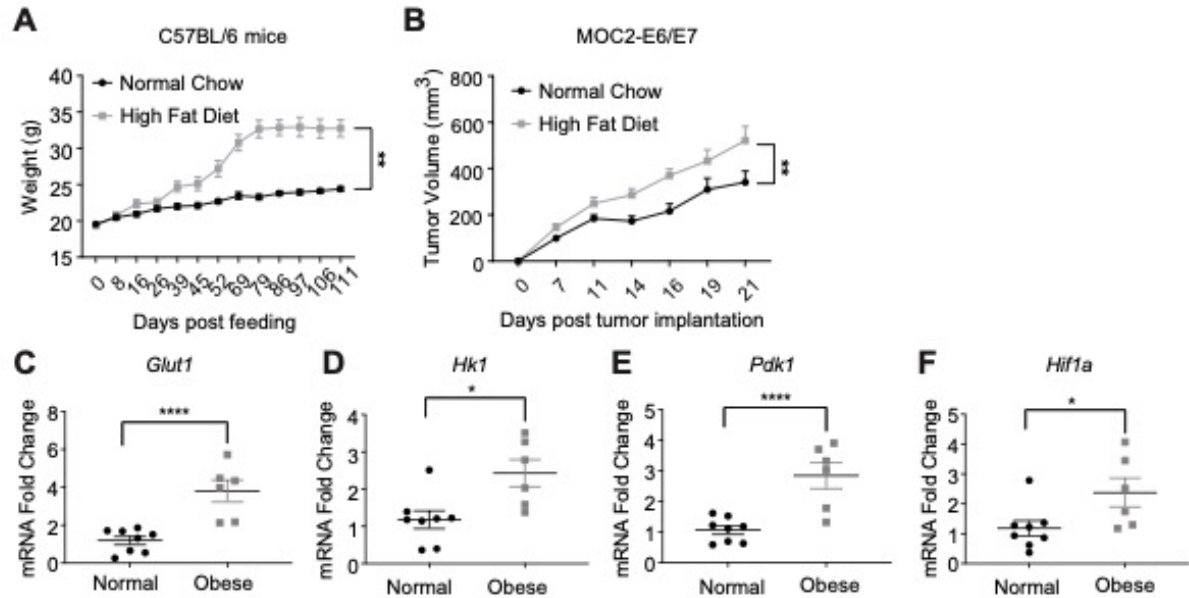
Figure 2-1: Obesity mediates an increased tumor burden & altered metabolic profile

(A) Weight curves from C57BL/6 mice fed either normal chow or 60% kcal high fat diet for 15 weeks. Weight differences between groups were assessed using the generalized estimating equation model (**$P < 0.01$). **(B)** MOC2-E6/E7 cancer cells were implanted into the right flank of mice fed either normal chow or a high fat diet and monitored for tumor burden (n=16 mice per condition). Tumor burden between groups was compared using the generalized estimating equation model. **(C-F)** Transcripts of the glycolysis pathway intermediates *Glut1*, *Hk1*, *Pdk1*, and *Hif1a* were quantified from whole excised tumor via qPCR (n=8 normal weight mice; n=6 obese mice). All comparisons between 2 groups were made using a 2-tailed unpaired *t*-test (*$P < 0.05$ and ****$P < 0.0001$).

To further assess the effects of obesity on the tumor microenvironment, we purified TILs

and spleens using Ficoll-Paque gradient and analyzed via flow cytometry. Our gating strategy

was as follows: Lymphocytes, single cells, Zombie Aqua negative (viability), CD45-positive,

TCRβ-positive, CD4-positive (Figure 2-2 A-F). In our analysis, we found decreased infiltration

of pro-inflammatory $TCRβ^+CD4^+IFNγ^+$ (Figure 2-2 G-H) cells as well as decreased

TCRβ⁺CD4⁺ PD-1⁺ T-cells (Figure 2-2 I-J), a population associated with activated IFN-I

signaling (103).
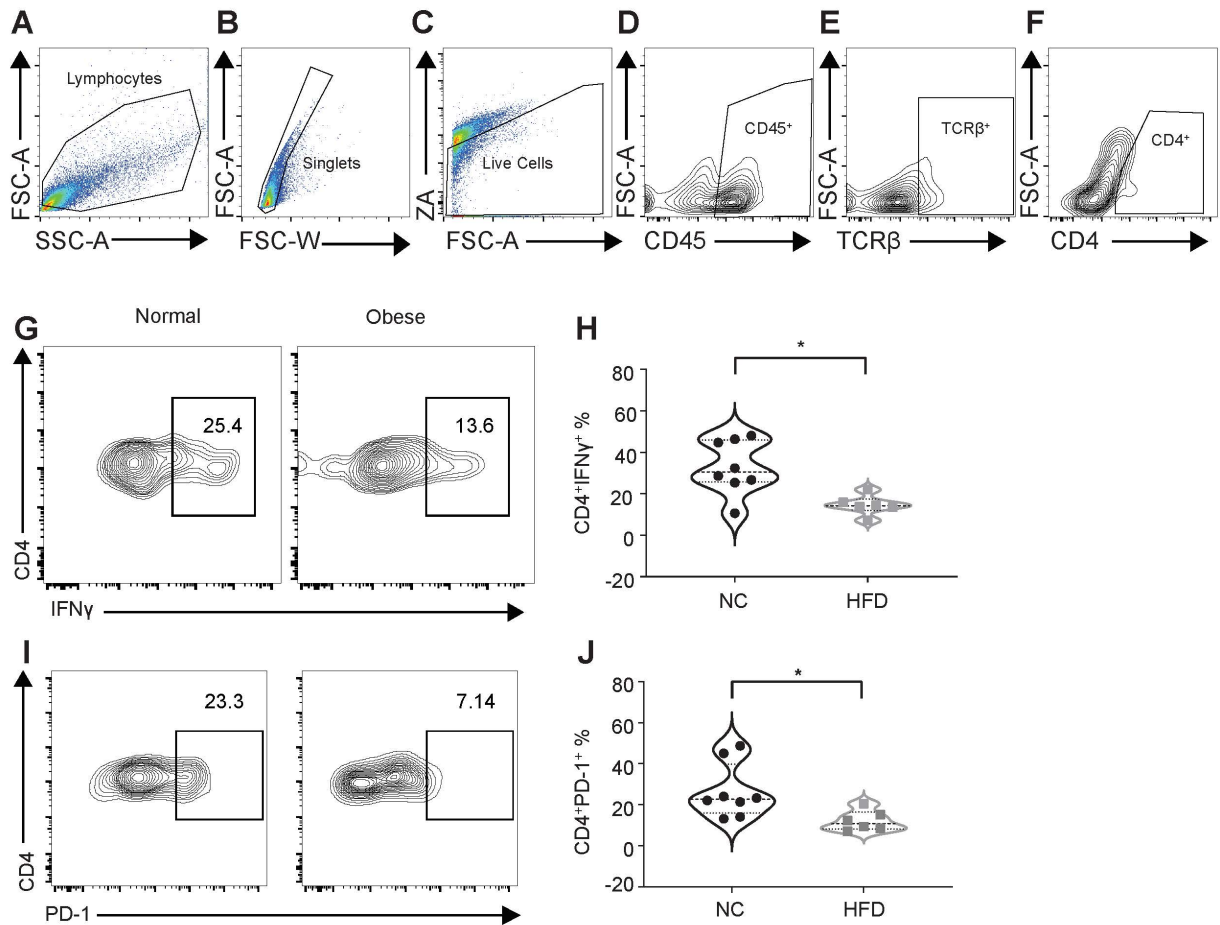
Figure 2-2: Obesity mediates an immunosuppressed tumor microenvironment

(A-F) Gating strategy was as follows: Lymphocytes, single cells, Zombie Aqua negative (viability), CD45-positive, TCRβ-positive, CD4-positive. **(G-J)** Frequency of **(G-H)** CD4⁺ IFNγ⁺ and **(I-J)** CD4⁺ PD-1⁺ T-cells assessed from ficoll-purified tumor infiltrating lymphocytes from normal weight and obese mice via flow cytometry (n=8 normal weight mice; n=6 obese mice).. All comparisons between 2 groups were made using a 2-tailed unpaired *t*-test (*$P <$ 0.05).

Furthermore, to characterize the complete cancer-associated landscape between groups, we performed single-cell RNA sequencing (scRNA-seq) on Ficoll-Paque isolated CD45^{+} immune cells as well as epithelial cell adhesion molecule (EpCAM)-positive cells, to render genetic exploration of immune and highly proliferative tumor cells. After filtering, we integrated high-quality transcriptomes and identified 20 distinct cell clusters (Figure 2-3 A-D). Of note, we found a reduction in signatures from a Sting1+CD40+ M1-like macrophage population (cluster 6) and increased frequency of M2-like macrophages (cluster 3) in tumors from obese mice. Also uncovered were reductions in Ki67-positive and –negative Tbet[+] Tcells (clusters 11 and 19) and an expansion of B cells (cluster 16) in the obese tumor set (Figure 2-3 E-I).
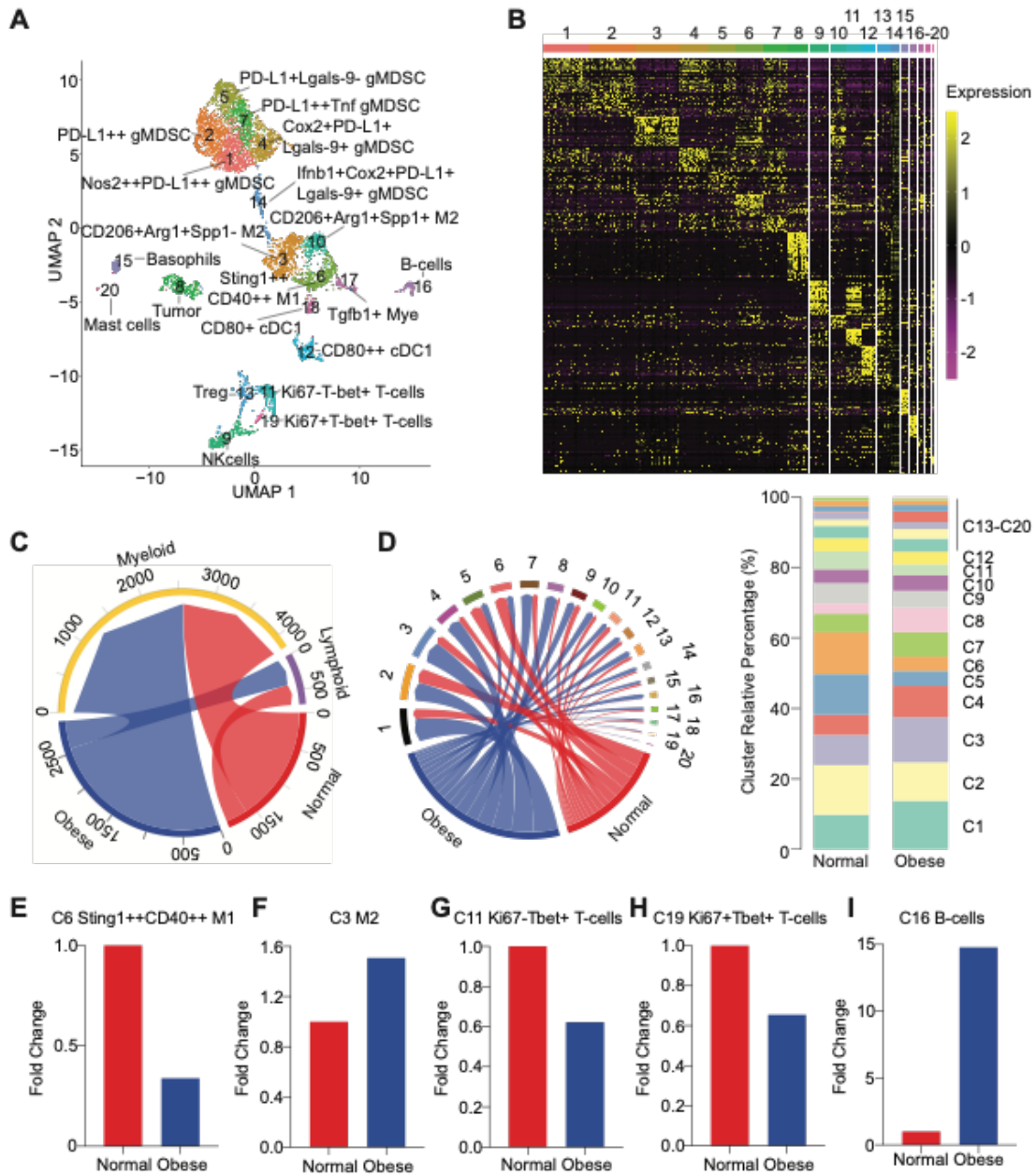
Figure 2-3: scRNA-seq analysis reveals an immunosuppressed tumor microenvironment from obese hosts.

(A) Tumors from normal weight and obese mice were harvested at day 21 after implantation. TILs were purified and pooled (n=5 mice/condition) and subjected to single-cell RNA-sequencing expression patterns of immune and tumor cell subsets. After filtering, 5,154 high-quality transcriptomes were integrated for UMAP analysis. Divergent myeloid, lymphoid, and epithelial lineages were defined by the top 2,025 genes with the highest cell-to-cell variation. **(B)** Cluster expression graphic displayed from groups in (A). **(C)** Correlations between myeloid

and lymphoid subsets and the two experimental groups. **(D)** Correlations between distinct clusters and expression between the two experimental groups. **(E-I)** Analysis of differential cluster expression between two experimental groups. Clusters with differential expression patterns were 6 (Sting1+CD40+ M1-like macrophage population), 3 (M2-like macrophages), 11 and 19 (Ki67-positive and –negative Tbet$^+$ T-cells), and 16 (an expansion of B cells).

Recent evidence has suggested that obese cancer patients may experience worse clinical outcomes in response to cyclic dinucleotide (CDN) therapies which activate STING (104). To test this theory in vivo, we implanted one-million MOC2/E6-E7 tumors into mice fed normal chow or high fat diet (Supp. Figure 2-1 A). On day 7, we treated mice with either Mock PBS or 50 μg of 2'3'-cGAM(PS)$_2$, a potent STING agonist, intratumorally, and continued once per week for three weeks. The administered 2'3'-cGAMP contains a phosphorothioated modification which is more stable in vivo than conventional 2'3'-cGAMP (105). At endpoint, we found that tumor burden in obese mice was reduced after CDN therapy, but at a less efficacious rate than normal weight mice, indicating the influence of fatty acids in suppressing host IFN-I-associated anti-tumor immune responses.
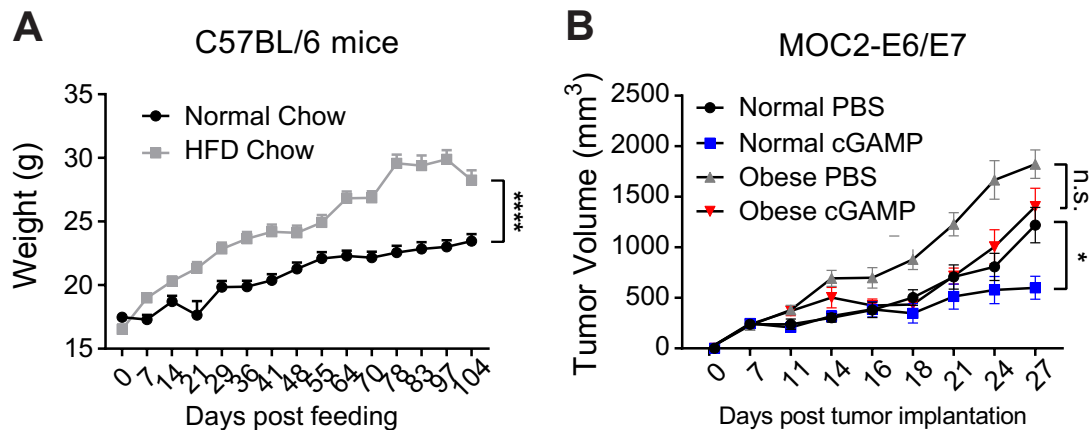
Supplemental Figure 2-1: Efficacy of cyclic dinucleotide therapy is reduced in tumor-bearing obese mice

(A) Weight curves from C57BL/6 mice fed either normal chow or 60% kcal high fat diet for 14 weeks. Weight differences between groups were assessed using the generalized estimating equation model (****$P<0.0001$). **(B)** Mock (PBS, 100 µL) or 2'3'-cGAM(PS)$_2$ (Rp/Sp) [50 µg/100 µL] was administered intratumorally once per week for three weeks following implantation of MOC2-E6/E7 tumor. Comparisons were made at endpoint using an unpaired *t*-test, non-parametric comparison (*$P < 0.05$)

Palmitic acid, but not oleic acid, suppresses STING-mediated IFN-I production and signaling in both cancer & immune cells

To further characterize the role of adiposity in mediating suppression of STING-related IFN-I responses within both cancer and immune cell compartments, we utilized the functional activity of palmitic acid, a saturated fatty acid and a key component of adipose tissue, which comprises significant proportions of depot fat as well as free fatty acids in blood (106, 107). Palmitate, an ester of palmitic acid, is used in vitro to model the effects of obesity (98, 108, 109). To examine both cancer and immune cell responses to saturated fatty acids, we pretreated both MOC2-E6/E7 WT cells and bone marrow-derived macrophages with either mock (10% BSA in ultrapure water) or 200µM palmitate-BSA, as previously described (97, 98) for 24 hours. We then activated the STING pathway via transfection of either 1µg/mL STING expression plasmid in MOC2-E6/E7 WT cells or 1µg/mL 2'3'-cGAMP in bone marrow-derived macrophages for 16 hours. STING plasmid is transfected into MOC2-E6/E7 due to model cell-intrinsic HPV16-mediated suppression of endogenous STING (101). We subsequently collected RNA and performed qPCR analysis on IFN-I related gene signatures *Ifnb1*, *Cxcl10*, and *Mx1*. We found that within both MOC2 cells (Figure 2-4 A-C) and the immune cell compartment (Figure 2-4 D-F), IFN-I related gene expression was suppressed after treatment with palmitate. We also collected supernatant from the transfected cells and found suppression of IFNβ production occurred in both cancer (Figure 2-4 G) and immune (Figure 2-4 H) cells. Lastly, we

34

characterized the expression of intermediates of the STING pathway via Western blot, noting

that palmitate treatment reduces expression of p-TBK1, p-IRF3, and p-STING in both MOC2

and BMDMs (Figure 2-4 I-J) indicating that saturated fatty acids are a mechanism for

suppressing STING-mediated IFN-I production.
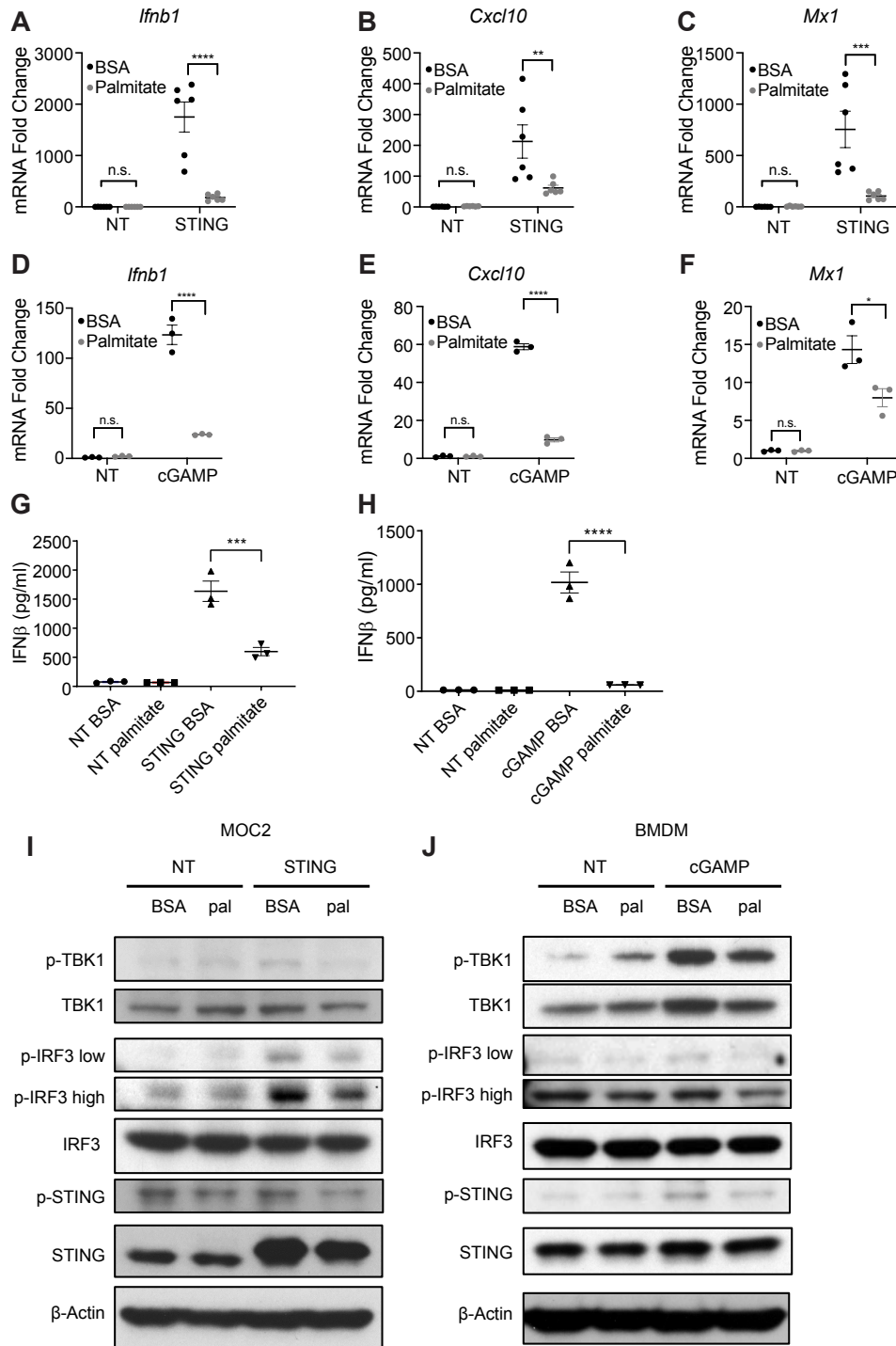
Figure 2-4: Palmitate suppresses STING-mediated IFN-I production and signaling in both cancer & immune cells

(A-C) MOC2-E6/E7 WT cells were pretreated with 200μM palmitate for 24 hours then transfected with 1μg/mL STING expression plasmid for 16 hours. Expression of murine *Ifnb1*,

Cxcl10, and *Mx1* was assessed via qPCR. **(D-F)** BMDMs were pretreated with 200μM palmitate for 24 hours then transfected with 1μg/mL 2'3'-cGAMP for 16 hours. Expression of murine *Ifnb1*, *Cxcl10*, and *Mx1* was assessed via qPCR. **(G)** MOC2-E6/E7 WT cells were pretreated with 200μM palmitate for 24 hours then transfected with 1μg/mL STING expression plasmid for 24 hours. Supernatant was subsequently collected and assessed for presence of IFNβ via ELISA. **(H)** BMDMs were pretreated with 200μM palmitate for 24 hours then transfected with 1μg/mL 2'3'-cGAMP for 24 hours. Supernatant was subsequently collected and assessed for presence of IFNβ via ELISA. All comparisons between 2 groups were made using a 2-tailed unpaired *t*-test (*$P < 0.05$; **$P < 0.01$; ***$P < 0.001$; ****$P < 0.0001$). **(I)** MOC2-E6/E7 WT and **(J)** BMDMs were pretreated with 200μM palmitate for 24 hours then transfected with **(I)** 1μg/mL STING or **(J)** 1μg/mL 2'3'-cGAMP for 16 hours. Cell lysate was collected and blotted for the presence of STING pathway-related proteins p-TBK1, TBK1, p-IFR3, IRF3, p-STING, STING as well as β-actin control.

We also assessed the role of unsaturated fatty acids in modulating STING-mediated IFN-I responses. Oleic acid is a dietary fatty acid that is known to counteract the effects of palmitic acid (110). As with palmitate, we examined cancer and immune cell IFN-I responses by first pretreating both MOC2-E6/E7 WT cells and BMDMs with either mock (10% BSA in ultrapure water) or 200μM oleate-BSA for 24 hours, followed by transfection of either 1μg/mL STING expression plasmid in MOC2-E6/E7 WT cells or 1μg/mL 2'3'-cGAMP in bone marrow-derived macrophages. After qPCR analysis, we found that oleate did not suppress the expression IFN-I related gene signatures *Ifnb1*, *Cxcl10*, and *Mx1* (Supp. Figure 2-2) indicating that unsaturated fatty acids do not modulate the IFN-I response in cancer cells.
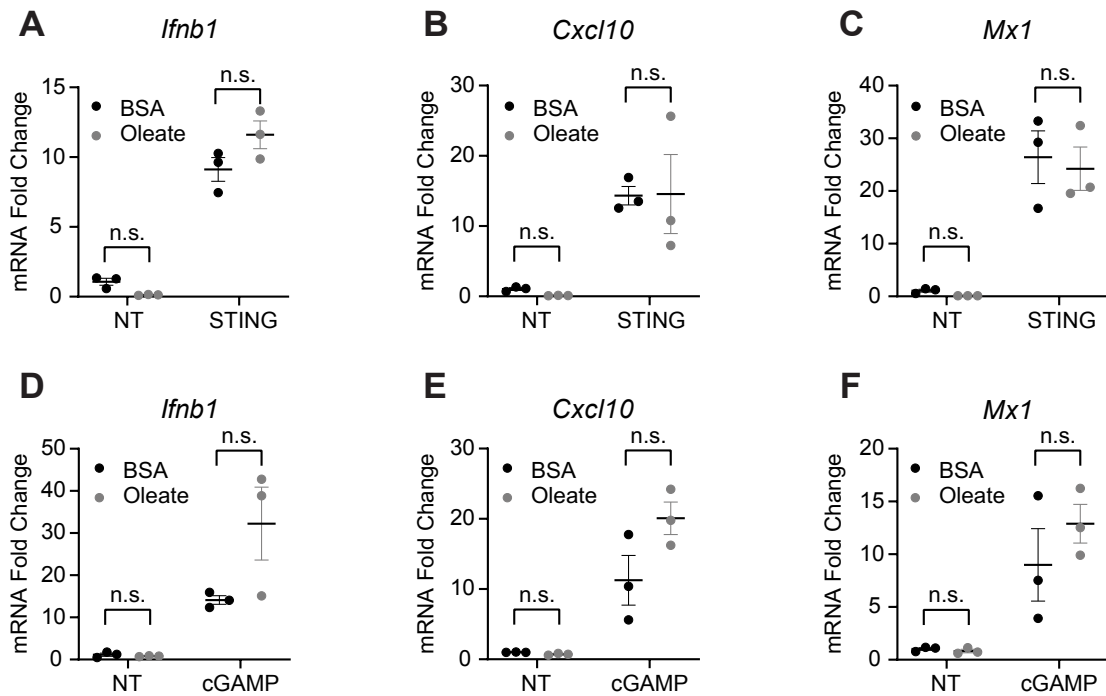
Supplemental Figure 2-2: Oleate does not suppress STING-mediated IFN-I production and signaling in either cancer or immune cells

(A-C) MOC2-E6/E7 WT were pretreated with 200μM palmitate for 24 hours then transfected with 1μg/mL STING expression plasmid for 16 hours. Expression of murine *Ifnb1*, *Cxcl10*, and *Mx1* was assessed via qPCR. **(D-F)** BMDMs were pretreated with 200μM palmitate for 24 hours then transfected with 1μg/mL 2'3'-cGAMP for 16 hours. Expression of murine *Ifnb1*, *Cxcl10*, and *Mx1* was assessed via qPCR. Comparisons between 2 groups were made using a 2-tailed unpaired *t*-test.

NLRC3 negatively regulates the dsDNA-dependent IFN-I response in human and mouse cancer

cells

Innate immune sensing pathways are critically important for regulating STING-mediated IFN-I

responses in HSNCC (101, 111). To further expand our understanding of potential cooperation

between innate immune sensors and adiposity, we extracted RNA from homogenized tumors

from normal weight and obese mice and assessed the presence of various innate immune sensors

which are responsible for mediating pro-inflammatory responses. Using qPCR, we identified

Nlrc3 as a gene signature upregulated in obese tumors (Figure 2-5 A-E). NLRC3, a nucleotide-binding, leucine-rich repeat protein, has been previously characterized as a negative regulator of IFN-I signaling within macrophages (112), by blocking the interaction of STING with its binding partner TANK-binding kinase 1 (TBK1), preventing the phosphorylation of IRF3, a key transcription factor for IFN-I production. To further characterize its function in the context of HNSCC, we utilized an *NLRC3*-targeting CRISPR/Cas9 lentivirus to knockout *NLRC3* expression within the Human HNSCC cell lines PCI-13 (Figure 2-5 F) and FaDu (Figure 2-5 L). EV- and *NLRC3*-knockout PCI-13 and FaDu cells were then transfected with either 1µg/mL STING expression plasmid or 1µg/mL poly(dA:dT) for 16 hours, and collected for qPCR analysis. Through this analysis, we found that NLRC3 loss in both PCI-13 (Figure 2-5 G-K) and FaDu (Figure 2-5 M-Q) cells led to increased expression of the STING-mediated IFN-I gene signatures *ISG15*, *ISG54*, and *MX1*, defining NLRC3 as a negative regulator of the cancer-intrinsic IFN-I response in human HNSCC cells.
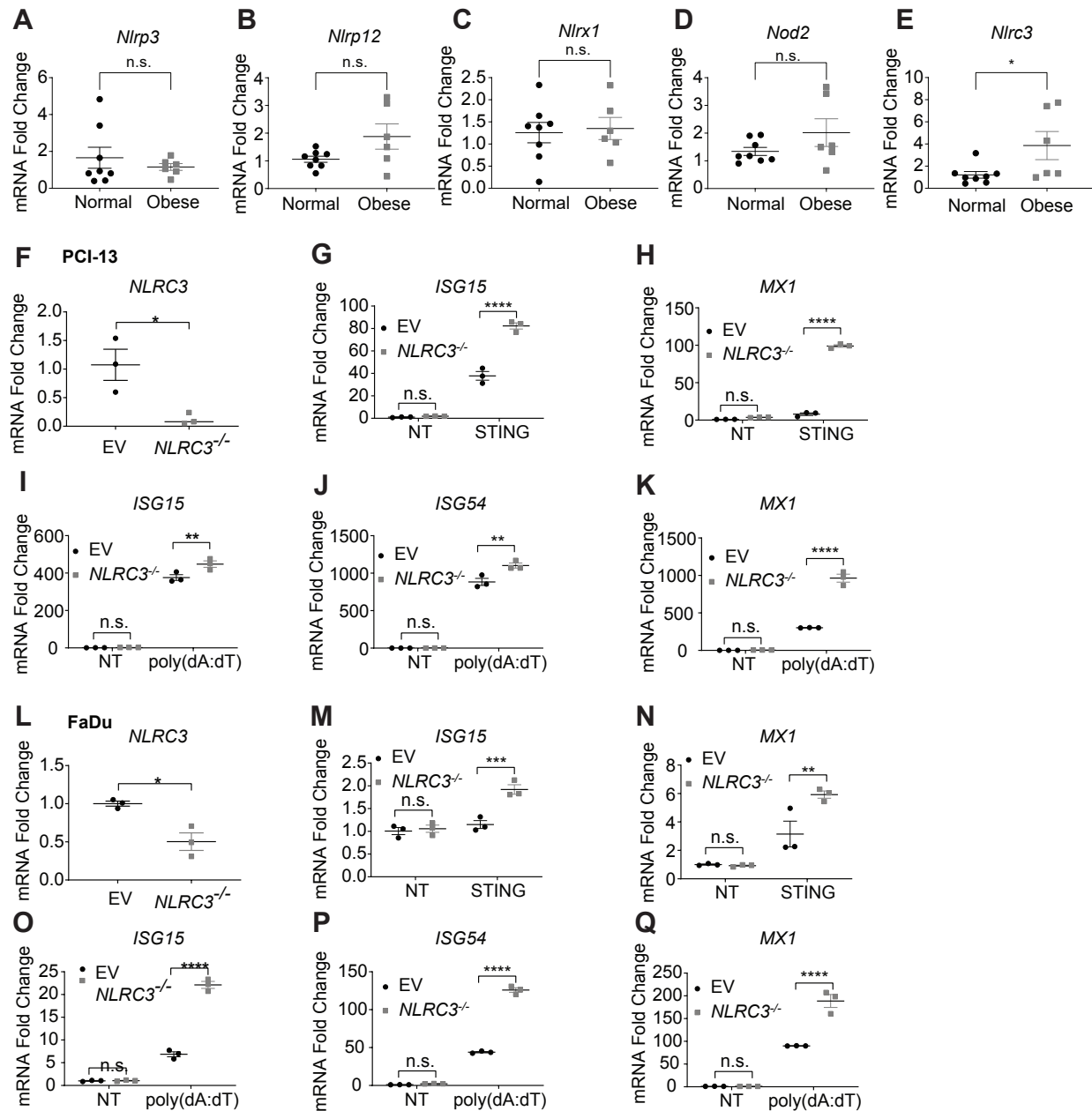
Figure 2-5: NLRC3 negatively regulates the dsDNA-dependent IFN-I response in human cancer cells

(A-E) Transcripts of the innate immune sensing regulators *Nlrp3*, *Nlrp12*, *Nlrx1*, *Nod2*, and *Nlrc3* were quantified from whole excised tumor via qPCR (n=8 normal weight mice; n=6 obese mice). **(F)** Human HNSCC cell line PCI-13 was transduced with an *NLRC3*-targeting CRISPR/Cas9 lentivirus. Knockout efficiency was quantified via qPCR. **(G-K)** EV- and *NLRC3*-knockout PCI-13 cells were transfected with either **(G-H)** 1µg/mL STING expression plasmid or **(I-K)** 1µg/mL poly(dA:dT) for 16 hours. Expression of human *ISG15*, *ISG54*, and *MX1* was

assessed via qPCR. **(L)** Human HNSCC cell line PCI-13 was transduced with an *NLRC3*-targeting CRISPR/Cas9 lentivirus. Knockout efficiency was quantified via qPCR. **(M-Q)** EV- and *NLRC3*-knockout FaDu cells were transfected with either **(M-N)** 1μg/mL STING expression plasmid or **(O-Q)** 1μg/mL poly(dA:dT) for 16 hours. Expression of human *ISG15*, *ISG54*, and *MX1* was assessed via qPCR. All comparisons between 2 groups were made using a 2-tailed unpaired *t*-test (*$P < 0.05$; **$P < 0.01$; ***$P < 0.001$; ****$P < 0.0001$).

Alongside these findings, we also examined the effects of NLRC3 loss in the mouse HNSCC cell line MOC2-E6/E7. These cells were transduced with an *Nlrc3*-targeting shRNA lentivirus and assessed via qPCR (Figure 2-6 A). An alamarBlue assay determined there were no differences in growth rates between cell lines (Figure 2-6 B). To further characterize the relationship between innate immune sensors and saturated fatty acids, MOC2-E6/E7 WT cells were treated with either mock BSA or 200μM palmitate-BSA and collected for RNA analysis. We found the *Nlrc3* expression was increased in palmitate-treated cells (Figure 2-6 C). To delineate the effects of *Nlrc3* on the murine cancer-intrinsic IFN-I response, EV- and shNlrc3-MOC2-E6/E7 cells were transfected with either 1μg/mL STING expression plasmid or 1μg/mL poly(dA:dT) for 16 hours. Subsequent qPCR analysis revealed increased expression levels of mouse *Ifnb1*, pan-*Ifnα*, *Cxcl9*, *Cxcl10*, and *Mx1* from both STING-transfected samples (Figure 2-6 D-H) as well as samples treated with poly(dA:dT) (Figure 2-6 I-M). We also characterized STING pathway intermediates via Western blot, finding that NLRC3 loss mediates increased p-TBK1 and p-IRF3, confirming the role of NLRC3 as a negative regulator of cancer-intrinsic IFN-I in murine cancer cells (Figure 2-6 N-O).
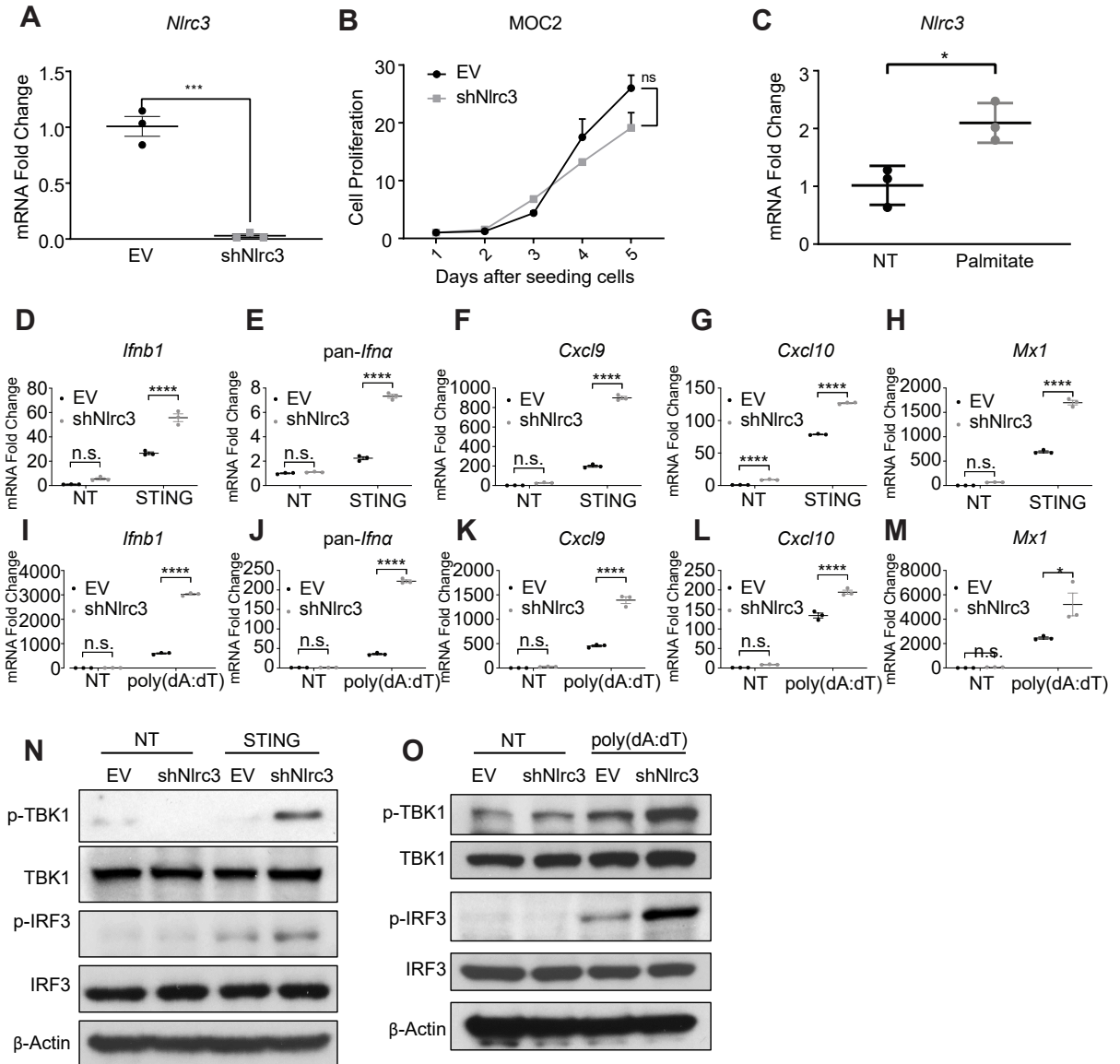
Figure 2-6: NLRC3 negatively regulates the dsDNA-dependent IFN-I response in murine cancer cells

(A) Mouse HNSCC MOC2-E6/E7 was transduced with an *Nlrc3*-targeting shRNA lentivirus. Knockdown efficiency was quantified via qPCR. **(B)** The proliferation of EV control and shNlrc3 MOC2-E6/E7 cells was assessed via an alamarBlue assay. Each group included 5 replicate wells. **(C)** *Nlrc3* expression was measured in MOC2-E6/E7 WT cells pretreated with 200µM palmitate for 24 hours via qPCR**. (D-M)** EV- and shNlrc3-MOC2-E6/E7 cells were transfected with either **(D-H)** 1µg/mL Sting expression plasmid or **(I-M)** 1µg/mL poly(dA:dT) for 16 hours. Expression of murine *Ifnb1*, pan-*Ifnα*, *Cxcl9*, *Cxcl10*, and *Mx1* was assessed via qPCR. All comparisons between 2 groups were made using a 2-tailed unpaired *t*-test (*$P < 0.05$; ***$P < 0.001$; ****$P < 0.0001$). **(N-O)** EV- and shNlrc3-MOC2-E6/E7 cells were transfected

with either **(N)** 1µg/mL Sting expression plasmid or **(O)** 1µg/mL poly(dA:dT) for 16 hours. Cell lysate was collected and blotted for the presence of STING pathway-related proteins p-TBK1, TBK1, p-IFR3, IRF3 as well as β-actin control.

Loss of cancer-intrinsic NLRC3 improves anti-tumor immune response

To understand the context of cancer-intrinsic NLRC3-mediated IFN-I suppression in vivo, we implanted one million EV- or shNlrc3-MOC2-E6/E7 cancer cells into the right flank of C57BL/6 mice and monitored tumor burden. We found that NLRC3 loss mediated a smaller tumor burden (Figure 2-7 A), as well as decreased tumor weights at endpoint (Figure 2-7 B). **(B)** Whole tumor was homogenized and assessed for the presence of T_H1/T_c1-related gene signatures. The signatures *Cxcl9*, *Cxcl10*, *Tnf*, and *Ifng* were found to be induced in shNlrc3-MOC2-E6/E7 cells, indicating increased infiltration of anti-tumor immune cell populations (Figure 2-7 C-F).
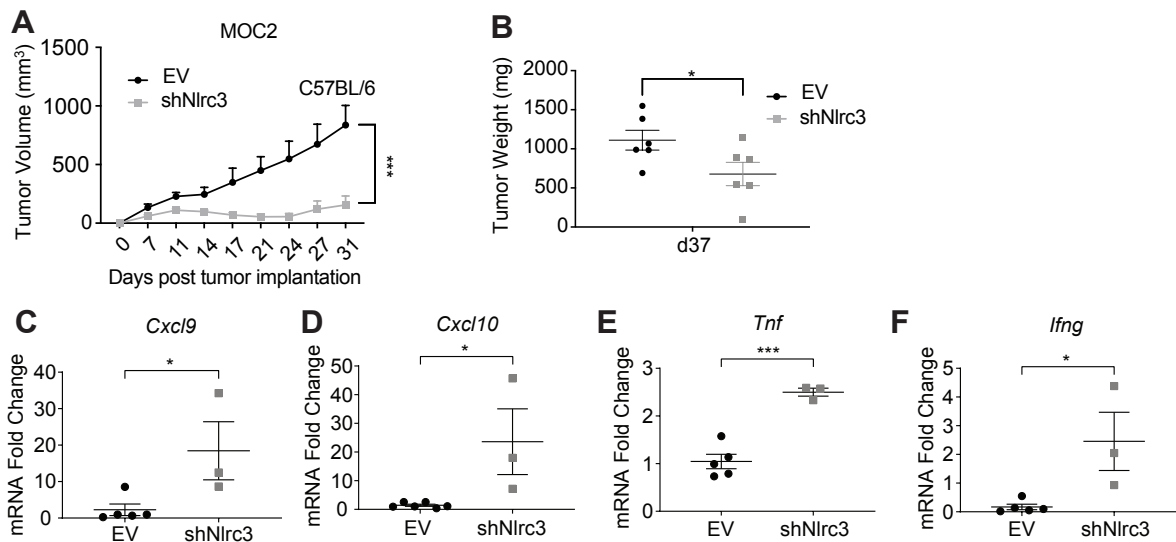
Figure 2-7: Loss of cancer-intrinsic NLRC3 promotes an anti-tumor immune profile

(A) EV- or shNlrc3-MOC2-E6/E7 cancer cells were implanted into the right flank of C57BL/6 mice and monitored for tumor burden (n=6 mice with EV-MOC2-E6/E7 tumors; n=5 mice with shNlrc3-MOC2-E6/E7 tumors). Tumor burden between groups was compared using the generalized estimating equation model (*$P < 0.05$). **(B)** Following mouse sacrifice, tumors were

resected and weighed before processing. **(C-F)** Transcripts of T_H1/T_c1-related gene signatures *Cxcl9*, *Cxcl10*, *Tnf*, and *Ifng* were quantified from whole excised tumor via qPCR (n=5 mice with EV-MOC2-E6/E7 tumors; n=3 mice with shNlrc3-MOC2-E6/E7 tumors). All comparisons between 2 groups were made using a 2-tailed unpaired *t* test All comparisons between 2 groups were made using a 2-tailed unpaired *t*-test (*$P < 0.05$; ***$P < 0.001$).

We also performed flow cytometry on Ficoll-Paque isolated TILs. Our gating strategy was as follows: Lymphocytes, single cells, Zombie Aqua negative (viability), CD45-positive (Figure 2-8 A-D). We found increased frequencies of TCRβ⁺ T-cells (Figure 2-8 E-F), TCRγδ⁺ T-cells (Figure 2-8 G-H), and CD8⁺ PD-1^{low} T-cells (Figure 2-8 I-J) from shNlrc3-MOC2-E6/E7 tumors.
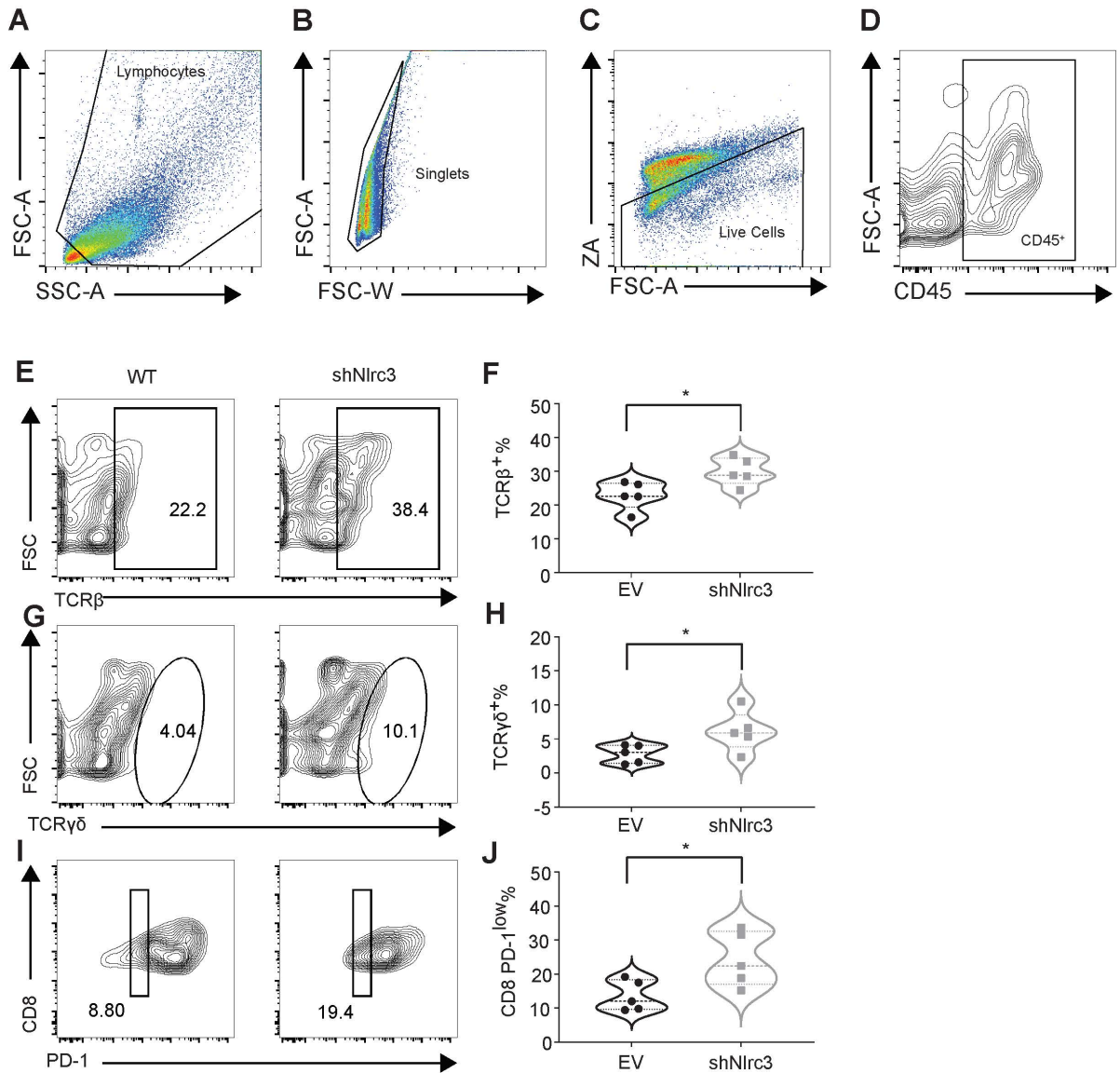
Figure 2-8: Loss of cancer-intrinsic NLRC3 improves the anti-tumor immune response

(A-F) Gating strategy was as follows: Lymphocytes, single cells, Zombie Aqua negative (viability), CD45-positive. **(E-F)** Frequency of TCRβ⁺ T-cells assessed from ficoll-purified tumor-infiltrating lymphocytes from normal weight and obese mice via flow cytometry (n=5 mice per condition). Gating strategy was as follows: Lymphocytes, single cells, Zombie Aqua negative (viability), CD45-positive. **(G-H)** Frequency of TCRγδ⁺ T-cells assessed from ficoll-purified tumor-infiltrating lymphocytes from normal weight and obese mice via flow cytometry (n=5 mice per condition). Gating strategy was as follows: Lymphocytes, single cells, Zombie Aqua negative (viability), CD45-positive. **(I-J)** Frequency of CD8⁺ PD-1^{low} T-cells assessed from ficoll-purified tumor-infiltrating lymphocytes from normal weight and obese mice via flow

cytometry (n=5 mice per condition). All comparisons between 2 groups were made using a 2-tailed unpaired *t*-test (*$P < 0.05$).

To better understand the specific context by which NLRC3 loss mediates improved tumor immunogenicity, we implanted EV- or shNlrc3-MOC2-E6/E7 cancer cells into the right flank of *Rag1^{-/-}* mice, which lack T and B cells (113)as well as *Ifnar1^{-/-}* mice that lack host downstream signaling. In both models, cancer-intrinsic NLRC3-mediated immune suppression was dependent on both adaptive immunity (Supp. Figure 2-3 A) and host IFN-I signaling pathways (Supp. Figure 2-3 B).
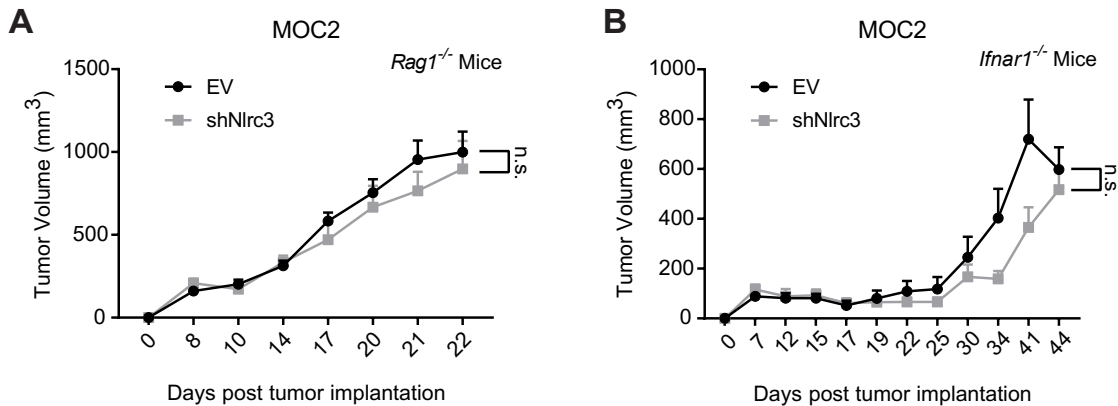
Supplemental Figure 2-3: Anti-tumor immunity mediated by loss of cancer-intrinsic NLRC3 is dependent on both host adaptive immunity and downstream IFN-I signaling.

(A) EV- or shNlrc3-MOC2-E6/E7 cancer cells were implanted into the right flank of mice *Rag1^{-/-}* mice and monitored for tumor burden (n=5 mice per condition). Tumor burden between groups was compared using the generalized estimating equation model. **(B)** EV- or shNlrc3-MOC2-E6/E7 cancer cells were implanted into the right flank of mice *Ifnar1^{-/-}* mice and monitored for tumor burden (n=7 mice per condition). Comparisons between 2 groups were made at endpoint using an unpaired *t*-test, non-parametric comparison.

Discussion

The role of STING-mediated IFN-I production and signaling in producing potent anti-tumor immune responses has been a promising avenue for treatment strategies aiming to enhance the immunogenicity of cold tumors. Traditionally, this pathway is induced by the engagement of cytosolic double-stranded DNA to cyclic GMP-AMP synthase (cGAS), catalyzing the formation of the second messenger molecule cyclic GMP-AMP (cGAMP). Subsequently, cGAMP acts on STING, to activate TBK1, resulting in phosphorylation of IRF3 and the transcription of IFN-I proteins. Unfortunately, in the clinic, CDNs alone have currently proven to enact limited efficacy towards regression of solid tumors (94). However, therapeutic modalities combining CDNs with other immune and metabolic targets could provide the necessary regulatory mechanisms needed to boost tumor immunogenicity (94).

In this chapter, we sought to delineate the interplay between saturated fatty acids associated with obesity and the tumor microenvironment. Obesity has previously been negatively correlated with head and neck patient outcomes, yet the linkages between tumor immune regulation and adiposity were unclear. We first sought to define how obesity affected tumor burden, by implanting MOC2-E6/E7 tumors into mice fed a high fat diet, a standard model for replicating the effects of obesity, as opposed to those fed a normal chow diet. We found that obese mice bore larger tumors, and through tumor microenvironment analysis via flow cytometry and single-cell RNA sequencing, we uncovered an immunosuppressed tumor landscape, including higher M2-like/M1-like ratios and well as reduced T-cell infiltration. From this, it was important to understand the mechanism by which this phenotype was enacted. By using palmitate, an abundant saturated fatty acid in adipose tissue, we modeled the effects of obesity on both cancer cell signaling pathways as well myeloid compartments in vitro.

47

Pretreatment of palmitate on both murine cancer cells and BMDMs led to suppressed IFN-I production, as demonstrated by qPCR and ELISA. This suggested that suppressed IFN-I signaling is a mode employed by saturated fatty acids to inhibit immune responses in cold tumors. To understand why this suppression occurs, we investigated a panel of innate immune sensors largely associated with pro-inflammatory pathways, including previously defined IFN-I regulators, to determine if fatty acids modulated the expression of such proteins. We found that *NLRC3* was induced both within tumors from obese mice as well as MOC2-E6/E7 cells treated with palmitate. To further analyze cancer-intrinsic NLRC3 on the IFN-I response, we deleted *NLRC3* expression via CRISPR/Cas9 in the human HPV-negative HNSCC cell lines PCI-13 and FaDu and knocked down *NLRC3* in MOC2-E6/E7 cells. Following activation of the STING pathway within these tumors, we found that lack of *NLRC3* mediated enhanced IFN-I production and signaling, confirming its importance as a negative regulator of IFN-I responses in cancer cells. Additional characterization revealed that loss of *NLRC3* in vivo greatly reduced tumor burden and increased frequencies of immunogenic infiltrates, indicating that NLRC3 could provide a promising target towards enhancing the efficacies of CDNs and other checkpoint inhibitors currently approved for treatments.

From this work, a novel interplay between saturated fatty acids and the activity of innate immune sensors has been uncovered, with interesting potential indications. It has been recently reported that NLRC3-mediated sequestration of STING is reversed by DNA binding to the leucine-rich repeat domain of NLRC3, which increases its ATPase activity and subsequently releases the STING/TBK1 complex (114). From this finding, the question emerges of how saturated fatty acids may directly or indirectly interact with NLRC3 machinery, and whether NLRC3 itself is a potentially targetable protein to enhance anti-tumor immunity. Future work

assessing the interplay between free fatty acids and innate immune sensors will hopefully further contribute to the improvement of STING-associated therapeutics administered for patients with non-immunogenic tumors.

CHAPTER 3 – Cancer-Specific IFNAR1 Downstream Signaling Is Associated With Worse Prognosis and Cancer Immune Escape

Abstract

Type-I interferon (IFN-I) signaling is critical to maintain cancer immunogenicity and is a key contributor to the anti-tumor response. However, recent studies have suggested that IFN-I signaling may also contribute to more aggressive tumor phenotypes, raising the possibility that IFN-I downstream signaling activation in cancer cells and myeloid populations may exert dichotomous roles. Here we examined the prognostic potential of cancer cell-specific IFN-I receptor downstream signaling in head and neck squamous cell carcinoma (HNSCC) using an expanded cohort of 195 patients by measuring protein levels of MX1, a sensitive surrogate marker of IFN-I induction. Kaplan-Meier analysis revealed that MX1-high tumors exhibited significantly worse overall survival, a finding which was confirmed in univariate and multivariate Cox regression models. To understand the mechanism driving this phenomenon, we administered mice with control or *Ifnar1*-deficient HNSCC cells. Notably, mice bearing *Ifnar1*-deficient tumors exhibited reduced overall tumor burden, reduced proportions of cancer stem cells and increased CD4$^+$ and CD8$^+$ T-cell infiltration. In particular, we observed immunosuppressive CD4+ PD1^{high} and CD8+ Tim3+ tumor infiltrating lymphocytes (TILs) were significantly reduced in shIfnar1 tumors, while CD8$^+$ PD-1^{low} TILs important for antitumor immunity were significantly increased. Finally, we also completed single cell RNA-sequencing (scRNA-Seq) with subsequent immune cell deconvolution to ascertain the extent to which the overall immune landscape is altered in *Ifnar1*-deficient tumors, which confirmed *Ifnar1*-deficient tumors exhibit

expansions in TILs with a concomitant loss of immunosuppressive myeloid cell populations. Thus, the beneficial role of IFN-I receptor activation is largely dependent on the myeloid compartment and cancer-specific IFN-I receptor engagement is associated with more aggressive cancer outcomes and poor immunogenicity.

Introduction

As immune checkpoint blockade (ICB) is being moved into a first line setting for cancer treatment, co-targeting resistance mechanisms have become central to the outcomes of immunotherapies. Conceptually, there are two broad resistance mechanisms. The first is tumor and myeloid upregulation of the expression of the inhibitory immune checkpoint receptor ligands, such as programmed cell death ligand 1 (PD-L1), to dampen the activation of effector T-cells. The second class of resistance mechanisms is due to the lack of immune priming signals with minimal inflammatory infiltration in the tumor stroma. The first class of mechanisms can be efficiently targeted by leveraging combinatorial ICBs. However, most tumors show features that fall into the second category. The induction of type-I interferon (IFN-I) signaling has been shown as a powerful priming approach to enhance antigen-presenting cells maturation and effector expansion, which sensitizes hypoimmunogenic cold tumors to ICB in several preclinical cancer models (21, 87, 88).

According to data from the Centers for Disease Control and Prevention, human papillomavirus (HPV)[+] Head and Neck Squamous Cell Carcinoma (HNSCC) was one of the only five cancer types that increased from 1975 to 2009; and the increase is predicted to continue until at least the year 2060 (115, 116). Notably, in contrast to the generally more favorable response profiles to chemotherapy among patients with HPV[+] tumors, the Hazard Ratios for

nivolumab were almost identical between the HPV$^+$ and HPV$^-$ groups despite the presence of

viral epitopes (7, 8). Similarly, pembrolizumab ICB resulted in little survival improvement over

standard-of-care in patients with HPV$^+$ tumors (9). Our recent study found that HPV potently

suppresses IFN-I priming signals and encourages cancer immune escape (101). In pre-clinical

models, we and others engineered IFN-I-inducing vaccines targeting the HPV16 E6/E7 epitopes

and showed that IFN-I is essential to prepare the tumor microenvironment for a better response

of ICB-mediated tumor-specific cytotoxic T-cell immunity (16, 23, 87).

Not surprisingly, IFN-I-inducing agents have entered clinical trials, including agonists for a

central adaptor molecule stimulator of interferon response cGAMP interactor 1 (STING1), which

was shown pivotal for radiotherapy-mediated benefits and necessary priming for ICB in animal

studies (21). There are three known human *STING1* alleles, which showed different sensitivities

to its physiological ligand cGAMP. Novel cyclic di-nucleotides have been engineered to activate

all known *STING1* alleles. However, a substantial subset of patients remains resistant to even

these broadly activating cyclic di-nucleotides (117). In addition, discrepancies are present in

studies assessing the role of IFN-I in cancer outcomes. For example, genome instability creates

micronuclei whose rupture activates the STING1-IFN-I pathway. This encourages cancer

metastasis and genetic suppression of chromosomal instability delays metastasis even in highly

aneuploid tumor mouse models (118). Higher expression levels of the Bloom Syndrome RecQ-

like Helicase (*BLM*) and exonuclease 1 (*EXO1*), which facilitate the generation of STING1-

inducing DNA fragments, are associated with poor prognosis in response to radiotherapy (119).

Although the activation of the IFN-I pathway is essential for innate immune detection of

cancer, it is equally important to understand the mechanisms underpinning the discrepancies in

these different studies. Unlike the type II and type III interferons, whose production are restricted

to a small collection of cell types, IFN-I is highly evolutionarily conserved and almost all normal cell types express IFN-I induction machinery and its receptor IFNAR1. The activation of a spectrum of pattern recognition receptors, including the Toll-like receptors (TLRs), RNA sensors such as DExD/H-Box Helicase 58 (DDX58, aka Retinoic Acid-inducible Gene I or RIG-I), Interferon Induced with Helicase C Domain 1 (IFIH1, aka Melanoma Differentiation-Associated Protein 5 or MDA5), and DNA sensor cyclic GMP-AMP Synthase (cGAS), lead to the phosphorylation of IRF3 and NF-κB. Nuclear phospho-IRF3 and phospho-p65 form an enhanceosome to drive the generation of IFN-I, which includes 13 subtypes of IFN-α, IFN-β, IFN-ω, IFN-ε, and IFN-κ. IFN-I functions in an autocrine or paracrine fashion to engage its receptor constituted by IFNAR1 and IFNAR2 on the plasma membrane. Upon activation, tyrosine kinases Tyrosine Kinase 2 (TYK2) and Janus Kinase 1 (JAK1) are phosphorylated, which leads to the phosphorylation of the Signal Transducers and Activators of Transcription (STAT)1 and STAT2. Within the IFNAR1 transcriptional program, *MX1* is a transgene that is specifically induced by IFN-I and used as a sensitive surrogate marker for IFNAR1 signaling.

Thus, the generation of IFN-I and its downstream signaling upon binding to IFNAR1 are two separate events for cancer cells. The secreted IFN-I may function in a paracrine fashion to stimulate the myeloid compartment, which drives most of the observed benefits. However, we and others have shown that multiple solid tumors including HPV⁻ and HPV⁺ HNSCC show deficiencies in the IFN-I induction pathway to evade innate immune detection. Notably, their IFN-I downstream JAK-STAT pathways are often intact, which can be also activated through the Epidermal Growth Factor Receptor (EGFR) pathway (120). Although IFNAR1 downstream signaling activation in myeloid cells enhances its antigen processing efficiency and cross-

priming of CD8^{+} T-cells, the role of IFNAR1 downstream signaling in cancer cells in regulating

the tumor immune microenvironment remains insufficiently characterized.

In this study, we performed a cohort analysis of 195 HNSCC patients to assess the

prognostic significance of IFNAR1 signaling activation in cancer cells and determine whether

suppression of the IFNAR1 pathway specifically in cancer cells improves intra-tumoral immune

infiltration.

Materials and Methods

Clinical samples and tissue microarray.

Patients with previously untreated HNSCC were recruited by the University of Michigan Head

and Neck Cancer Specialized Program of Research Excellence (SPORE) between 2008 to 2012

for a longitudinal study. The patient demographic information and clinical characteristics are

summarized in Supplementary Table 2. The tumors from 218 patients, with a median follow-up

of 60 months, were incorporated into a tissue microarray (TMA). For each tumor, 3

representative 5-µm cores, identified by head and neck pathologist Jonathan McHugh

(Department of Pathology, University of Michigan, Ann Arbor, MI, USA), were included, each

of which contained tumor tissue and surrounding stroma to varying degrees. TMAs were stained

with anti-MX1 antibody (1:600; Cell Signaling Technology, catalog #37849S). The secondary

antibody was biotinylated goat anti-rabbit antibody (Vectastain ABC HRP Kit, PK-4001, Vector

Laboratories). Immunohistochemical (IHC) staining intensity was quantitated in tumor tissue for

each core by selecting a region of interest (ROI) using Aperio ImageScope, followed by

quantification according to the following formula: Score = $(255-I^{avg} * Positivity)$, where I^{avg} was

the average intensity and positivity was the number of positive cells. IHC scores were averaged

from the 3 cores, and those that were missing or had insufficient tumor parenchyma were excluded from subsequent analysis. In total, MX1 IHC scores were available for 195 patients. In experiments involving multivariate Cox regression modeling to control for CD4+ and CD8+ TILs, immunohistochemistry was performed for CD4 and CD8 followed by manual counting of intratumoral CD4 and CD8 numbers for each TMA, in triplicate, by trained observers blinded to the clinical information.

Statistics

Univariate Cox linear regression modeling was used to explore the association between MX1 expression in TMAs and patient clinical variables (e.g. nodal metastasis, stage, etc.). The association between MX1 IHC scores and patient survival was conducted using both univariate and multivariate Cox regression models as indicated in Table 1. To dichotomize tumors into MX1-low and MX1-high groups, a threshold score was estimated by the change point in a Cox regression model, generating a change point cutoff score of 41. Statistical significance in survival probability between MX1-low and MX1-high TMAs was evaluated by Kaplan-Meier survival curves and a log-rank test. As a secondary method, we compared overall survival (OS) and recurrence-free time (RFT) in patients exhibiting MX1 scores in the highest quartile (MX1 score $\geq$ 31.79) vs. patients with lower scores. Statistical analysis between 2 independent groups was made using unpaired, 2-tailed Student's t tests. Tumor burden between groups was compared using the generalized estimating equation model. Statistical significance is indicated in all figures according to the following scale: *$P < 0.05$; **$P < 0.01$; ***$P < 0.001$; and ****$P < 0.0001$. All graphs are presented as the mean $\pm$ SEM.

Animals

Eight-week-old C57BL/6 (strain 000664), were purchased from The Jackson Laboratory and housed under specific pathogen–free conditions in a temperature- and light-controlled environment. Because sex is not a known prognosticator for HNSCC, both sexes were used equally. Syngeneic HNSCC models were established by inoculation of 1 million empty vector (EV-MOC2-E6/E7) control or shIfnar1-MOC2-E6/E7 cells subcutaneously in the right flank. Beginning on day 7 after tumor implantation, tumors were measured using a digital Vernier caliper every 2–3 days, and tumor volume was calculated according to the formula 1/2 (length x width^2). Tumor weight was measured after animals were sacrificed followed excision. All mice were euthanized at the indicated time points followed by tumor, spleen, and/or TIL harvesting for subsequent analysis. All animal procedures were performed in accordance with the protocol approved by the Institutional Animal Care and Use Committee at the University of Michigan (PRO00008517).

Cell culture

The MOC2-E6/E7 cell line was cultured in 60% IMDM (SH30228.01, HyClone) with 30% F12 nutrient mix (11764-054, Gibco), 5% FBS, 4 μg/mL puromycin, 5 μg/mL insulin, 40 ng/mL hydrocortisone, 5 ng/mL EGF, 100 U/mL penicillin, and 100 mg/mL streptomycin. Cells were maintained in a humidified incubator at 37°C with 5% CO2. The MOC2-E6/E7 cell line was originally obtained from Harvard University and validated by immunoblotting for HPV16 E7 protein in Figure S3 of our previous publication (16). To generate EV-MOC2-E6/E7 and shIfnar1-MOC2-E6/E7 cell lines, MOC2-E6/E7 cells were transduced with empty vector control (EV) or shIfnar1-expressing lentiviruses followed by puromycin selection. The selecting

concentration of puromycin was determined by the establishment of a kill curve, via addition of various doses of puromycin into wild-type MOC2 cells. The determined concentration used was 120 μg/mL puromycin. qPCR on murine *Ifnar1* and *Isg54* was performed to validate the knockdown efficiency. Murine pLKO.1-shIFNAR1-puro and pLKO.1–empty vector–puro lentiviral constructs were obtained from Sigma-Aldrich (catalog SHCLNG-NM_010508 and SHC001V, respectively). Lentiviral packaging vectors were provided by Jenny P.Y. Ting at the University of North Carolina at Chapel Hill (Chapel Hill, North Carolina, USA).

Gene expression qPCR

Total RNA was extracted using QIAshredder and the RNeasy Plus Mini Kit (catalog 79654 and 74134, respectively; Qiagen). RNA concentration was measured using a Nanodrop Spectrophotometer (Thermo Fisher Scientific). RNA was reverse-transcribed into cDNA using High-Capacity cDNA Reverse Transcription Kit and RNAse inhibitor (4368814 and N8080119, Applied Biosystems). Primers were synthesized by Integrated DNA Technologies and included: *Isg54* forward 5′-TCTGGTCACCTGGGGAAACTATG-3′, reverse 5′-TTCTCAATCCTGTAGGGGCTGG-3′; *Ifnar1* forward 5′-TCCCCGCAGTATTGATGAGT-3′, reverse 5′-CTGGTCTGTGAGCTGTACTT-3′.

AlamarBlue assay

Empty vector control or shIFNAR1 MOC2-E6/E7 cells were seeded at a density of 500 cells per well in 96-well microplates with a flat black bottom (3904, Corning). Every 24 hours from day 1 to day 4, corresponding wells were supplemented with 10% alamarBlue (DAL1025, Invitrogen), and the plate was subsequently incubated at 37°C for 4 hours. The fluorescence intensity

(excitation 560, emission 590 nm) of these wells was measured using a Biotek plate reader and Gen5 program (version 2.09), and 5 replicates per group were examined simultaneously.

Flow cytometry

Immune cells from tumors and spleens were purified as we have previously described (16). Briefly, tumors were excised from mice and minced into pieces, followed by dissociation by passing through a 70-μm cell strainer to obtain a single-cell suspension. Spleens were processed by mechanical dissociation, followed by lysis of red blood cells (A10492-01, Gibco). Ficoll-Paque PLUS (17-1440-03, GE Healthcare Life Sciences) was added to the bottom of each tube containing single cell suspensions in RPMI1640, followed by density-gradient centrifugation to purify immune cells. Purified immune cells were stained for multi-fluorophore flow cytometric analysis with the following antibodies: anti-CD45 (clone 30-F11, BioLegend), anti-CD3 (clone 17A2, BD Biosciences), anti-CD4 (clone RM4-5, BioLegend), anti-CD8 (clone 53-6.7, BioLegend), anti-CD44 (clone IM7, BioLegend), anti-CD366 [Tim3] (clone RMT3-23, Biolegend), and anti-PD-1 (clone 29F1A12, Biolegend). Cells were also stained for viability using Fixable Viability Dye (FVD) eFluor 780 (65-0865-14, Thermo Fisher Scientific) or Zombie Aqua (423101, BioLegend) diluted 1:1000 in PBS at 4°C for 30 minutes. Acquisition and compensation were conducted on a Beckman Coulter CytoFLEX flow cytometer. FlowJo version 10 software was used for data analysis.

ALDH assay

This assay was performed using the ALDEFLUOR™ Kit (01700, STEMCELL Technologies). In part, empty vector control or shIFNAR1 MOC2-E6/E7 in vitro lines were resuspended into

ALDEFLUOR™ Assay Buffer (01701, STEMCELL Technologies) at a working concentration of 1×10^5. Following ALDEFLUOR staining, cells were stained with anti-CD44, and analyzed on a Beckman Coulter CytoFLEX flow cytometer.

Single cell RNA-sequencing and immune cell deconvolution

Whole tumor lysate was treated with ACK Lysing Buffer (A1049201, ThermoFisher), then processed through an EasySep Dead Cell Removal (Annexin V) Kit (17899, STEMCELL Technologies). Cell suspension was submitted in $1 \times$ PBS + 0.04% BSA for $10 \times$ Genomics 3'-single cell processing and RNA-Seq at a depth of at least 30,000 reads per cell. We utilized the following criteria to select high-quality transcriptomes: (i) the qualified cells must have a unique feature counts between 200 and 7,500; (ii) the mitochondrial reads must be fewer than 10%; (iii) the transcriptomes must have unique molecular identifiers counts over 500. We integrated 12,907 high-quality transcriptomes for downstream analyses. We utilized the sctransform tool to remove the library size effect and the mutual nearest neighbors algorithm to remove the batch effect for final integration. We selected the top 3,000 genes with the highest cell-to-cell variation as well as features to stabilize the immune population structure. The additional features include *Cxcr5, Cd69, Aim2, Irf5, Irf1, Irf3, Lgals9, Ly6e, Nos2, Il6, Tnf, Isg15, Gsdmd, Cd8a, Cd40, Cd80, Cd86, Il10, Tgfb1, Tmem173, Cd274, Cxcl9, Mrc1, Siglec15, Trdc, Cd2, Trac, Cd4, Cd8b1, Foxp3, Trbc1, Trbc2, Gzmb, Eomes, Icos, Cd3d, Cd3e, Ifng, Ncr1, Cd19, Cd79a, Cd79b, Itgam, Itgax, Batf3, Xcr1, Gata3, Ctla4, Rorc, Il17a, Bcl6, Havcr2, Tnfrsf4, Tigit, Cxcl10, Mx1, Ifnb1, Il3ra, Nrp1, Fcer1a, Tbx21, Lag3, Ifnl3, Pdcd1, Cd14, Ifna4, Ly6g, Ly6c1,* and *Lyz2*. We obtained the top 50 principal components from the integrated data set.

Results

High MX1 protein expression levels in cancer cells are associated with poor prognosis in HNSCC patients

Tissue microarrays (TMAs) were generated utilizing specimens from 195 patients with HNSCC. The majority of specimens were collected from patients with advanced stage disease (15% stage 3; 65% stage 4) and were relatively representative of the natural distribution across disease sites, including larynx (17%), oral cavity (46%), oropharynx (30%), and hypopharynx/other (7%). Other parameters evaluated in this patient cohort, summarized in Table 3-1, included age, gender, adult comorbidity evaluation (ACE) score, HPV status, and history or present use of tobacco products and alcohol consumption.

Variable	Subgroup	N (%)
Age Category	<60	108 (55%)
	60-80	76 (39%)
	>80	11 (6%)
Sex	Male	147 (75%)
	Female	48 (25%)
Stage	0/1	20 (10%)
	2	20 (10%)
	3	29 (15%)
	4	126 (65%)
Disease Site	Larynx	34 (17%)
	Oral Cavity	89 (46%)
	Oropharynx	59 (30%)
	Hypopharynx/Other	13 (7%)
ACE Comorbidities Score	none	58 (30%)
	mild	89 (46%)
	moderate	32 (16%)
	severe	15 (7%)
HPV Status	negative	114 (58%)
	positive	60 (31%)
	invalid/missing	21 (11%)
Alcohol consumption	never	21 (11%)
	current	131 (67%)
	former (quit >12 months)	43 (22%)
Smoker (cigarettes)	never	45 (23%)
	current	92 (47%)
	former (quit >12 months)	58 (30%)

Table 3-1 – **Baseline demographic and clinical information corresponding to the TMAs analyzed from an expanded cohort of 195 HNSCC patients (mean follow-up of 60 months)**

To assess the prognostic value of cancer cell-specific IFNAR1 downstream signaling, we analyzed MX1 protein levels by immunohistochemical staining of the TMAs. MX1 exhibited a diffuse cytoplasmic staining pattern that was highly variable in density among different tumors.

MX1 is also stained in the infiltrating immune cells, as expected. To specifically examine the

role of cancer-specific IFNAR1 activation, we manually selected tumor parenchyma for 585

cores, with three cores representing one tumor, prior to quantitation (Figure 3-1a). Cancer-

specific MX1 staining scores were quantitated using Aperio ImageScope, as we previously

reported (101). These results supported the heterogeneous nature of MX1 distribution, with

descriptive statistics summarized in Table 3-2.

Mean	Standard deviation	Median	Minimum	Maximum	25th Percentile	75th Percentile
22.0143	16.9247	18.5335	0.11441	86.2481	9.32779	31.9399

Table 3-2 – **Descriptive statistics for MX1 immunohistochemical staining scores obtained by Aperio ImageScope quantification of TMAs from 195 HNSCC patients**

To analyze the association with relevant clinical variables, MX1 scores were considered in their

continuous form (the raw score) or in a dichotomized form wherein tumors were divided into

MX1-high and MX1-low groups using the change point threshold in Cox regression modeling,

generating a change point cutoff score of 41. No significant association was observed between

MX1 score and disease site or nodal metastasis, although a trend existed between the raw MX1

score and advanced cancer stage ($P = 0.09$) (Supplemental Figure 3-1).

MX1 Score: 5.19
Survival Time: 61.67

MX1 Score: 4.18
Survival Time: 71.26

MX1 Score: 45.06
Survival Time: 4.60

MX1 Score: 51.09
Survival Time: 20.86
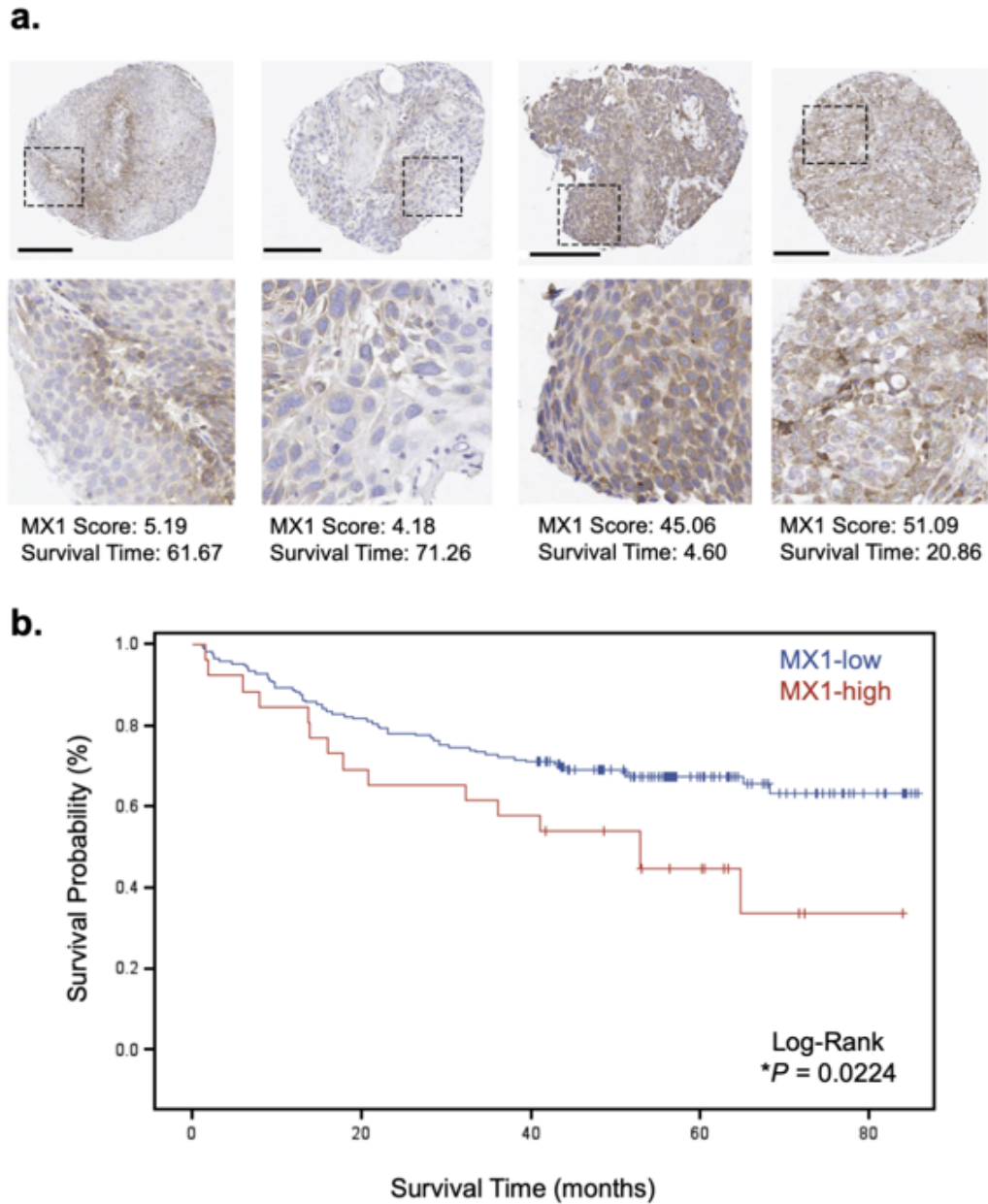
Figure 3-1 – High MX1 protein levels is a negative prognosticator in head and neck squamous cell carcinoma.

MX1 immunohistochemistry in TMAs from HNSCC patients reveals cytoplasmic staining of variable intensity across specimens **(A)** Raw MX1 scores and survival time are indicated for each representative TMA. Scale bar: 200 µm. **(B)** MX1 staining scores were segregated into MX1-low or MX1-high groups and the Kaplan-Meier survival curves of each group were compared using a log-rank test.
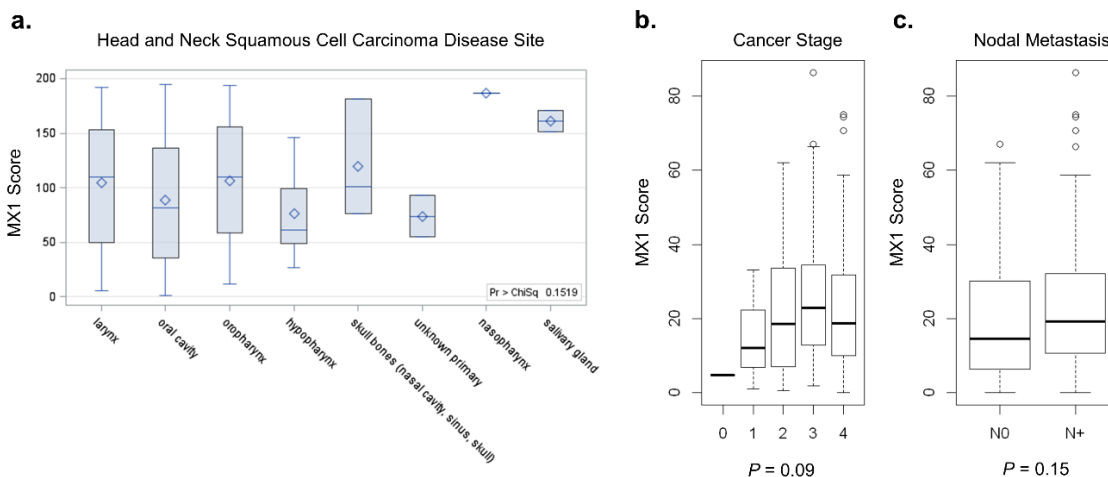
Supplemental Figure 3-1 – **Association of MX1 immunohistochemical scores with disease site, cancer stage, and nodal metastasis**

Raw MX1 scores were generated by quantifying MX1 immunohistochemical staining in TMAs from 195 HNSCC patients, followed by correlation with primary disease site **(a.)**, cancer stage **(b.)**, or status of nodal metastasis **(c.)**. No statistical differences were observed between MX1 and any of these variables, although a non-statistically significant positive association was observed between MX1 score and increased HNSCC cancer stages ($P = 0.09$). Univariate Cox linear regression modeling was used to analyze the association between MX1 score and each variable.

We next examined the impact of MX1 protein expression on HNSCC patient overall survival

(OS). The Kaplan-Meier survival curves were compared between MX1-high and MX1-low

groups using a log-rank test, which revealed that MX1-high staining was significantly correlated

with worse overall survival ($P = 0.02$; Figure 3-1b). Utilizing a univariable Cox regression model

where MX1 is the single predictor of outcome, we found that the MX1-high group was

correlated with significantly worse overall survival ($P = 0.02$), but no association was observed

with recurrence-free survival (RFS; $P = 0.28$; Table 3-3). We also built a multivariate Cox

regression model controlling for age, clinical stage, disease site, ACE scores, HPV status,

smoking, and CD4$^+$ T-cells among tumor infiltrating leukocytes (TILs), and found that MX1-

high staining remained correlated with significantly worse overall survival ($P = 0.04$; Table 3-3).

Notably, using a multivariate Cox regression model that controls for these factors, but instead controls for CD8^{+} T-cells among tumor infiltrating leukocytes (TILs), MX1-high tumors are no longer associated with worse prognosis ($P = 0.42$; Table 3-3), suggesting that high MX1 staining in cancer cells negatively predicts patient outcome in a CD8^{+} T-cell-dependent manner.

MX1 Group	Overall Survival (OS)		Recurrence-Free Survival (RFS)	
Univariate model	HR (95% CI)[1]	P-value	HR (95% CI)	P-value
MX1 score (1 unit increase)	1.00 (0.99, 1.02)	0.12	1.01 (0.99, 1.02)	0.35
MX1-high (≥ 41)	1.97 (1.11, 3.48)	**0.02**	1.49 (0.73, 3.06)	0.28
Multivariate model (CD4+)	HR (95% CI)	P-value	HR (95% CI)	P-value
MX1 score (1 unit increase)	1.01 (1.00, 1.03)	0.14	1.00 (0.99, 1.03)	0.43
MX1-high (≥ 41)	1.96 (1.02, 3.74)	**0.04**	1.73 (0.77, 3.87)	0.18
Multivariate model (CD8+)	HR (95% CI)	P-value	HR (95% CI)	P-value
MX1 score (1 unit increase)	1.00 (0.99, 1.02)	0.66	1.00 (0.98, 1.02)	0.99
MX1-high (≥ 41)	1.30 (0.68, 2.48)	0.42	1.25 (0.56, 2.78)	0.58

[1] Abbreviations: HR: hazard ratio; CI: confidence interval.

Table 3-3 – **Association between MX1 score and overall survival or recurrence-free survival**

Displayed above is a univariate model or multivariate models controlling for patient age, clinical stage, disease site, comorbidities, HPV status, smoking history, and CD4^{+} (middle) or CD8^{+} TILs (bottom).

As a secondary method of dividing patients by their MX1 immunohistochemical scores, we compared Kaplan-Meier curves for overall survival (OS) and recurrence-free time (RFT) in patients exhibiting MX1 scores in the highest quartile (MX1 score ≥ 31.79) vs. patients with lower scores. Interestingly, patients exhibiting MX1 scores in the highest quartile tended to exhibit worse overall survival ($P = 0.186$; not shown) and recurrence-free survival ($P = 0.049$; not shown). In a univariate Cox regression model, patients exhibiting MX1 scores in the highest

quartile tended to exhibit worse prognosis in terms of OS ($P = 0.07209$) and RFT ($P = 0.05563$; Table 3-4). This association was generally stronger when controlling for individual clinical parameters such as patient age, stage, site, ACE score, smoking status, and CD4+ or CD8+ accounts using multivariate Cox regression modeling (Table 3-4).

MX1 Group	Overall Survival (OS)		Recurrence-Free Survival (RFS)	
Univariate model	HR (95% CI)[1]	P-value	HR (95% CI)	P-value
MX1-upper quartile vs. lower	1.66 (0.96, 2.90)	0.072	1.90 (0.99, 3.65)	0.056
Multivariate model (MX1-upper quartile vs. lower)	HR (95% CI)	P-value	HR (95% CI)	P-value
Controlling for age[2]	1.03 (1.01, 1.05)	**0.014**	1.01 (0.98, 1.03)	0.562
Controlling for stage[3]	2.40 (1.12, 5.14)	**0.025**	3.24 (1.09, 9.60)	**0.034**
Controlling for site[4]	2.55 (1.26, 5.15)	**0.001**	2.33 (0.94, 5.77)	0.066
Controlling for ACE score[5]	5.30 (1.99, 14.2)	**0.001**	3.99 (1.37, 11.6)	**0.011**
Controlling for smoking history[6]	3.78 (1.58, 9.06)	**0.003**	1.79 (0.73, 4.34)	0.201
Controlling for CD4+ TILs[7]	0.68 (0.52, 0.90)	**0.006**	0.74 (0.56, 0.98)	**0.034**
Controlling for CD8+ TILs[8]	0.93 (0.77, 1.13)	0.472	0.98 (0.80, 1.19)	0.804

[1] Abbreviations: HR: hazard ratio; CI: confidence interval.

Table 3-4 – **Association between MX1 scores in the highest quartile vs. all other patients in terms of overall survival or recurrence-free survival**

Loss of IFNAR1 downstream signaling in HNSCC cells reduces tumor burden and improves the tumor immune microenvironment

To directly determine the role of cancer-specific IFNAR1 downstream signaling in tumor immunogenicity, we utilized an established MOC2-E6/E7 syngeneic HNSCC model (16), which does not produce IFN-I upon transfection with STING1 agonists (101). We produced a

derivative model in which the Ifnar1 receptor is knocked down (MOC2-E6/E7-shIfnar1) leading

to loss of cancer cell-intrinsic IFNAR1 signaling (Figure 3-2a-b). Defective downstream IFN-I

signaling had no effect on cell proliferation in vitro (Figure 3-2c). Interestingly, when we

implanted empty vector control (MOC2-E6/E7-EV) and Ifnar1-deficient tumor cells into

C57BL/6 hosts, we observed a significant reduction in tumor growth in the Ifnar1-deficient

tumor group (Figure 3-2d-e).
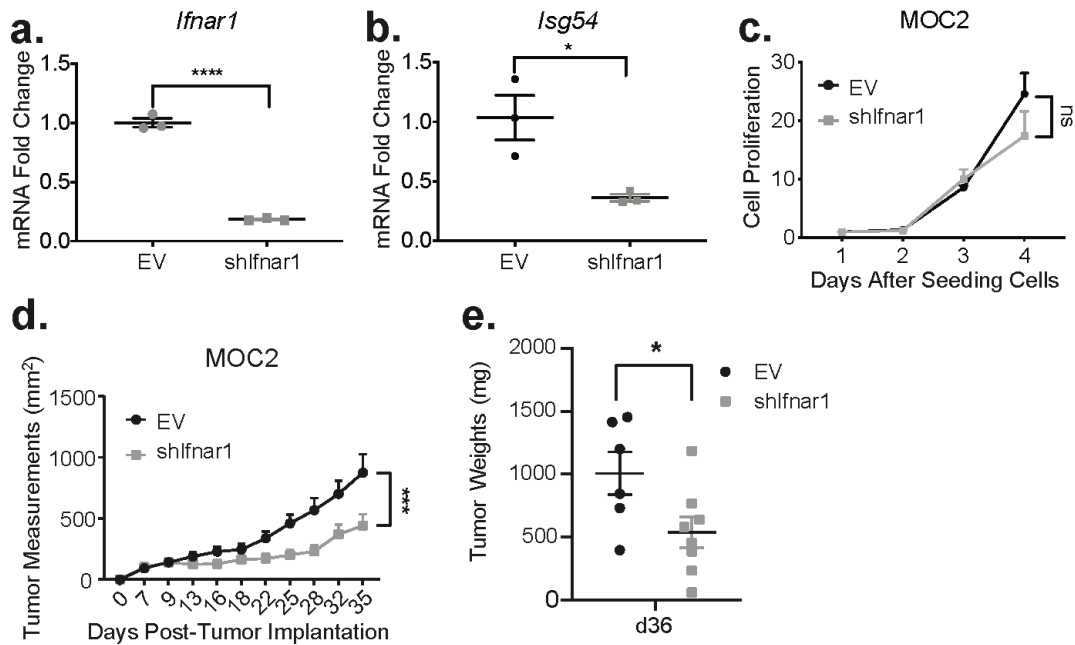
Figure 3-2 – **Loss of IFN-I signaling in HNSCC cells reduces tumor burden.**

(**A**) qPCR was performed to quantitate the transcript levels of *Ifnar1* and (**B**) the downstream
IFN-I target gene *Isg54* in EV control and shIfnar1 MOC2-E6/E7 cells. (**C**) The proliferation of
EV control and shIfnar1 MOC2-E6/E7 cells was measured via an alamarBlue assay. Each group
included 5 replicate wells. (**D-E**) One million EV control or IFNAR1-deficient MOC2-E6/E7
cells were implanted subcutaneously in the right flank of C57BL/6 hosts. (**D**) Tumor
measurements were performed every 2–4 days and (**E**) tumor weight was measured followed
harvesting at day 36. All Comparisons between 2 groups were made using a 2-tailed
unpaired *t* test (**$*P < 0.01$, $****P < 0.0001$**).

When we examined the cancer cell compartment in vitro, we noticed that Ifnar1 deficiency reduced the fraction of cells showing features of cancer stem cells (Figure 3-3a-b), which have been demonstrated to be more resistant to immune killing (121). We separated the TILs through a Ficoll-Paque gradient and found an enhancement in both CD4$^+$ and CD8$^+$ T-cell infiltration in Ifnar1-deficient tumors (Figure 3-3c-f), suggestive of the elicitation of a T-cell-inflamed microenvironment in a highly aggressive cold tumor model.
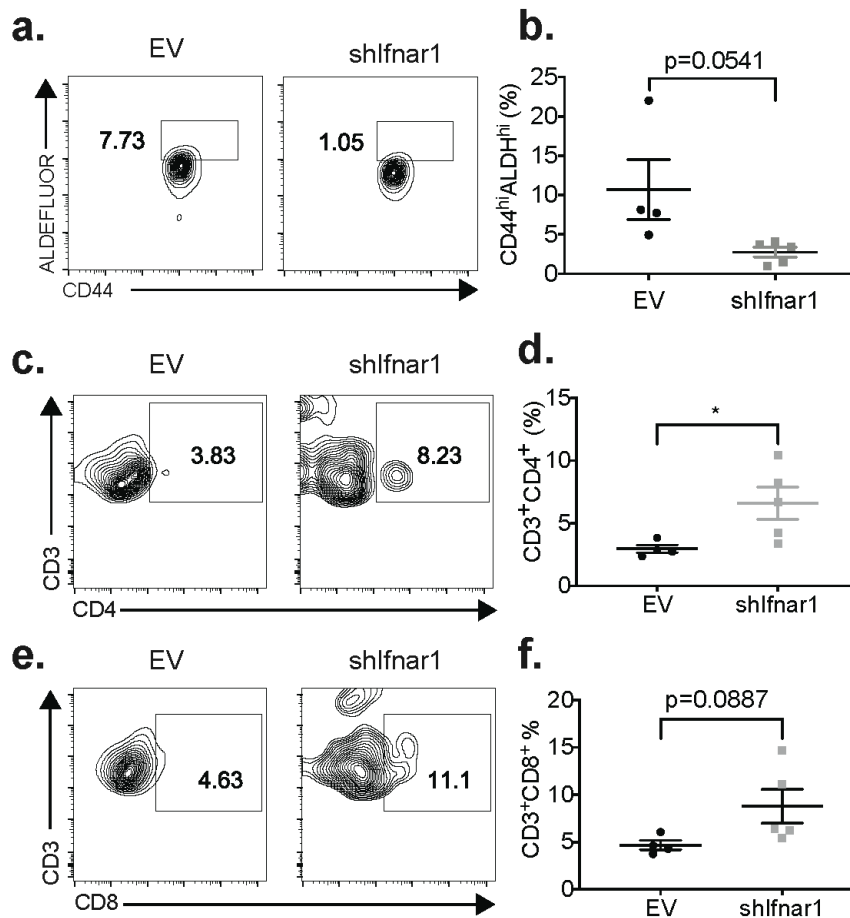
Figure 3-3 – **Loss of IFN-I signaling in HNSCC cells promotes cancer stemness and TIL infiltration**

(A-B) To assess presence of cancer stem cells, EV control and shIFNAR1 MOC2-E6/E7 cells were treated using the ALDEFLUOR Assay Kit and analyzed via flow cytometry for aldehyde dehydrogenase-high. Gating strategy was as follows: MOC2 cells, single cells, CD44-high. **(C-F)** Tumors were harvested 36 days following implantation, and tumor infiltrating lymphocytes (TILs) were separated using a Ficoll-Paque gradient. **(C-D)** The proportion of CD3+ CD4+ TILs were assessed by flow cytometry. Gating strategy was as follows: Lymphocytes, single cells, Zombie Aqua negative (viability), CD45-positive. **(E-F)** The proportion of CD3+ CD8+ TILs were assessed by flow cytometry. Gating strategy was as follows: Lymphocytes, single cells, Zombie Aqua negative (viability), CD45-positive. All Comparisons between 2 groups were made using a 2-tailed unpaired t test (*$P < 0.05$).

To more completely characterize the phenotype of CD4+ and CD8+ TILs, we again separated TILs from control and Ifnar1-deficient tumors. Notably, while no changes were observed in immune subsets in the spleen, we observed a significant reduction in immunosuppressive CD4+/PD1^{high} and CD8+/Tim3+ TILs in Ifnar1-deficient tumors (Figure 3-4a-f), as well as an increase in the fraction of CD8+/PD1^{low} TILs required for antitumor immunity (Figure 3-4g-i).
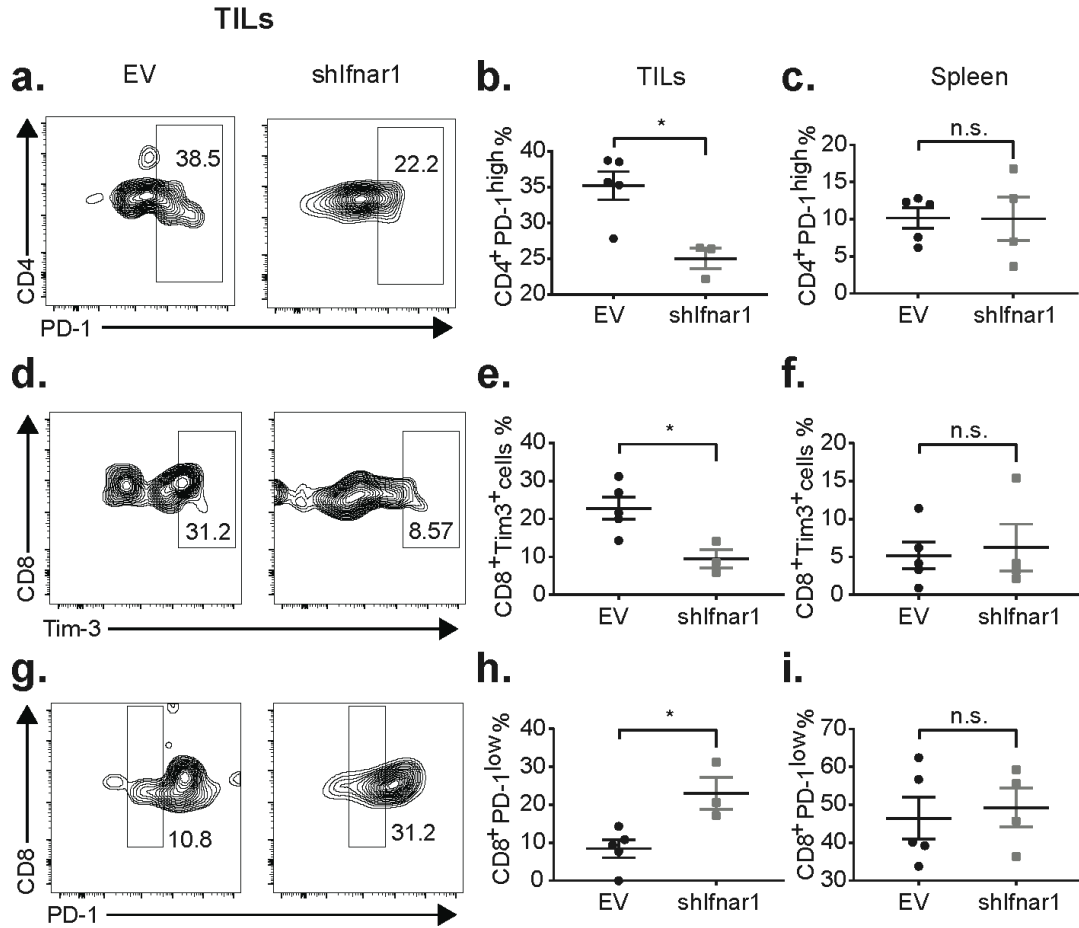
Figure 3-4 – **Loss of IFN-I signaling in cancer cells promotes a more inflamed tumor microenvironment.**

(**A-C**) Tumors or spleens were harvested 36 days following tumor implantation, and lymphocytes were isolated using a Ficoll-Paque gradient. The proportion of CD4+ PD1^{high} TILs or splenic T cells were assessed by flow cytometry. Gating strategy was as follows: Lymphocytes, single cells, Zombie Aqua negative (viability), CD45-positive, CD3 positive. (**D-F**) The proportion of CD8+ Tim3+ TILs or splenic T cells were assessed by flow cytometry. Gating strategy was as follows: Lymphocytes, single cells, Zombie Aqua negative (viability), CD45-positive, CD3 positive. (**G-I**) The proportion of CD8+ PD1^{low} TILs or splenic T cells were assessed by flow cytometry. Gating strategy was as follows: Lymphocytes, single cells, Zombie Aqua negative (viability), CD45-positive, CD3 positive.

Cancer-specific IFN-I downstream signaling impacts the global immune landscape

Collectively, our flow cytometry analyses of TILs suggest that mice bearing Ifnar1-deficient tumors exhibit a shift towards a more immunologically "hot" tumor microenvironment. To comprehensively characterize the impact of tumor-intrinsic IFN-I signaling on the tumor immune microenvironment, we performed single-cell RNA-sequencing (scRNA-seq) to render the intratumoral immune landscape. We performed Ficoll-Paque purification, followed by CD45$^+$ FACS sorting, to enrich intra-tumoral leukocytes. After filtering, we integrated 12,907 high-quality transcriptomes and identified 20 cell clusters (Figure 3-5a), which showed distinct immune lineage segregation and smooth functional transition. The majority of the intratumoral leukocytes consisted of the myeloid cells, including myeloid-derived suppressor cells (MDSCs, clusters 1, 2, 5, 7, 8, 9, and 12), M2-like macrophages (cluster 13), and conventional dendritic cells type 1 (cDC1, cluster 20). The CD4$^+$ T-cells were separated to regulatory T-cells (Treg, cluster 15) and a stem-like cluster with high expression levels of Tcf7 (cluster 3). The effector populations included Tbet$^+$CD8$^+$ T-cells (cluster 6), Tcf7$^+$CD8$^+$ T-cells (cluster 18), natural killer (NK) cells (cluster 17), and γδ T-cells (cluster 16). We also identified Cxcr5$^+$ B-cells (clusters 4, 10, and 11) and a minute population of basophils (cluster 19) (Figure 3-5a). Global intratumoral immune microenvironment remodeling was noted when tumor cells were deficient in downstream IFN-I signaling (Figure 3-5b-c). Inhibition of cancer-specific Ifnar1 signaling transduction expanded the frequencies of CD8$^+$ T-cells by 5.4 folds, Tcf7$^+$CD4$^+$ T-cells by 7.3 folds, and γδ T-cells by 3.6 folds. There was an about 50% reduction in MDSCs. Also observed was a 7.6-fold expansion of Cxcr5$^+$ B-cells in the Ifnar1-deficient tumors (Figure 3-5b-c).

Thus, using clinical specimens as well as parallel flow cytometry and single-cell analysis, we found that activation of downstream IFN-I signaling in cancer cells not only led to lymphoid

71

contraction within the tumors but also resulted in dysfunctional CD8$^+$ T-cells profiles. To

delineate the impact of cancer-intrinsic IFN-I activation upon the differentiation of CD8$^+$ T-cells,

we separated the CD8$^+$ subsets (clusters 6 and 18) and performed Potential of Heat-diffusion for

Affinity-based Transition Embedding (PHATE) analysis, which revealed the functional

development pathways of CD8$^+$ T-cells. We found that the CD8$^+$ T-cells in empty vector control

and Ifnar1-deficient tumors assumed divergent functional commitments. MOC2 has been

established as a hypoimmunogenic HNSCC model that is refractory to ICBs (122, 123). In

agreement, we found that the CD8$^+$ T-cells in control tumors largely committed to a terminal

exhaustion phenotype with high expression levels of *Pd-1* and *Tim-3*. These cells were low on

activation markers such as *Cd28* and *Cd69* as well as stemness markers *Tcf7* and *Slamf6*. In

contrast, increased frequency of CD8$^+$ T-cells in Ifnar1-deficient tumors expressed high levels of

Cxcr3, which is rapidly induced upon activation of Th1 effectors (124). Notably, most of these

CD8$^+$ T-cells in Ifnar1-deficient tumors preserved stemness features, which are critical in

maintaining cancer immunogenicity (125, 126). Glutaminolysis has been shown to be activated

in Th1 cells to support their effector function (127-129). Interestingly, we found that the

terminally exhausted CD8$^+$ T-cells in control tumors largely lost the expression of a glutamine

transporter *Slc38a2*. However, *Slc38a2* was highly expressed in CD8$^+$ T-cells that also expressed
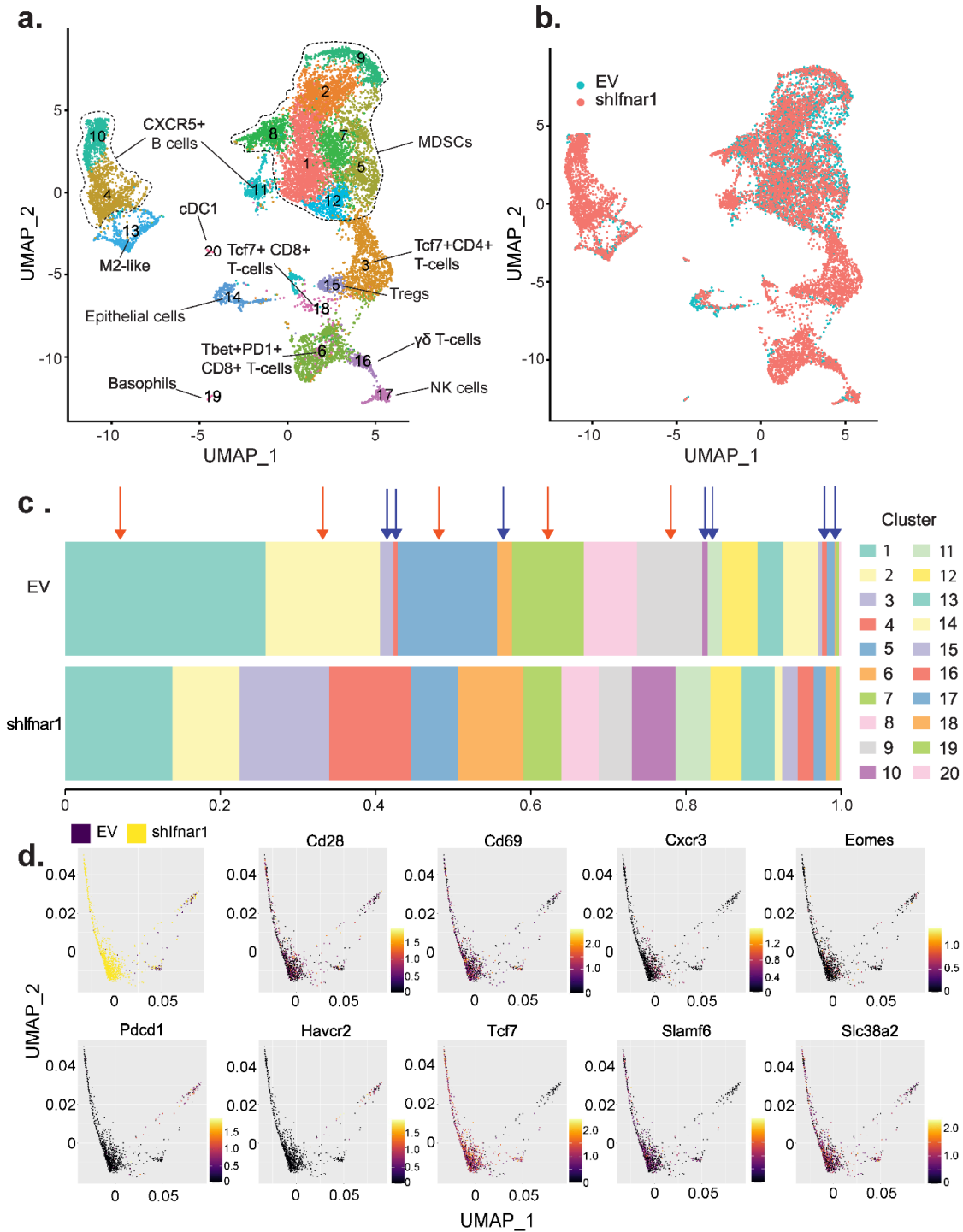
a stemness marker *Tcf7* (Fig. 3-5d).

Figure 3-5 – **Analysis of the tumor immune landscape by single cell RNA-sequencing with immune cell deconvolution.**

(A-C) MOC2-E6/E7-EV control and MOC2-E6/E7-shIfnar1 tumors were harvested at day 36 after implantation. TILs were purified and pooled from six mice per group and subjected to single-cell RNA-sequencing. (**A**) After filtering, 12,907 high-quality transcriptomes were integrated for UMAP analysis. Divergent myeloid and lymphoid lineages were defined by top 3,000 genes with the highest cell-to-cell variation and enforced features of 69 immune cell marker genes. (**B**) UMAP analyses demonstrating the tumor immune landscape in EV control (green) and Ifnar1-deficient (red) tumors are shown. (**C**) Comparison of the relative proportion of cell types identified in EV control and Ifnar1-deficient tumors. Ifnar1-deficient tumors exhibited a marked decrease in the proportion of several cell types (red arrows), which was particularly pronounced among myeloid-derived suppressor cells (MDSCs, clusters 1, 2, 5, 7, 8, 9, and 12). In Ifnar1-deficient tumors, increased enrichment was observed in the proportion of $Tcf7^+CD4^+$ TILs (cluster 3), $CD8^+$ T-cells (clusters 6 and 18), $\gamma\delta$ T-cells (cluster 16), as well as $CXCR5^+$ B-cells (clusters 4, 10, and 11), as indicated by blue arrows. (**D**) PHATE analyses were performed to reveal the divergent differentiation trajectories of the $CD8^+$ T-cells (clusters 6 and 18 from Fig. 5a) in empty vector control (black) and Ifnar1-deficient tumors (yellow). The expression patterns of functional markers across the $CD8^+$ T-cell landscape were highlighted in the rest of the panels, with red showing the highest expression levels and black showing the lowest expression levels.

Discussion

Much progress has been made towards understanding cancer resistance to ICB. A preexisting tumor antigen-specific T-cell pool is required for optimal response to immunotherapy. STING-mediated IFN-I activation underpins the success of multiple innate

immune priming strategies that aim to enrich the tumor-specific T-cell pool. Irradiation, inhibition of DNA damage repair, and direct stimulation with cyclic dinucleotides are utilized to trigger DNA-induced STING1 activation. However, the efficacy of this broad class of innate immune priming treatments is challenged by unknown mechanisms that dampen tumor sensitivity to STING1 stimulation. The main focus on the immune remodeling effect of STING1 agonists had been on the M1-like repolarization of the myeloid cells. This study aims to understand whether cancer-specific IFN-I downstream signaling contributes to immunosuppression. We first assessed whether cancer intrinsic IFNAR1 signaling is clinically significant for patients with HNSCC. Utilizing univariate and multivariate Cox regression models, we found that high MX1 protein levels in cancer cells were associated with worse overall survival. MX1 is a sensitive surrogate marker for IFNAR1 downstream signaling activation, suggesting that sustained IFNAR1 engagement was an unfavorable prognosticator in HNSCC. Notably, the association between cancer-specific MX1 expression and worse outcomes is dependent on the number of intra-tumoral CD8$^+$ T-cells.

The current IFN-I agonists were administered to globally activate IFNAR1 signaling in both immune cells and other cell types, including cancer cells. The beneficial effect of STING1-IFN-I activation is dependent on myeloid reprograming (21, 130). Activation of IFNAR1 signaling not only enhances antigen processing, antigen presentation, MHC molecule upregulation, but also improves trafficking and recruitment of innate and adaptive immune cells to the otherwise T-cell-deficient tumor stroma. However, IFNAR1 activation in cancer cells promotes cancer stemness and potentiates a T-cell exclusion local niche. IFN-I stimulation not only makes cancer cells assume stemness features to develop resistance to immune killing but reprograms the global tumor immune microenvironment. We performed parallel flow cytometry and single-cell RNA-

Seq to reveal the divergent myeloid and lymphoid remodeling imposed by cancer-specific IFN-I signaling disruption. We found that Ifnar1-deficient tumors harbors reduced MDSCs and expanded effectors including CD8$^+$ T-cells, non-Treg CD4$^+$ T-cells, and γδ T-cells. Notably, blocking cancer-specific IFN-I signaling not only expands CD8$^+$ T-cell pool but remodels its differentiation trajectory. We utilized a well-established cold cancer model and indeed found that majority of the intratumoral CD8$^+$ T-cells have committed to terminal exhaustion with double expression of Pd-1 and Tim-3. However, Ifnar1-deficient tumors expands Tcf7$^+$ stem-like effector T-cells, which preserves high proliferation potential and responsiveness to ICB. Mechanistically, cancer stem cells in HNSCC are a small yet highly tumorigenic population which selectively express PD-L1 and dampen autologous CD8$^+$ T-cell activation (121). Thus, cancer-intrinsic IFNAR1 signaling activation likely initiates a transcriptional program that is overlapping with the cancer stemness program to dampen the anti-tumor effect of STING1 stimulation.

CHAPTER 4 – Conclusions and Future Directions

Summary

Head and neck squamous cell carcinomas (HNSCCs) are defined as immunologically cold (16), which presents unique challenges in the development of novel therapeutics towards improving immune responses (131). Alongside this, a phase 3 clinical trial of the checkpoint inhibitor nivolumab, an anti-PD-1 monoclonal antibody, yielded only a 13.3% response rate in HNSCC patients (7). Thus, the goal of the research outlined within this dissertation was to further delineate both activating and inhibitory mechanisms which influence tumor development and immune cell evasion. To answer such questions, we approached the field through the examination of type I interferon (IFN-I) regulation, which enacts broad anti-tumor functional activity, by activating effector and myeloid immune cell populations (21, 89-91). Though previous research has examined the therapeutic benefits of myeloid cell IFN-I production (21, 130), the effects of cancer-intrinsic IFN-I production and downstream tumor-specific IFNAR1 engagement had yet to be assessed. In chapter 2, we examined how cancer-intrinsic IFN-I production is suppressed in obese hosts, leading to increased tumor burden and a highly immunosuppressed tumor microenvironment. We further identified the gene *NLRC3* as upregulated in obese tumors, and as a negative regulator of the cancer-intrinsic IFN-I response. In addition, the efficacy of NLRC3-deficiency in mediating an improved anti-tumor immune response was shown to be dependent on both host adaptive immunity and host IFN-I signaling. In chapter 3, we investigated the role of cancer-intrinsic IFN-I downstream signaling towards

modulating the tumor microenvironment. We first discovered that *MX1*, a "metagene" associated

with downstream IFNAR1 engagement (46) was correlated with worse HNSCC patient survival.

We also found that cancer-intrinsic IFNAR1-deficiency led to reduced overall tumor burden,

reduced proportions of cancer stem cells, and reduced immunosuppressive tumor-infiltrating

lymphocytes (TILs) subsets in hosts. Altogether, the work outlined in this document has

uncovered that the therapeutic benefits of IFN-Is in mediating cancer immune escape are largely

dependent on myeloid and cancer cell IFN-I production and myeloid IFN-I downstream

signaling, and that paracrine and autocrine signaling effects of IFNAR1 activation on cancer

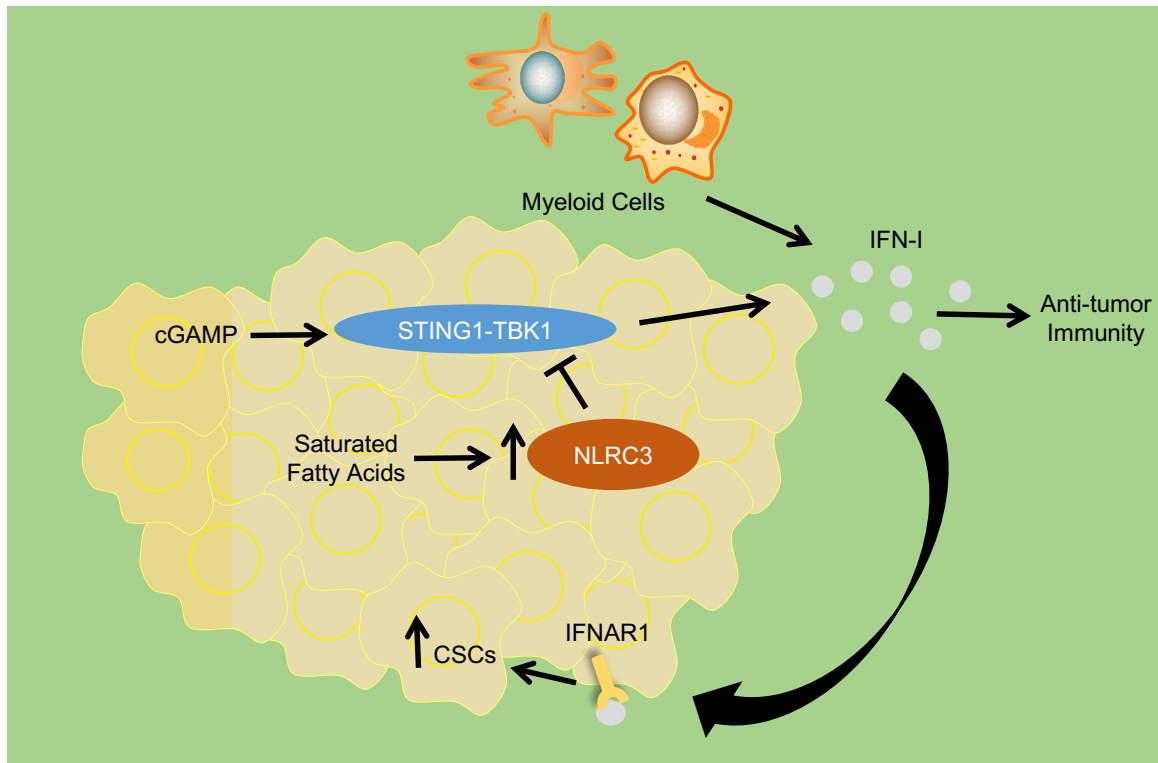cells are deleterious for host anti-tumor immune cell responses and patient outcomes (Figure 4-

1).

Figure 4-1 – **Schematic of differential outcomes between cancer-intrinsic IFN-I production
& downstream IFNAR1 engagement**

The work outlined in this dissertation has uncovered the differential regulation of tumor progression that occurs by the STING-mediated type I interferon pathway. We uncover that IFN-I production and signaling from the host, as well as is IFN-I production from the cancer cell is beneficial for the development of anti-tumor immunity, and this process is suppressed by the presence of saturated fatty acids, which induces the IFN-I regulator NLRC3. However, IFN-I signaling from the cancer cell promotes tumor immune escape by expanding cancer stem cells, proving deleterious for patient outcomes.

Objectives, Major Findings, and Implications from Chapter 2

The inflammatory processes associated with obesity and associated metabolic disorders have previously been linked to driving angiogenesis and expedited tumor development, through a variety of immunosuppressive factors, such as HIF-1α and TGF-β, which buttress cellular growth (132). In concordance with this work, innate immune regulators have additionally been implicated in interacting with reactive oxygen species induced by free fatty acid synthesis, leading to disordered inflammation (133). However, until now, we have not fully understood the mechanisms by which adiposity mediates tumor immune suppression. In chapter 2, we sought to first to determine how obesity modulates head and neck squamous cell carcinoma (HNSCC) progression and the associated microenvironment in vivo, and then to further explore the effects of saturated fatty acids on regulating cancer and immune cell-associated type I interferon (IFN-I) production.

As mentioned previously, obesity has been correlated with worse head and neck cancer patient tumor growth (94); however, body mass cannot alone indicate patient outcomes (134), and mechanistic studies underlying these correlations were not clear. To assess the effects of obesity on host HNSCC burden, we utilized the previously characterized MOC2-E6/E7 tumor model, which is syngeneic to C57BL/6 mice (16). C57BL/6 mice were fed either a normal chow diet or a high fat diet for twelve weeks, then implanted with MOC2-E6/E7 cells. Obese mice displayed a larger tumor burden than normal weight mice, and through tumor microenvironment

analysis, we uncovered an immunosuppressed landscape that included suppressed T-cell expansions and increased M2-like macrophage populations. This work suggests that effector cell cytokine and chemokine signaling is altered by components of adipose tissue. We also found that obesity modulated glycolytic processes within tumor cells.

To find the fatty acid compartment which could be promoting aggressive tumor growth in obese hosts, we used both palmitate, an abundant saturated fatty acid in adipose tissue, as well as oleate, an unsaturated fatty acid, to model to effects of obesity within cell culture. Pretreatment of palmitate on both murine cancer cells and BMDMs led to suppressed type I interferon (IFN-I) production, whereas pretreatment with oleate did not produce this effect. Alongside this, we hypothesized that obese patients, who potentially bear a range of metabolic defects, would be less responsive to cyclic dinucleotide (CDN) therapy. We thus treated tumor-bearing normal weight and obese mice with 2'3'-cGAMP for three weeks and found that the effects of CDN therapy were reduced in relation to obesity.

To understand why saturated fatty acids caused this effect, we investigated a panel of innate immune sensors associated with IFN-I signaling pathways by qPCR within obese tumors, including *NLRX1* (101) and *NLRP3* (135). In this analysis, we found that *NLRC3*, a known regulator of the myeloid IFN-I response (112), was upregulated in tumors from obese mice. This novel finding indicates that saturated fatty acids directly interact with innate immune sensing pathway machinery within both cancer and immune cells to influence inflammatory processes. To characterize NLRC3-mediated effects on the cancer-intrinsic IFN-I, we both knocked out (via CRISPR/Cas9 in human HNSCC cells) and knocked down (via shRNA in MOC2-E6/E7) *NLRC3* expression, then stimulated cells with agonists of the IFN-I pathway. These experiments revealed that NLRC3 in negatively regulates IFN-I production in cancer cells. In vivo loss of

cancer-intrinsic NLRC3 led to reduced tumor burdens and increased infiltrates of TCRβ⁺ and TCRγδ⁺ cells. In addition, further experiments utilizing *Rag1*-deficient and *Ifnar1*-deficient mice confirmed the necessity of host adaptive immune cell responses and host downstream IFNAR1 signaling towards the effects of cancer-intrinsic NLRC3 loss.

Recent work has suggested that chronic inflammation in obese patients leads to better response rates to checkpoint therapies (136). However, it has also been reported in cancer models that components of adipose tissue, such as leptin, contribute to increased PD-1 expression and dysregulated T-cell activation (137). Thus, from our work analyzing the relationship between the innate immune sensor NLRC3 and saturated fatty acids, certain important future directions emerge. The first concerns the regulation of NLRC3 itself. Our findings in chapter 2 suggest that saturated fatty acids induce *NLRC3* expression, but one limitation to our study is that much is still unknown concerning direct regulators of NLRC3 transcription and functional activation. Previous reports have indicated that saturated fatty acids are potent drivers of ER stress and cellular injury, which subsequently promotes immunosuppressive myeloid cell expansion in the tumor microenvironment (138, 139), as well as activation of the pathogen recognition receptor NLRP3 (140). Potential in vivo carbon tracing experiments utilizing [^{13}C]-glucose, which have been used to uncover differential use of glucose in T-cells in vivo (141), could also further uncover if dysregulated metabolites of glycolysis interact with NLRC3 machinery to enhance its activity.

It has been recently reported that NLRC3-mediated sequestration of STING is reversed by DNA binding to the leucine-rich repeat domain of NLRC3 (114). It is a possibility that saturated fatty acids may directly interact on NLRC3 sensing domains, or through an ER stress-mediated molecular reprogramming. We additionally acknowledge that one technical limitation

to this study is the lack of a functional NLRC3 antibody. However, qPCR analysis of NLRC3, in addition to downstream induction of IFN-related gene signatures, and protein analysis of the STING pathway intermediates confirm cancer-intrinsic NLRC3 loss. Another interesting question pertains to the effects of weight loss on HNSCC tumor burden, and whether transient cancer cell-saturated fatty acid interaction may contribute to a fluctuating IFN-I and anti-tumor immune response. Lastly, a question emerges concerning host-intrinsic NLRC3 as a potentially targetable protein to enhance anti-tumor immunity. By uncovering how IFN-I signaling expands or retracts effectors in the tumor microenvironment, this mechanism can be used to enhance current combinatorial treatment modalities.

Objectives, Major Findings, and Implications from Chapter 3

Much has been previously addressed concerning the immune priming effects of IFN-I production on skewing anti-tumor immune responses towards effector phenotypes. However, not much has been understood concerning the mechanisms of downstream cancer-intrinsic IFNAR1 engagement and signaling in tumor modulation. Thus, in this chapter, our objective was to better characterize the mechanisms driving cancer resistance to STING-inducing priming therapies, we dissected the differences between IFNAR1 signaling in cancer cells from the IFN-I signaling in immune cells. From this work, we uncovered that downstream IFNAR1 signaling activation in cancer cells, via the surrogate "metagene" *MX1*, is associated with poor clinical outcomes. In addition, by blocking IFNAR1 signaling in the tumor cells, we noted expansions of stem-like effector T-cells, restriction of myeloid cell-derived suppressor cells (MDSCs), and global reduction in tumor burden. In our stemness assay, we examined the proliferative properties of the MOC2-E6/E7 cell line in vitro. However, a more comprehensive approach for future work would

be to assess the cancer stem cell compartment from our shIfnar1-MOC2-E6/E7 in vivo tumor models.

We postulate that the future development of robust IFN-I-inducing formulations is important to rapidly control tumors through myeloid reprogramming while avoiding prolonged stimulation of HNSCC cells, which triggers an adaptive mechanism promoting resistance to innate immune priming strategies. One possibility by which this resistance mechanism occurs is through the protein complex NF-κB. NF-κB activation is known to be critical for IFN-I induction. It is frequently activated in HNSCC (142), and its activation in tumor cells enhances HNSCC invasion and resistance to therapy (143-145). Thus, the duration of immune activation therapy is also likely shaping the evolution of tumor resistance. Most preclinical models for STING1 agonists testing were based on relatively acute administration into implantable subcutaneous tumor models. Chronic STING1 stimulation likely results in sustained NF-κB activation in tumor cells. This pathway encourages transcriptional programs associated with stemness that is associated with a more tolerogenic local immune niche.

To enhance the therapeutic effectiveness and avoid chronic STING1 stimulation, several robust delivery vehicles have been engineered for STING1 agonists. Controlled release of STING1 agonists using a peptide hydrogel significantly extends the survival of tumor-bearing mice compared to treatment with free STING1 agonists treatment alone (23). When STING1 agonists are delivered using nanoparticles in combination with ICB, tumor-specific CD8$^+$ T-cells are significantly expanded (16). Similarly, two other delivery systems including endosomolytic polymersomes nanoparticles and biodegradable polymer acetylated dextran microparticles also enhance the efficacy of STING1 (146, 147). Nanoparticles and microparticles are preferably taken up by myeloid cells and protect cargo from rapid degradation. Due to the unfavorable

pharmacokinetics property of free cGAMP, the integration of these delivery systems is a highly promising strategy to enhance myeloid response and avoid chronic stimulation of the IFNAR1 signaling in cancer cells. Finally, we speculate that targeting cancer stemness could be a viable treatment option, should targeted STING1 therapies produce downstream cancer-specific IFNAR1 activation. For one, the anti-CD44v6 monoclonal antibody bivatuzumab has been administered in phase I clinical trials for recurrent/metastatic HNSCC (148). We hypothesize that combinatorial therapies such as these will alleviate detrimental off-target effects and improve tumor regression outcomes.

Final Thoughts

The research outlined in this dissertation expands our understanding of the pleiotropic, differential mechanisms by which STING-mediated IFN-I production and signaling enacts both immune cell effector cell expansion as well as immune evasion by the induction of cancer stem cells. We highlight a novel strategy by which obesity constrains anti-tumor immunity, by the promotion of an innate immune sensor. It is certainly a goal of future work to further reveal the nature of NLRC3 regulation and sensing. More accurate NLRC3 antibodies, as well as characterization of *Nlrc3*-deficient tumors within *Nlrc3*$^{-/-}$ hosts will expand our understanding of interaction between host- and tumor-intrinsic IFN-I regulatory mechanisms. Extensive immune cell profiling of the myeloid compartment from these tumors would additionally broaden our knowledge of cellular-mediated mechanisms aiding immunosuppression. Thus, we postulate that future investigations examining such interactions will provide greater context towards our understanding of sensing-mediated immunosuppression. We additionally speculate that future pharmacologic agents will deliver targeted STING1 agonists to activate and expand cytolytic effector cell populations while mitigating the harmful effects of cancer IFNAR1 engagement.

84

APPENDIX

Chapter 1

Portions of this chapter have been published:
Heath BR, Michmerhuizen NL, Donnelly CR, Sansanaphongpricha K, Sun D, Brenner JC, Lei YL. <u>Head and Neck Cancer Immunotherapy beyond the Checkpoint Blockade.</u> *Journal of Dental Research* (2019) 2019 Sep;98(10):1073-1080.

<u>Author contributions:</u> Heath BR, Michmerhuizen NL and Sun D contributed to the direction and composition of the manuscript. Donnelly CR, Sansanaphongpricha K and Brenner JC contributed to manuscript design. Lei YL was responsible for the overall conception, direction, and composition of this project.

Chapter 2

This chapter is currently in preparation as an article for journal submission:
Heath BR, Gong W, Broses LJ, Luo X, Xie Y, Lei YL. <u>The innate immune sensor NLRC3 influences obesity-mediated IFN-I suppression and cancer immune escape.</u>

<u>Author contributions:</u> Heath BR conducted experiments and contributed to the direction and composition of the manuscript. Gong W, Broses LJ, Luo X and Xie Y performed experiments and conducted data analyses. Lei YL was responsible for the overall conception, direction, and composition of this project.

Chapter 3 & Chapter 4

Portions of these chapters are adapted from a publication under review at OncoImmunology:
Donnelly CR*, Heath BR*, Gong W*, Donnelly LA, Bellile E, Ji RR, Brenner JC, Chinn S, Wen H, Wang J, Wolf GT, Xie Y, Lei YL. <u>Cancer-specific IFNAR1 downstream signaling promotes cancer stemness and effector CD8$^+$ T-cell exhaustion</u> * represents equal contribution

<u>Author contributions:</u> Donnelly CR and Heath BR conducted experiments and contributed to the composition of the manuscript, including editing. Gong W, Wang, J, Donnelly LA, Bellile E and Xie, Y performed experiments and conducted data analyses. Lei YL was responsible for the overall conception, direction, and composition of this project, with intellectual input from Brenner JC, Chinn S, Wen H, Wolf GT, and Ji RR.

REFERENCES

1.   Bray F, Ferlay J, Soerjomataram I, Siegel RL, Torre LA, and Jemal A. Global cancer statistics 2018: GLOBOCAN estimates of incidence and mortality worldwide for 36 cancers in 185 countries. *CA Cancer J Clin.* 2018;68(6):394-424.

2.   Merhi M, Raza A, Inchakalody VP, Nashwan AJJ, Allahverdi N, Krishnankutty R, et al. Squamous Cell Carcinomas of the Head and Neck Cancer Response to Programmed Cell Death Protein-1 Targeting and Differential Expression of Immunological Markers: A Case Report. *Front Immunol.* 2018;9:1769.

3.   Maxwell JH, Grandis JR, and Ferris RL. HPV-Associated Head and Neck Cancer: Unique Features of Epidemiology and Clinical Management. *Annu Rev Med.* 2016;67:91-101.

4.   Yom SS, Mallen-St Clair J, and Ha PK. Controversies in Postoperative Irradiation of Oropharyngeal Cancer After Transoral Surgery. *Surg Oncol Clin N Am.* 2017;26(3):357-70.

5.   Herman S, Rogers HD, and Ratner D. Immunosuppression and squamous cell carcinoma: a focus on solid organ transplant recipients. *Skinmed.* 2007;6(5):234-8.

6.   Gonzalez JL, Reddy ND, Cunningham K, Silverman R, Madan E, and Nguyen BM. Multiple Cutaneous Squamous Cell Carcinoma in Immunosuppressed vs Immunocompetent Patients. *JAMA Dermatol.* 2019.

7.   Ferris RL, Blumenschein G, Jr., Fayette J, Guigay J, Colevas AD, Licitra L, et al. Nivolumab for Recurrent Squamous-Cell Carcinoma of the Head and Neck. *N Engl J Med.* 2016;375(19):1856-67.

8.   Ferris RL, Blumenschein G, Jr., Fayette J, Guigay J, Colevas AD, Licitra L, et al. Nivolumab vs investigator's choice in recurrent or metastatic squamous cell carcinoma of the head and neck: 2-year long-term survival update of CheckMate 141 with analyses by tumor PD-L1 expression. *Oral oncology.* 2018;81:45-51.

9.   Cohen EEW, Soulieres D, Le Tourneau C, Dinis J, Licitra L, Ahn MJ, et al. Pembrolizumab versus methotrexate, docetaxel, or cetuximab for recurrent or metastatic head-and-neck squamous cell carcinoma (KEYNOTE-040): a randomised, open-label, phase 3 study. *Lancet.* 2019;393(10167):156-67.

10.   Sharma P, and Allison JP. Immune checkpoint targeting in cancer therapy: toward combination strategies with curative potential. *Cell.* 2015;161(2):205-14.

11.   Hamid O, Robert C, Daud A, Hodi FS, Hwu WJ, Kefford R, et al. Safety and tumor responses with lambrolizumab (anti-PD-1) in melanoma. *The New England journal of medicine.* 2013;369(2):134-44.

12.   Tumeh PC, Harview CL, Yearley JH, Shintaku IP, Taylor EJ, Robert L, et al. PD-1 blockade induces responses by inhibiting adaptive immune resistance. *Nature.* 2014;515(7528):568-71.

13.   Rizvi NA, Hellmann MD, Snyder A, Kvistborg P, Makarov V, Havel JJ, et al. Cancer immunology. Mutational landscape determines sensitivity to PD-1 blockade in non-small cell lung cancer. *Science (New York, NY.* 2015;348(6230):124-8.

14.   Alexandrov LB, Nik-Zainal S, Wedge DC, Aparicio SA, Behjati S, Biankin AV, et al. Signatures of mutational processes in human cancer. *Nature.* 2013;500(7463):415-21.

15.   Wuebben EL, and Rizzino A. The dark side of SOX2: cancer - a comprehensive overview. *Oncotarget.* 2017;8(27):44917-43.

16.   Tan YS, Sansanaphongpricha K, Xie Y, Donnelly CR, Luo X, Heath BR, et al. Mitigating SOX2-potentiated Immune Escape of Head and Neck Squamous Cell Carcinoma with a STING-inducing Nanosatellite Vaccine. *Clin Cancer Res.* 2018;24(17):4242-55.

17.   Boumahdi S, Driessens G, Lapouge G, Rorive S, Nassar D, Le Mercier M, et al. SOX2 controls tumour initiation and cancer stem-cell functions in squamous-cell carcinoma. *Nature.* 2014;511(7508):246-50.

18.   Lee SH, Oh SY, Do SI, Lee HJ, Kang HJ, Rho YS, et al. SOX2 regulates self-renewal and tumorigenicity of stem-like cells of head and neck squamous cell carcinoma. *British journal of cancer.* 2014;111(11):2122-30.

19.   Liu K, Jiang M, Lu Y, Chen H, Sun J, Wu S, et al. Sox2 cooperates with inflammation-mediated Stat3 activation in the malignant transformation of foregut basal progenitor cells. *Cell stem cell.* 2013;12(3):304-15.

20.   Siegle JM, Basin A, Sastre-Perona A, Yonekubo Y, Brown J, Sennett R, et al. SOX2 is a cancer-specific regulator of tumour initiating potential in cutaneous squamous cell carcinoma. *Nat Commun.* 2014;5:4511.

21.   Deng L, Liang H, Xu M, Yang X, Burnette B, Arina A, et al. STING-Dependent Cytosolic DNA Sensing Promotes Radiation-Induced Type I Interferon-Dependent Antitumor Immunity in Immunogenic Tumors. *Immunity.* 2014;41(5):843-52.

22.   Gajewski TF, Woo SR, Zha Y, Spaapen R, Zheng Y, Corrales L, et al. Cancer immunotherapy strategies based on overcoming barriers within the tumor microenvironment. *Current opinion in immunology.* 2013;25(2):268-76.

23.   Leach DG, Dharmaraj N, Piotrowski SL, Lopez-Silva TL, Lei YL, Sikora AG, et al. STINGel: Controlled release of a cyclic dinucleotide for enhanced cancer immunotherapy. *Biomaterials.* 2018;163:67-75.

24.   Song S, Peng P, Tang Z, Zhao J, Wu W, Li H, et al. Decreased expression of STING predicts poor prognosis in patients with gastric cancer. *Sci Rep.* 2017;7:39858.

25.   Xia T, Konno H, Ahn J, and Barber GN. Deregulation of STING Signaling in Colorectal Carcinoma Constrains DNA Damage Responses and Correlates With Tumorigenesis. *Cell Rep.* 2016;14(2):282-97.

26.   Cerami E, Gao J, Dogrusoz U, Gross BE, Sumer SO, Aksoy BA, et al. The cBio cancer genomics portal: an open platform for exploring multidimensional cancer genomics data. *Cancer Discov.* 2012;2(5):401-4.

27.   Cancer Genome Atlas N. Comprehensive genomic characterization of head and neck squamous cell carcinomas. *Nature.* 2015;517(7536):576-82.

28.   Lui VW, Hedberg ML, Li H, Vangara BS, Pendleton K, Zeng Y, et al. Frequent mutation of the PI3K pathway in head and neck cancer defines predictive biomarkers. *Cancer discovery.* 2013;3(7):761-9.

29.   Wang Z, Martin D, Molinolo AA, Patel V, Iglesias-Bartolome R, Degese MS, et al. mTOR co-targeting in cetuximab resistance in head and neck cancers harboring PIK3CA and RAS mutations. *Journal of the National Cancer Institute.* 2014;106(9).

30.   Sugiura A, and Rathmell JC. Metabolic Barriers to T Cell Function in Tumors. *J Immunol.* 2018;200(2):400-7.

31. Siska PJ, and Rathmell JC. T cell metabolic fitness in antitumor immunity. *Trends in immunology.* 2015;36(4):257-64.

32. Delgoffe GM, and Powell JD. Feeding an army: The metabolism of T cells in activation, anergy, and exhaustion. *Molecular immunology.* 2015;68(2 Pt C):492-6.

33. Topalian SL, Taube JM, Anders RA, and Pardoll DM. Mechanism-driven biomarkers to guide immune checkpoint blockade in cancer therapy. *Nature reviews Cancer.* 2016;16(5):275-87.

34. Palucka AK, and Coussens LM. The Basis of Oncoimmunology. *Cell.* 2016;164(6):1233-47.

35. Hanahan D, and Weinberg RA. Hallmarks of cancer: the next generation. *Cell.* 2011;144(5):646-74.

36. Courtnay R, Ngo DC, Malik N, Ververis K, Tortorella SM, and Karagiannis TC. Cancer metabolism and the Warburg effect: the role of HIF-1 and PI3K. *Mol Biol Rep.* 2015;42(4):841-51.

37. Shayan G, Srivastava R, Li J, Schmitt N, Kane LP, and Ferris RL. Adaptive resistance to anti-PD1 therapy by Tim-3 upregulation is mediated by the PI3K-Akt pathway in head and neck cancer. *Oncoimmunology.* 2017;6(1):e1261779.

38. Spranger S, Bao R, and Gajewski TF. Melanoma-intrinsic beta-catenin signalling prevents anti-tumour immunity. *Nature.* 2015;523(7559):231-5.

39. Luke JJ, Bao R, Sweis RF, Spranger S, and Gajewski TF. WNT/beta-catenin Pathway Activation Correlates with Immune Exclusion across Human Cancers. *Clin Cancer Res.* 2019;25(10):3074-83.

40. Ang KK, Harris J, Wheeler R, Weber R, Rosenthal DI, Nguyen-Tan PF, et al. Human papillomavirus and survival of patients with oropharyngeal cancer. *The New England journal of medicine.* 2010;363(1):24-35.

41. Bauman JE, Cohen E, Ferris RL, Adelstein DJ, Brizel DM, Ridge JA, et al. Immunotherapy of head and neck cancer: Emerging clinical trials from a National Cancer Institute Head and Neck Cancer Steering Committee Planning Meeting. *Cancer.* 2017;123(7):1259-71.

42. Kansy BA, Shayan G, Jie HB, Gibson SP, Lei YL, Brandau S, et al. T cell receptor richness in peripheral blood increases after cetuximab therapy and correlates with therapeutic response. *Oncoimmunology.* 2018;7(11):e1494112.

43. Saloura V, Fatima A, Zewde M, Kiyotani K, Brisson R, Park JH, et al. Characterization of the T-Cell Receptor Repertoire and Immune Microenvironment in Patients with Locoregionally Advanced Squamous Cell Carcinoma of the Head and Neck. *Clin Cancer Res.* 2017;23(16):4897-907.

44. Haanen J. Converting Cold into Hot Tumors by Combining Immunotherapies. *Cell.* 2017;170(6):1055-6.

45. Dunn GP, Koebel CM, and Schreiber RD. Interferons, immunity and cancer immunoediting. *Nature reviews.* 2006;6(11):836-48.

46. Sistigu A, Yamazaki T, Vacchelli E, Chaba K, Enot DP, Adam J, et al. Cancer cell-autonomous contribution of type I interferon signaling to the efficacy of chemotherapy. *Nat Med.* 2014;20(11):1301-9.

47. Kuai R, Ochyl LJ, Bahjat KS, Schwendeman A, and Moon JJ. Designer vaccine nanodiscs for personalized cancer immunotherapy. *Nat Mater.* 2017;16(4):489-96.

48.   Hornung V, Rothenfusser S, Britsch S, Krug A, Jahrsdorfer B, Giese T, et al. Quantitative expression of toll-like receptor 1-10 mRNA in cellular subsets of human peripheral blood mononuclear cells and sensitivity to CpG oligodeoxynucleotides. *J Immunol.* 2002;168(9):4531-7.

49.   Edwards AD, Diebold SS, Slack EM, Tomizawa H, Hemmi H, Kaisho T, et al. Toll-like receptor expression in murine DC subsets: lack of TLR7 expression by CD8 alpha+ DC correlates with unresponsiveness to imidazoquinolines. *European journal of immunology.* 2003;33(4):827-33.

50.   Wu TT, and Zhou SH. Nanoparticle-based targeted therapeutics in head-and-neck cancer. *Int J Med Sci.* 2015;12(2):187-200.

51.   Peer D, Karp JM, Hong S, Farokhzad OC, Margalit R, and Langer R. Nanocarriers as an emerging platform for cancer therapy. *Nat Nanotechnol.* 2007;2(12):751-60.

52.   Gillison ML, Trotti AM, Harris J, Eisbruch A, Harari PM, Adelstein DJ, et al. Radiotherapy plus cetuximab or cisplatin in human papillomavirus-positive oropharyngeal cancer (NRG Oncology RTOG 1016): a randomised, multicentre, non-inferiority trial. *Lancet.* 2019;393(10166):40-50.

53.   Mehanna H, Robinson M, Hartley A, Kong A, Foran B, Fulton-Lieuw T, et al. Radiotherapy plus cisplatin or cetuximab in low-risk human papillomavirus-positive oropharyngeal cancer (De-ESCALaTE HPV): an open-label randomised controlled phase 3 trial. *Lancet.* 2019;393(10166):51-60.

54.   Deng L, Liang H, Burnette B, Beckett M, Darga T, Weichselbaum RR, et al. Irradiation and anti-PD-L1 treatment synergistically promote antitumor immunity in mice. *The Journal of clinical investigation.* 2014;124(2):687-95.

55.   Oweida A, Lennon S, Calame D, Korpela S, Bhatia S, Sharma J, et al. Ionizing radiation sensitizes tumors to PD-L1 immune checkpoint blockade in orthotopic murine head and neck squamous cell carcinoma. *Oncoimmunology.* 2017;6(10):e1356153.

56.   Miyauchi S, Kim SS, Pang J, Gold KA, Gutkind JS, Califano J, et al. Immune modulation of head and neck squamous cell carcinoma and the tumor microenvironment by conventional therapeutics. *Clin Cancer Res.* 2019.

57.   Reits EA, Hodge JW, Herberts CA, Groothuis TA, Chakraborty M, Wansley EK, et al. Radiation modulates the peptide repertoire, enhances MHC class I expression, and induces successful antitumor immunotherapy. *J Exp Med.* 2006;203(5):1259-71.

58.   Verbrugge I, Hagekyriakou J, Sharp LL, Galli M, West A, McLaughlin NM, et al. Radiotherapy increases the permissiveness of established mammary tumors to rejection by immunomodulatory antibodies. *Cancer Res.* 2012;72(13):3163-74.

59.   Oweida A, Hararah MK, Phan A, Binder D, Bhatia S, Lennon S, et al. Resistance to Radiotherapy and PD-L1 Blockade Is Mediated by TIM-3 Upregulation and Regulatory T-Cell Infiltration. *Clin Cancer Res.* 2018;24(21):5368-80.

60.   Sharabi AB, Nirschl CJ, Kochel CM, Nirschl TR, Francica BJ, Velarde E, et al. Stereotactic Radiation Therapy Augments Antigen-Specific PD-1-Mediated Antitumor Immune Responses via Cross-Presentation of Tumor Antigen. *Cancer Immunol Res.* 2015;3(4):345-55.

61.   Wirsdorfer F, Cappuccini F, Niazman M, de Leve S, Westendorf AM, Ludemann L, et al. Thorax irradiation triggers a local and systemic accumulation of immunosuppressive CD4+ FoxP3+ regulatory T cells. *Radiat Oncol.* 2014;9:98.

62.   Hato SV, Khong A, de Vries IJ, and Lesterhuis WJ. Molecular pathways: the immunogenic effects of platinum-based chemotherapeutics. *Clin Cancer Res.* 2014;20(11):2831-7.

63.   Tesniere A, Schlemmer F, Boige V, Kepp O, Martins I, Ghiringhelli F, et al. Immunogenic death of colon cancer cells treated with oxaliplatin. *Oncogene.* 2010;29(4):482-91.

64.   Apetoh L, Ghiringhelli F, Tesniere A, Obeid M, Ortiz C, Criollo A, et al. Toll-like receptor 4-dependent contribution of the immune system to anticancer chemotherapy and radiotherapy. *Nature medicine.* 2007;13(9):1050-9.

65.   Tran L, Allen CT, Xiao R, Moore E, Davis R, Park SJ, et al. Cisplatin Alters Antitumor Immunity and Synergizes with PD-1/PD-L1 Inhibition in Head and Neck Squamous Cell Carcinoma. *Cancer Immunol Res.* 2017;5(12):1141-51.

66.   Kim NR, and Kim YJ. Oxaliplatin regulates myeloid-derived suppressor cell-mediated immunosuppression via downregulation of nuclear factor-kappaB signaling. *Cancer Med.* 2019;8(1):276-88.

67.   Huang X, Guan D, Shu YQ, Liu LK, and Ni F. Effect of Cisplatin on the Frequency and Immuno-inhibitory Function of Myeloid-derived Suppressor Cells in A375 Melanoma Model. *Asian Pac J Cancer Prev.* 2015;16(10):4329-33.

68.   Vincent J, Mignot G, Chalmin F, Ladoire S, Bruchard M, Chevriaux A, et al. 5-Fluorouracil selectively kills tumor-associated myeloid-derived suppressor cells resulting in enhanced T cell-dependent antitumor immunity. *Cancer Res.* 2010;70(8):3052-61.

69.   Suzuki E, Kapoor V, Jassar AS, Kaiser LR, and Albelda SM. Gemcitabine selectively eliminates splenic Gr-1+/CD11b+ myeloid suppressor cells in tumor-bearing animals and enhances antitumor immune activity. *Clinical cancer research : an official journal of the American Association for Cancer Research.* 2005;11(18):6713-21.

70.   Alizadeh D, and Larmonier N. Chemotherapeutic targeting of cancer-induced immunosuppressive cells. *Cancer Res.* 2014;74(10):2663-8.

71.   Kodumudi KN, Woan K, Gilvary DL, Sahakian E, Wei S, and Djeu JY. A novel chemoimmunomodulating property of docetaxel: suppression of myeloid-derived suppressor cells in tumor bearers. *Clin Cancer Res.* 2010;16(18):4583-94.

72.   Ko JS, Zea AH, Rini BI, Ireland JL, Elson P, Cohen P, et al. Sunitinib mediates reversal of myeloid-derived suppressor cell accumulation in renal cell carcinoma patients. *Clin Cancer Res.* 2009;15(6):2148-57.

73.   Bruchard M, Mignot G, Derangere V, Chalmin F, Chevriaux A, Vegran F, et al. Chemotherapy-triggered cathepsin B release in myeloid-derived suppressor cells activates the Nlrp3 inflammasome and promotes tumor growth. *Nat Med.* 2013;19(1):57-64.

74.   Lesterhuis WJ, Punt CJ, Hato SV, Eleveld-Trancikova D, Jansen BJ, Nierkens S, et al. Platinum-based drugs disrupt STAT6-mediated suppression of immune responses against cancer in humans and mice. *J Clin Invest.* 2011;121(8):3100-8.

75.   Ramakrishnan R, Assudani D, Nagaraj S, Hunter T, Cho HI, Antonia S, et al. Chemotherapy enhances tumor cell susceptibility to CTL-mediated killing during cancer immunotherapy in mice. *J Clin Invest.* 2010;120(4):1111-24.

76.   Sun LL, Yang RY, Li CW, Chen MK, Shao B, Hsu JM, et al. Inhibition of ATR downregulates PD-L1 and sensitizes tumor cells to T cell-mediated killing. *Am J Cancer Res.* 2018;8(7):1307-16.

77.   Vendetti FP, Karukonda P, Clump DA, Teo T, Lalonde R, Nugent K, et al. ATR kinase inhibitor AZD6738 potentiates CD8+ T cell-dependent antitumor activity following radiation. *The Journal of clinical investigation.* 2018;128(9):3926-40.

78.   Lyssiotis CA, and Kimmelman AC. Metabolic Interactions in the Tumor Microenvironment. *Trends Cell Biol.* 2017;27(11):863-75.

79.   Choi SY, Collins CC, Gout PW, and Wang Y. Cancer-generated lactic acid: a regulatory, immunosuppressive metabolite? *J Pathol.* 2013;230(4):350-5.

80.   Le Bourgeois T, Strauss L, Aksoylar HI, Daneshmandi S, Seth P, Patsoukis N, et al. Targeting T Cell Metabolism for Improvement of Cancer Immunotherapy. *Front Oncol.* 2018;8:237.

81.   Pilon-Thomas S, Kodumudi KN, El-Kenawi AE, Russell S, Weber AM, Luddy K, et al. Neutralization of Tumor Acidity Improves Antitumor Responses to Immunotherapy. *Cancer Res.* 2016;76(6):1381-90.

82.   Robey RB, and Hay N. Is Akt the "Warburg kinase"?-Akt-energy metabolism interactions and oncogenesis. *Semin Cancer Biol.* 2009;19(1):25-31.

83.   Cash H, Shah S, Moore E, Caruso A, Uppaluri R, Van Waes C, et al. mTOR and MEK1/2 inhibition differentially modulate tumor growth and the immune microenvironment in syngeneic models of oral cavity cancer. *Oncotarget.* 2015;6(34):36400-17.

84.   Moore EC, Cash HA, Caruso AM, Uppaluri R, Hodge JW, Van Waes C, et al. Enhanced Tumor Control with Combination mTOR and PD-L1 Inhibition in Syngeneic Oral Cavity Cancers. *Cancer Immunol Res.* 2016;4(7):611-20.

85.   Ferris RL. Immunology and Immunotherapy of Head and Neck Cancer. *J Clin Oncol.* 2015;33(29):3293-304.

86.   Mandal R, Şenbabaoğlu Y, Desrichard A, Havel JJ, Dalin MG, Riaz N, et al. The head and neck cancer immune landscape and its immunotherapeutic implications. *JCI Insight.* 2016;1(17).

87.   Fu J, Kanne DB, Leong M, Glickman LH, McWhirter SM, Lemmens E, et al. STING agonist formulated cancer vaccines can cure established tumors resistant to PD-1 blockade. *Sci Transl Med.* 2015;7(283):283ra52.

88.   Luo M, Wang H, Wang Z, Cai H, Lu Z, Li Y, et al. A STING-activating nanovaccine for cancer immunotherapy. *Nat Nanotechnol.* 2017;12(7):648-54.

89.   Diamond MS, Kinder M, Matsushita H, Mashayekhi M, Dunn GP, Archambault JM, et al. Type I interferon is selectively required by dendritic cells for immune rejection of tumors. *J Exp Med.* 2011;208(10):1989-2003.

90.   Ivashkiv LB, and Donlin LT. Regulation of type I interferon responses. *Nat Rev Immunol.* 2014;14(1):36-49.

91.   Corrales L, Glickman LH, McWhirter SM, Kanne DB, Sivick KE, Katibah GE, et al. Direct Activation of STING in the Tumor Microenvironment Leads to Potent and Systemic Tumor Regression and Immunity. *Cell Rep.* 2015;11(7):1018-30.

92.   King SN, Dunlap NE, Tennant PA, and Pitts T. Pathophysiology of Radiation-Induced Dysphagia in Head and Neck Cancer. *Dysphagia.* 2016;31(3):339-51.

93.   Lambert EM, Gunn GB, and Gidley PW. Effects of radiation on the temporal bone in patients with head and neck cancer. *Head Neck.* 2016;38(9):1428-35.

94.   Le Naour J, Zitvogel L, Galluzzi L, Vacchelli E, and Kroemer G. Trial watch: STING agonists in cancer therapy. *Oncoimmunology.* 2020;9(1):1777624.

95.   Park J, Morley TS, Kim M, Clegg DJ, and Scherer PE. Obesity and cancer—mechanisms underlying tumour progression and recurrence. *Nature Reviews Endocrinology.* 2014;10(8):455-65.

96.   Etemadi A, O'Doherty MG, Freedman ND, Hollenbeck AR, Dawsey SM, and Abnet CC. A prospective cohort study of body size and risk of head and neck cancers in the NIH-AARP diet and health study. *Cancer Epidemiol Biomarkers Prev.* 2014;23(11):2422-9.

97.   Boland LK, Burand AJ, Boyt DT, Dobroski H, Di L, Liszewski JN, et al. Nature vs. Nurture: Defining the Effects of Mesenchymal Stromal Cell Isolation and Culture Conditions on Resiliency to Palmitate Challenge. *Front Immunol.* 2019;10:1080.

98.   Pascual G, Avgustinova A, Mejetta S, Martín M, Castellanos A, Attolini CS, et al. Targeting metastasis-initiating cells through the fatty acid receptor CD36. *Nature.* 2017;541(7635):41-5.

99.   Lei Y, Wen H, Yu Y, Taxman DJ, Zhang L, Widman DG, et al. The mitochondrial proteins NLRX1 and TUFM form a complex that regulates type I interferon and autophagy. *Immunity.* 2012;36(6):933-46.

100.   Lang P, Hasselwander S, Li H, and Xia N. Effects of different diets used in diet-induced obesity models on insulin resistance and vascular dysfunction in C57BL/6 mice. *Sci Rep.* 2019;9(1):19556.

101.   Luo X, Donnelly CR, Gong W, Heath BR, Hao Y, Donnelly LA, et al. HPV16 drives cancer immune escape via NLRX1-mediated degradation of STING. *J Clin Invest.* 2020;130(4):1635-52.

102.   Stinkens R, Goossens GH, Jocken JW, and Blaak EE. Targeting fatty acid metabolism to improve glucose metabolism. *Obes Rev.* 2015;16(9):715-57.

103.   Terawaki S, Chikuma S, Shibayama S, Hayashi T, Yoshida T, Okazaki T, et al. IFN-α directly promotes programmed cell death-1 transcription and limits the duration of T cell-mediated immunity. *J Immunol.* 2011;186(5):2772-9.

104.   Gessani S, and Belardelli F. Type I Interferons as Joint Regulators of Tumor Growth and Obesity. *Cancers (Basel).* 2021;13(2).

105.   Li L, Yin Q, Kuss P, Maliga Z, Millán JL, Wu H, et al. Hydrolysis of 2'3'-cGAMP by ENPP1 and design of nonhydrolyzable analogs. *Nat Chem Biol.* 2014;10(12):1043-8.

106.   Kingsbury KJ, Paul S, Crossley A, and Morgan DM. The fatty acid composition of human depot fat. *Biochem J.* 1961;78(3):541-50.

107.   Korbecki J, and Bajdak-Rusinek K. The effect of palmitic acid on inflammatory response in macrophages: an overview of molecular mechanisms. *Inflamm Res.* 2019;68(11):915-32.

108.   Ahmad R, Al-Roub A, Kochumon S, Akther N, Thomas R, Kumari M, et al. The Synergy between Palmitate and TNF-α for CCL2 Production Is Dependent on the TRIF/IRF3 Pathway: Implications for Metabolic Inflammation. *J Immunol.* 2018;200(10):3599-611.

109.   Mayer CM, and Belsham DD. Palmitate Attenuates Insulin Signaling and Induces Endoplasmic Reticulum Stress and Apoptosis in Hypothalamic Neurons: Rescue of Resistance and Apoptosis through Adenosine 5′ Monophosphate-Activated Protein Kinase Activation. *Endocrinology.* 2010;151(2):576-85.

110.   Palomer X, Pizarro-Delgado J, Barroso E, and Vázquez-Carrera M. Palmitic and Oleic Acid: The Yin and Yang of Fatty Acids in Type 2 Diabetes Mellitus. *Trends Endocrinol Metab.* 2018;29(3):178-90.

111. Saulters E, Woolley JF, Varadarajan S, Jones TM, and Dahal LN. STINGing viral tumours: What we know from head and neck cancers. *Cancer Res.* 2021.

112. Zhang L, Mo J, Swanson KV, Wen H, Petrucelli A, Gregory SM, et al. NLRC3, a member of the NLR family of proteins, is a negative regulator of innate immune signaling induced by the DNA sensor STING. *Immunity.* 2014;40(3):329-41.

113. Mombaerts P, Iacomini J, Johnson RS, Herrup K, Tonegawa S, and Papaioannou VE. RAG-1-deficient mice have no mature B and T lymphocytes. *Cell.* 1992;68(5):869-77.

114. Li X, Deng M, Petrucelli AS, Zhu C, Mo J, Zhang L, et al. Viral DNA Binding to NLRC3, an Inhibitory Nucleic Acid Sensor, Unleashes STING, a Cyclic Dinucleotide Receptor that Activates Type I Interferon. *Immunity.* 2019;50(3):591-9.e6.

115. Jemal A, Simard EP, Dorell C, Noone AM, Markowitz LE, Kohler B, et al. Annual Report to the Nation on the Status of Cancer, 1975-2009, featuring the burden and trends in human papillomavirus(HPV)-associated cancers and HPV vaccination coverage levels. *Journal of the National Cancer Institute.* 2013;105(3):175-201.

116. Gillison ML, Chaturvedi AK, Anderson WF, and Fakhry C. Epidemiology of Human Papillomavirus-Positive Head and Neck Squamous Cell Carcinoma. *Journal of clinical oncology : official journal of the American Society of Clinical Oncology.* 2015;33(29):3235-42.

117. Flood BA, Higgs EF, Li S, Luke JJ, and Gajewski TF. STING pathway agonism as a cancer therapeutic. *Immunological reviews.* 2019;290(1):24-38.

118. Bakhoum SF, Ngo B, Laughney AM, Cavallo JA, Murphy CJ, Ly P, et al. Chromosomal instability drives metastasis through a cytosolic DNA response. *Nature.* 2018;553(7689):467-72.

119. Erdal E, Haider S, Rehwinkel J, Harris AL, and McHugh PJ. A prosurvival DNA damage-induced cytoplasmic interferon response is mediated by end resection factors and is limited by Trex1. *Genes & development.* 2017;31(4):353-69.

120. Concha-Benavente F, Srivastava RM, Trivedi S, Lei Y, Chandran U, Seethala RR, et al. Identification of the Cell-Intrinsic and -Extrinsic Pathways Downstream of EGFR and IFNgamma That Induce PD-L1 Expression in Head and Neck Cancer. *Cancer research.* 2016;76(5):1031-43.

121. Lee Y, Shin JH, Longmire M, Wang H, Kohrt HE, Chang HY, et al. CD44+ Cells in Head and Neck Squamous Cell Carcinoma Suppress T-Cell-Mediated Immunity by Selective Constitutive and Inducible Expression of PD-L1. *Clin Cancer Res.* 2016;22(14):3571-81.

122. Zhou L, Mudianto T, Ma X, Riley R, and Uppaluri R. Targeting EZH2 Enhances Antigen Presentation, Antitumor Immunity, and Circumvents Anti-PD-1 Resistance in Head and Neck Cancer. *Clin Cancer Res.* 2020;26(1):290-300.

123. Moore E, Clavijo PE, Davis R, Cash H, Van Waes C, Kim Y, et al. Established T Cell-Inflamed Tumors Rejected after Adaptive Resistance Was Reversed by Combination STING Activation and PD-1 Pathway Blockade. *Cancer Immunol Res.* 2016;4(12):1061-71.

124. Kim CH, Rott L, Kunkel EJ, Genovese MC, Andrew DP, Wu L, et al. Rules of chemokine receptor association with T cell polarization in vivo. *The Journal of clinical investigation.* 2001;108(9):1331-9.

125. Siddiqui I, Schaeuble K, Chennupati V, Fuertes Marraco SA, Calderon-Copete S, Pais Ferreira D, et al. Intratumoral Tcf1(+)PD-1(+)CD8(+) T Cells with Stem-like Properties

Promote Tumor Control in Response to Vaccination and Checkpoint Blockade Immunotherapy. *Immunity.* 2019;50(1):195-211 e10.

126. Miller BC, Sen DR, Al Abosy R, Bi K, Virkud YV, LaFleur MW, et al. Subsets of exhausted CD8(+) T cells differentially mediate tumor control and respond to checkpoint blockade. *Nature immunology.* 2019;20(3):326-36.

127. Chisolm DA, Savic D, Moore AJ, Ballesteros-Tato A, Leon B, Crossman DK, et al. CCCTC-Binding Factor Translates Interleukin 2- and alpha-Ketoglutarate-Sensitive Metabolic Changes in T Cells into Context-Dependent Gene Programs. *Immunity.* 2017;47(2):251-67 e7.

128. Edwards DN, Ngwa VM, Raybuck AL, Wang S, Hwang Y, Kim LC, et al. Selective glutamine metabolism inhibition in tumor cells improves antitumor T lymphocyte activity in triple-negative breast cancer. *The Journal of clinical investigation.* 2021;131(4).

129. Buck MD, O'Sullivan D, and Pearce EL. T cell metabolism drives immunity. *The Journal of experimental medicine.* 2015;212(9):1345-60.

130. Hou Y, Liang H, Rao E, Zheng W, Huang X, Deng L, et al. Non-canonical NF-kappaB Antagonizes STING Sensor-Mediated DNA Sensing in Radiotherapy. *Immunity.* 2018;49(3):490-503 e4.

131. Outh-Gauer S, Alt M, Le Tourneau C, Augustin J, Broudin C, Gasne C, et al. Immunotherapy in head and neck cancers: A new challenge for immunologists, pathologists and clinicians. *Cancer Treat Rev.* 2018;65:54-64.

132. Divella R, De Luca R, Abbate I, Naglieri E, and Daniele A. Obesity and cancer: the role of adipose tissue and adipo-cytokines-induced chronic inflammation. *J Cancer.* 2016;7(15):2346-59.

133. Jin C, and Flavell RA. Innate sensors of pathogen and stress: linking inflammation to obesity. *J Allergy Clin Immunol.* 2013;132(2):287-94.

134. Iyengar NM, Gucalp A, Dannenberg AJ, and Hudis CA. Obesity and Cancer Mechanisms: Tumor Microenvironment and Inflammation. *J Clin Oncol.* 2016;34(35):4270-6.

135. Yu X, Du Y, Cai C, Cai B, Zhu M, Xing C, et al. Inflammasome activation negatively regulates MyD88-IRF7 type I IFN signaling and anti-malaria immunity. *Nat Commun.* 2018;9(1):4964.

136. Woodall MJ, Neumann S, Campbell K, Pattison ST, and Young SL. The Effects of Obesity on Anti-Cancer Immunity and Cancer Immunotherapy. *Cancers (Basel).* 2020;12(5).

137. Wang Z, Aguilar EG, Luna JI, Dunai C, Khuat LT, Le CT, et al. Paradoxical effects of obesity on T cell function during tumor progression and PD-1 checkpoint blockade. *Nat Med.* 2019;25(1):141-51.

138. Xu S, Nam SM, Kim JH, Das R, Choi SK, Nguyen TT, et al. Palmitate induces ER calcium depletion and apoptosis in mouse podocytes subsequent to mitochondrial oxidative stress. *Cell Death Dis.* 2015;6:e1976.

139. Cubillos-Ruiz JR, Bettigole SE, and Glimcher LH. Tumorigenic and Immunosuppressive Effects of Endoplasmic Reticulum Stress in Cancer. *Cell.* 2017;168(4):692-706.

140. Menu P, Mayor A, Zhou R, Tardivel A, Ichijo H, Mori K, et al. ER stress activates the NLRP3 inflammasome via an UPR-independent pathway. *Cell Death Dis.* 2012;3:e261.

141. Ma EH, Verway MJ, Johnson RM, Roy DG, Steadman M, Hayes S, et al. Metabolic Profiling Using Stable Isotope Tracing Reveals Distinct Patterns of Glucose Utilization by Physiologically Activated CD8. *Immunity.* 2019;51(5):856-70.e5.

142. Yang X, Cheng H, Chen J, Wang R, Saleh A, Si H, et al. Head and Neck Cancers Promote an Inflammatory Transcriptome through Coactivation of Classic and Alternative NF-kappaB Pathways. *Cancer Immunol Res.* 2019;7(11):1760-74.

143. Rehman AO, and Wang CY. CXCL12/SDF-1 alpha activates NF-kappaB and promotes oral cancer invasion through the Carma3/Bcl10/Malt1 complex. *Int J Oral Sci.* 2009;1(3):105-18.

144. Yang Z, Liao J, Cullen KJ, and Dan H. Inhibition of IKKbeta/NF-kappaB signaling pathway to improve Dasatinib efficacy in suppression of cisplatin-resistant head and neck squamous cell carcinoma. *Cell Death Discov.* 2020;6:36.

145. Li Z, Liao J, Yang Z, Choi EY, Lapidus RG, Liu X, et al. Co-targeting EGFR and IKKbeta/NF-kappaB signalling pathways in head and neck squamous cell carcinoma: a potential novel therapy for head and neck squamous cell cancer. *British journal of cancer.* 2019;120(3):306-16.

146. Shae D, Becker KW, Christov P, Yun DS, Lytton-Jean AKR, Sevimli S, et al. Endosomolytic polymersomes increase the activity of cyclic dinucleotide STING agonists to enhance cancer immunotherapy. *Nat Nanotechnol.* 2019;14(3):269-78.

147. Watkins-Schulz R, Tiet P, Gallovic MD, Junkins RD, Batty C, Bachelder EM, et al. A microparticle platform for STING-targeted immunotherapy enhances natural killer cell- and CD8(+) T cell-mediated anti-tumor immunity. *Biomaterials.* 2019;205:94-105.

148. Yang L, Shi P, Zhao G, Xu J, Peng W, Zhang J, et al. Targeting cancer stem cell pathways for cancer therapy. *Signal Transduct Target Ther.* 2020;5(1):8.